A Study Of Single-lane Roundabouts For Connected Automated Vehicles

A Microscopic Control Model And Queueing Models

Master Thesis

Huan Wu

TU Delft

A Study Of Single-lane Roundabouts For Connected Automated Vehicles

A Microscopic Control Model And Queueing Models

by

Student Name	Student Number
Huan Wu	4505565

Supervisors: Prof.dr.ir. G. Jongbloed, Dr.ir.Maria Salomons, and Dr.ir.L.G.H.Fortuijn.
Faculty: Electrical Engineering, Mathematics and Computer Science, TUDelft

TU Delft

Acknowledgement

First and foremost, I would like to express my deepest gratitude to **Prof.dr.ir. Geurt Jongbloed**. Based on my research interests, Geurt kindly connected me with **Dr.ir. Maria Salomons** and **Dr.ir. Bertus Fortuijn** from the Faculty of Civil Engineering and Geosciences. I am sincerely thankful to all of you for providing me with the opportunity to work on the single-lane roundabout optimization project.

During our meetings, Geurt consistently demonstrated profound expertise, identifying the shortcomings in my research and guiding me towards effective solutions. His insightful feedback significantly enriched my understanding of statistical analysis, elevating my academic capabilities to a higher standard.

I am equally grateful to Maria for her invaluable guidance. She not only taught me how to write reports in a more academic style but also patiently explained specialized knowledge in transportation whenever I needed support. Her encouragement and mentorship were essential throughout this journey.

I would also like to extend my heartfelt thanks to Bertus for sharing his expertise in roundabout optimization. His meticulous attention to detail helped me identify minor errors in my thesis and address deficiencies in the references I cited. His provision of appropriate literature ensured the academic integrity of my work.

Moreover, I deeply appreciate the care and concern that Geurt, Maria, and Bertus showed for both my physical and mental well-being throughout the project. Their humanity and kindness highlighted the compassionate side of academia, for which I am profoundly grateful.

I am also indebted to my undergraduate advisor, **Prof.dr. Richard Boucherie**, for his guidance at the beginning of this project. At that time, I was unfamiliar with the analysis of an $M/G/1/k$ queueing model, and his provision of relevant literature was instrumental in helping me build a strong foundation for my research.

In addition, I wish to thank my friend **Shikuan Li**, a master's student in Computer Science at TUDelft, for engaging in fruitful discussions on object-oriented programming, which greatly benefited my project. My gratitude also goes to **Bonan Wu**, a master's student in Civil Engineering at Beijing Forestry University, for teaching me how to use VISSIM simulation software, which played a crucial role in my research.

Lastly, I would like to extend my deepest appreciation to my parents for their unwavering support and understanding. Their belief in me has always been a source of strength and motivation.

To all those who have supported and guided me during this journey, thank you for your contributions to the successful completion of this work.

Huan Wu
Delft, January 2025

Abstract

Abstract

This study focuses on optimizing the efficiency of single-lane roundabouts for connected automated vehicles (CAVs). While roundabouts are vital for traffic management, their performance declines significantly under high traffic volumes. By leveraging vehicle-to-vehicle communication and the cooperative decision-making capabilities of CAVs, this research develops a microscopic control model that not only minimizes sojourn times (maximizes efficiency) but also provides precise trajectory control for each individual vehicle. Besides, a theoretical $M/G/1/k$ queueing model is employed to calculate the expected sojourn time, serving as a baseline to compare CAV-controlled scenarios with human-driven conditions.

The results demonstrate that the proposed microscopic control model significantly reduces the expected sojourn time for vehicles entering the roundabout. For a single-lane roundabout with a capacity of 17 vehicles per leg, compared to uncontrolled scenarios simulated in VISSIM, the control model achieves empirical efficiency improvements of 26%, 80%, 91%, and 90% under arrival rates of 200, 400, 600, and $800 pcu/h$ per leg, respectively. These empirical findings align closely with theoretical predictions from the $M/G/1/k$ queueing model, which estimate efficiency gains of 18%, 78%, 89%, and 90%. Moreover, the control model demonstrates robustness under extreme traffic conditions, maintaining high efficiency and passenger comfort.

This research provides valuable insights into the integration of CAVs into traffic systems and contributes both practically and theoretically to the modernization of roundabout traffic management.

Key words: Connected Automated Vehicles, Single-lane Roundabouts, Microscopic Control Model, $M/G/1/k$ Queueing Model, Sojourn Time Optimization, Efficiency of Roundabouts, Trajectory.

Contents

Nomenclature

Abbreviations

Abbreviation	Definition
CAVs	connected automated vehicles
MLE	maximum likelihood estimator
PGF	probability generating function
LST	Laplace-Stiejes transform
AVG	automatic vehicle guidance
cdf	cumulative distribution function
ecdf	empirical cumulative distribution function
pdf	probability density function
SCV	squared coefficient of variation
DTMC	discrete time Markov Chain
SE	shifted exponential distribution
M	M3 distribution
LN	lognormal distribution
K-S	Kolmogorov-Smirnov
AIC	Akaike Information Criterion
AIC	Bayesian Information Criterion
i.i.d	identically independently distributed
Q1	25th percentile of the data
Q2	50th percentile of the data
Q3	75th percentile of the data
$MM()$	method of moment estimator

Symbols

Symbol	Definition	Unit
v_{max}	maximum speed limit on each leg	(m/s)
a_{max}	maximum acceleration limit on each leg	(m/s^2)
a_{min}	minimum acceleration limit on each leg	(m/s^2)
v_r	maximum speed limit in the circulating stream	(m/s)
d_{safe}	safety distance on each leg	(m)
x_0	distance of the leg in the control zone	(m)
$\lambda, \lambda_1, ..., \lambda_4$	arrival rate to the leg of the roundabout	(pcu/h)
VL	vehicle length	(m)
C_l	leg capacity	/
i	index of vehicle	/
j	index of leg	/
n_j	total number of vehicles on leg j	/
$A_{i,j}^{\text{max}}$	the maximum time at which vehicle i from leg j reaches the entry line	(s)
$A_{i,j}^{\text{min}}$	the minimum time at which vehicle i from leg j reaches the entry line	(s)
$v_{i,0}$	initial speed of vehicle i entering the control zone	(m/s)
r	radius of the single-lane roundabout	(m)

Symbol	Definition	Unit
S_i^j	sojourn time of vehicle i from leg j to travel from entering the control zone to merging into the roundabout	(s)
$t_{i,0}$	time at which vehicle i reaches the boundary of the control zone	(s)
$v'_{i,0}$	inter-mediate variable for calculating $A_{i,j}^{\mathsf{max}}$, it is defined as $\sqrt{\frac{2a_{\mathsf{max}}\lvert a_{\mathsf{min}}\rvert x_0+\lvert a_{\mathsf{min}}\rvert(v_{i,0})^2+a_{\mathsf{max}}(v_r)^2}{a_{\mathsf{max}}+\lvert a_{min}\rvert}}$	(m/s)
$\tilde{v}_{i,0}$	inter-mediate variable for calculating $A_{i,j}^{\mathsf{max}}$, it is defined as $\sqrt{\frac{a_{\mathsf{max}}(v_{i,0})^2+\lvert a_{\mathsf{min}}\rvert(v_r)^2-2a_{\mathsf{max}}\lvert a_{min}\rvert}{a_{\mathsf{max}}+\lvert a_{min}\rvert}}$	(m/s)
t_a	acceleration time for calculating $A_{i,j}^{\mathsf{min}}$, it is defined as $\frac{v_{\mathsf{max}}-v_{i,0}}{a_{\mathsf{max}}}$	(s)
t_c	cruising time for calculating $A_{i,j}^{\mathsf{min}}$, it is defined as $\frac{x_0-\frac{(v_{\mathsf{max}})^2-(v_{i,0})^2}{2a_{\mathsf{max}}}-\frac{(v_{\mathsf{max}})^2-(v_r)^2}{2\lvert a_{\mathsf{min}}\rvert}}{v_{\mathsf{max}}}$	(s)
t_d	deceleration time for calculating $A_{i,j}^{\mathsf{min}}$, it is defined as $\frac{v_{\mathsf{max}}-v_r}{\lvert a_{\mathsf{min}}\rvert}$	(s)
c_1, c_2, c_3, c_4	conflict points attached to leg $1, 2, 3, 4$, respectively	/
$C_j^{j'}$	set of conflict points for vehicles from leg j and j', it is defined as $\{c_1, c_2, c_3, c_4\}$	/
c	general notation of conflict points, $c \in C_j^{j'}$	/
$BI_{i,i'}^c$	A binary variable that equals 1 if vehicle i reaches the conflict point c prior to i'; otherwise, it equals 0.	/
t_C	critical time	(s)
t_M	minimum headway time	(s)
t_F	follow-on time	(s)
$a_{i,1}$	vehicle i's acceleration in the first segment of the Second Phase Optimization	(m/s^2)
$v_{i,*}$	vehicle i's cruising speed in the second segment of the Second Phase Optimization	(m/s)
$a_{i,2}$	vehicle i's acceleration in the third segment of the Second Phase Optimization	(m/s^2)
$t_{i,1}$	end time of the first segment in the Second Phase Optimization	(s)
$t_{i,2}$	end time of the second segment in the Second Phase Optimization	(s)
Δt	change in time or time step	(s)
$v_i(t+\Delta t)$	vehicle i's speed at next time step	(m/s)
$x_i(t+\Delta t)$	vehicle i's position at next time step	(m)
S	sojourn time in a queueing system	(s)
B	service time in a queueing system	(s)
W	waiting or queueing time in a queueing system	(s)
L	number of customers in a queueing system, including the one in service	/
L_q	number of customers in the queue, excluding the one in service	/
$\{C(t)\}$	Delayed Process in the circulating stream of the single-lane roundabout, which is the arrival process of the circulating stream to the conflict point	/
$C_i(t)$	inter-arrival time or inter-event time in the process $\{C(t)\}$	(s)

Symbol	Definition	Unit
$C_1(t)$	the first inter-event time in the process $\{C(t)\}$, which is the event time of Equilibrium Process within the Delayed Process	(s)
B_0	the time that the first vehicle at the entry line has to wait under the Non-Delayed Renewal Process of the circulating stream	(s)
L_k^d	the number of customers left behind after the kth departure in a queueing system	/
A_k	the number of customers that arrive during the service time of kth customer in a queueing system	/
$p_{i,j}$	transition probability of the DTMC $\{L_k^d\}_{k=0}^{\infty}$	/
α_n	probability that there are n arrivals during a service time B	/
$P_{M/G/1}$	transition probability matrix in the $M/G/1$ queueing system	/
$P_{M/G/1/k}$	transition probability matrix in the $M/G/1/k$ queueing system, where k is the capacity of the system	/
$\boldsymbol{\pi}$	stationary probability vector in the $M/G/1/k$ queueing system	/
C_s^2	squared coefficient of variation of the service time in a queueing system	/
ρ	utilization of a queueing system	/
p_k	blocking probability in the $M/G/1/k$ queueing system	/
$L(t)$	number of customers in a queueing system at time t	/
S_i	the time that a customer i spends in a queueing system	(s)
T_i	the arrival time of customer i to a queueing system	(s)
$N(t)$	the number of customers that have arrived in a queueing system up to time t	/
D_i	the departure time of customer i from a queueing system	(s)
H_0	null hypothesis	/
H_1	alternative hypothesis	/
θ	parameter(s) in the statistical model (distribution model)	/
$Avg(S_V)$	average sojourn time of vehicles in the Vissim simulation	(s)
$\mathbb{E}(S_{uc}^{qk})$	expected uncontrolled sojourn time calculated from the $M/G/1/k$ queueing model	(s)
$\mathbb{E}(S_c)$	mean controlled sojourn time from the control model	(s)
a_n	probability of having n customers in a queueing system upon arrival, it is defined as $\mathbb{P}(L^a = n)$	/
d_n	probability of having n customers in a queueing system upon departure, it is defined as $\mathbb{P}(L^d = n)$	/
p_n	probability of having n customers in a queueing system, it is defined as $\mathbb{P}(L = n)$	/

1

Introduction

1.1. Background and Context

Roundabouts are widely regarded as an effective solution for managing traffic flow at intersections, especially in urban areas. They help reduce congestion and improve safety by promoting continuous movement, as opposed to traditional traffic signals or stop signs that cause vehicles to halt frequently. Single-lane roundabouts, in particular, offer the advantage of efficiently handling moderate traffic volumes with minimal delay[23]. However, as traffic volumes increase, even these roundabouts can become congested, resulting in increased waiting times and reduced efficiency. Therefore, improving the performance of single-lane roundabouts has become a critical area of research.

Recent advancements in connected automated vehicles (CAVs) technology have introduced new possibilities for optimizing traffic flow. CAVs are installed with sophisticated communication systems that allow them to exchange information, such as vehicle position, speed, and intentions, and operate autonomously without the need for human intervention. This ability to share information and make cooperative decisions enables vehicles to reduce collision risk and improve the overall efficiency of traffic networks. When applied to roundabouts, CAVs could potentially optimize the time for them to enter the roundabout, leading to smoother traffic flow and reduced queueing time[4].

However, the integration of CAVs into traditional roundabout models presents unique challenges. Traditional traffic flow models for roundabouts typically rely on the assumption that human drivers make independent decisions, an assumption that may not hold when autonomous vehicles with communication abilities are introduced. Additionally, existing studies on roundabouts primarily focus on conventional vehicles without considering the dynamic and cooperative nature of CAV systems. As a result, existing research lacks sufficient exploration of how CAVs influence the efficiency of single-lane roundabouts and the optimal strategies for managing their movements to enhance overall performance.

This research aims to address this gap by developing a microscopic control model specifically designed for CAVs in single-lane roundabouts. By considering vehicle-to-vehicle communication and dynamic gap acceptance, the model seeks to optimize the time for vehicles entering a single-lane roundabout. Once the optimal entering time is obtained, it will be used to derive a microscopic control to optimize the driving experience. Furthermore, this study combines the control model with queueing theory to assess the expected sojourn times for vehicles (time for vehicles to enter roundabouts) in both controlled and uncontrolled scenarios. The results of this study will provide valuable insights into how CAVs can be leveraged to improve roundabout efficiency, offering potential solutions for modernizing traffic management systems.

1.2. Problem Statement

Single-lane roundabouts are a widely used traffic management solution, yet they are susceptible to inefficiencies as traffic volumes increase. While conventional traffic flow models for roundabouts focus on driver behavior and interactions, the rise of CAVs introduces new opportunities and challenges for

optimizing roundabout efficiency which refers to the expected time for vehicles to enter the roundabouts (also named as expected sojourn time). Traditional roundabout models are often insufficient for fully capturing the cooperative behavior of CAVs, particularly in scenarios where vehicles can communicate and make collective decisions in real-time.

The primary challenge addressed in this research is the need to understand how CAVs can be integrated into existing roundabout systems to improve traffic flow, reduce delays, and increase overall efficiency. Specifically, it remains unclear how CAVs should adjust their speed and acceleration when entering a single-lane roundabout, how the control of these vehicles within a designated control zone affects overall roundabout performance, and how the efficiency of such systems gets improved compared to traditional human-driven conditions.

There is also limited understanding of the theoretical and practical implications of integrating CAVs into single-lane roundabouts, particularly when comparing controlled systems with real-world conditions. The current gap in literature lies in the lack of quantitative analysis on how CAVs, operating under a microscopic control model, can reduce waiting times and improve vehicle throughput in a single-lane roundabout. Furthermore, the comparison between a controlled system and human-driven scenarios has not been explored in detail, particularly in terms of the expected sojourn times for vehicles.

Thus, the problem lies in effectively designing a system that accounts for the cooperative, dynamic nature of CAVs, optimizes their entry and movement through roundabouts, and quantifies the improvement in roundabout efficiency under various driving conditions.

1.3. Research Questions

In the controlled scenario for Connected and Automated Vehicles (CAVs), the penetration of CAVs is 100%, and a typical single-lane roundabout with four entrances and four exits is assumed to be equipped with a control zone. This control zone includes the four entry legs and the circulating roadway inside the roundabout. Once a vehicle enters the control zone, the onboard computer will calculate its optimal sojourn time (the time it takes for a vehicle to move from entering the control zone to merging into the roundabout). When a new vehicle enters the control zone, it receives information about the sojourn times and exits of vehicles already within the zone. Using this information, the new vehicle calculates its own optimal sojourn time. This is how CAVs communicate with each other within the control zone. All sojourn times are collected by a central CPU, which then issues commands to guide the vehicles' trajectories to optimize their driving experience as they enter the roundabout. Specifically, it determines the acceleration or speed of vehicles within the control zone at any given time. As a result, no vehicle acts "selfishly"; all vehicles within the control zone follow the commands from the central CPU to determine their trajectories. However, once inside the roundabout, all vehicles are controlled to maintain the maximal limiting speed of the circulating roadway. Additionally, it is assumed that there is no path guidance within the control zone, meaning that all vehicles will travel along the center of each entry leg and the circulating roadway. Furthermore, vehicles are assumed to arrive at the control zone according to a Poisson Process and all legs have the same arrival rate. The detailed assumptions will be introduced in Sec.4.1.1.

To understand how CAVs communicate and are controlled within the control zone, one can refer to Fig. 1.1. In the figure, vehicles are ordered based on their time of entry into the control zone. For instance, when vehicle 1 enters the control zone, it will calculate its optimal sojourn time and send it to the central CPU. Based on this sojourn time, the central CPU will issue commands to guide its trajectory and ensure the optimal driving experience. When vehicle 3 enters the control zone, vehicles 1 and 2 are already inside. Vehicle 3 then will receive information about the optimal sojourn times and exits of vehicles 1 and 2. Using this information, vehicle 3 will calculate its own optimal sojourn time and send it to the central CPU. Afterward, it will follow the commands issued by the central CPU.

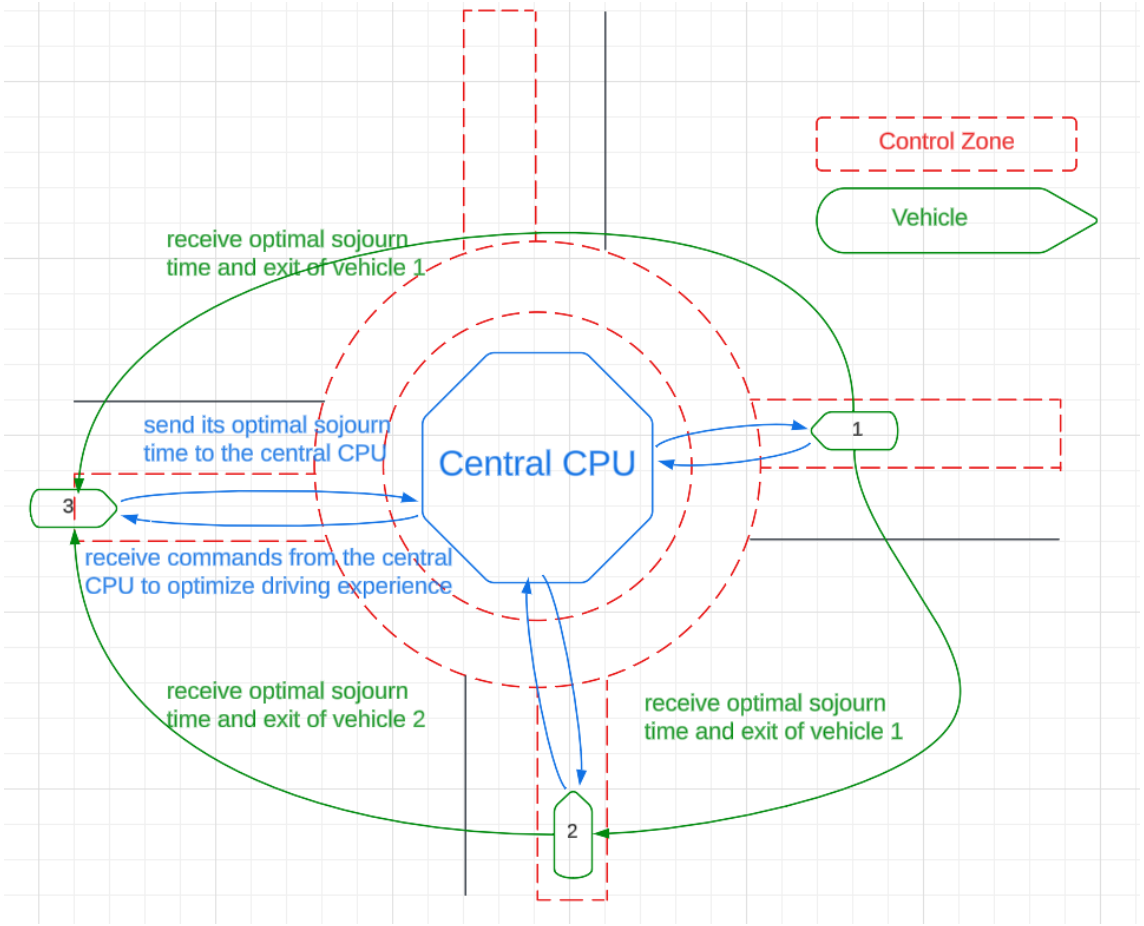

Figure 1.1: Concept of how CAVs communicate and are controlled.

To address the identified problem and explore the potential benefits of CAVs in single-lane roundabouts, this thesis aims to answer the following research questions:

1. **Given the arrival speed to the control zone, how to control each vehicle inside the control zone to maximize the efficiency of a single-lane roundabout and the driving experience of each driver?**

   Under the context of this research question, from a macroscopic perspective, the word “control” refers to determining the optimal sojourn time for each individual vehicle. However, from a microscopic perspective, the word “control” refers to what speed or acceleration should each individual vehicle take within a designated control zone during a specific period of time. In other words, from a macroscopic point of view, “control” refers to managing the optimal sojourn time for each individual vehicle. From a microscopic point of view,“control” refers to managing the trajectory of each vehicle.

   It should be noted that there are several possible *control types*. For example, under a *centralized control* scenario, a central CPU gathers information from all vehicles and makes decisions for each individual vehicle. In contrast, under a *decentralized control* scenario, each vehicle makes its own decisions using locally collected or shared information. In a *cooperative control* scenario, vehicles share data in order to make coordinated decisions. Meanwhile, in a *selfish* or *non-cooperative control* scenario, each vehicle independently optimizes its own performance without explicitly cooperating or sharing information with others. In this research, we employ a *hybrid control* approach. Specifically, when computing the expected sojourn time, an arriving vehicle receives information from vehicles already in the control zone. However, when determining the speed or acceleration for each individual vehicle, the central CPU issues commands based

on the information from all vehicles in the control zone.

By considering the ability of vehicles to communicate and cooperate, this research question first aims to minimize the total sojourn time for all vehicles (maximize efficiency for the single-lane roundabout) based on each vehicle's speed upon arrival to the control zone. Its output is the optimal individual sojourn time. Given the individual optimal sojourn times, we will then focus on determining the optimal speed and acceleration profiles for CAVs entering and navigating the roundabout, ensuring a comfortable driving experience for each driver. The output of it is the driving trajectory for each individual vehicle.

To better understand **Research Question 1**, Fig.1.2 indicates the input and output of it.

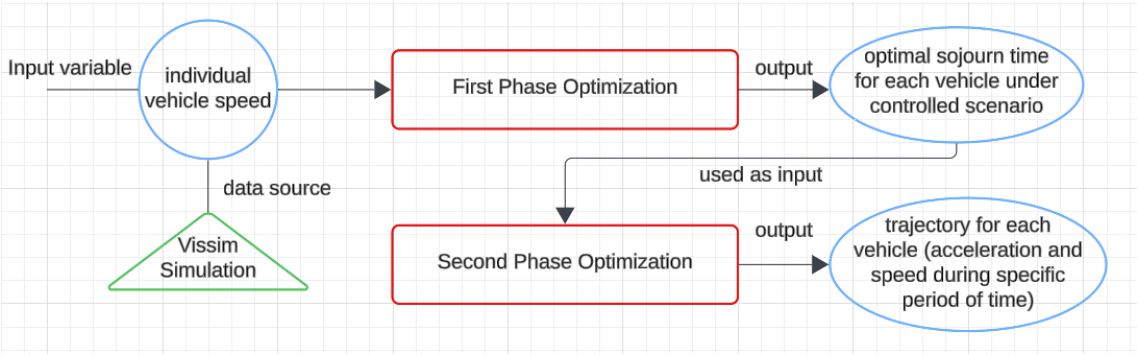

Figure 1.2: Explanation of Research Question 1.

2. **How to quantify the efficiency improved by controlling all CAVs within the control zone microscopically?**

   This question investigates the broader impact of controlling all CAVs within the control zone, assessing whether such control leads to improved roundabout performance in terms of reduced congestion, shorter sojourn times, and higher vehicle throughput. The comparison will be made between the control model and an uncontrolled scenario.

   To answer this research question, we will calculate the efficiency (expected sojourn time) for the controlled CAVs and compare it to the one obtained from the uncontrolled scenario. The average sojourn time can be obtained from the VISSIM simulation, which uses the built-in car-following model [27]. Although the results from the VISSIM simulation have been validated over the years and are reliable, it remains a simulation model. Therefore, we will develop a mathematical queueing model to theoretically calculate the expected sojourn time under an uncontrolled scenario. This motivates the proposal of our next research question.

3. **Under human-driven conditions (uncontrolled scenario), what is the theoretical expected sojourn time for vehicles from entering the control zone to merging into the roundabout on each leg?**

   This question examines the theoretical sojourn time for a vehicle under human driving conditions in a single-lane roundabout. The aim is to provide a baseline for comparison, allowing the expected performance of CAVs under the control model to be evaluated against human-driven scenarios.

   To answer this research question, an $M/G/1/k$ queueing model (Markovian arrival process, general service time distribution, single server with system capacity k) will be developed. The key parameter for calculating the expected sojourn time in this model is the distribution of the headway time, which refers to the time interval between consecutive vehicles in the circulating stream. In principle, headway time data should be obtained from real-world measurements. However, due to data availability constraints, we will use data from the VISSIM simulation, which mimics human-driven conditions. The car-following model (Wiedemann 74 model [17]), priority rules, gap acceptance, yielding behavior, conflict points, merging behavior, and driver behavior parameters are used by default in VISSIM. More specifically, in the Wiedemann 74 model, factors such as

vehicle headway times and reaction times help determine how vehicles adjust their speed and maintain safe distances while circulating in the roundabout. Regarding priority rules, vehicles entering the roundabout must yield to those already circulating, and VISSIM ensures that vehicles follow these real-world traffic rules. Moreover, gap acceptance is a crucial aspect of roundabout simulations. Vehicles entering the roundabout must accept a sufficient gap in the circulating traffic before entering. VISSIM uses parameters such as the critical gap to simulate how vehicles adjust to available gaps in traffic. Additionally, VISSIM models conflict points (where vehicle paths cross) and merging behavior (where vehicles from entry lanes merge into circulating lanes), allowing the simulation to account for delays and congestion at these points within the roundabout. Furthermore, parameters such as safety distance and follow-on time are also considered in the VISSIM simulation. Therefore, using the headway time data obtained from the VISSIM simulation to derive the theoretical expected sojourn time under human-driven conditions is considered reliable. The input and output for solving this research question are presented in Fig.1.3.

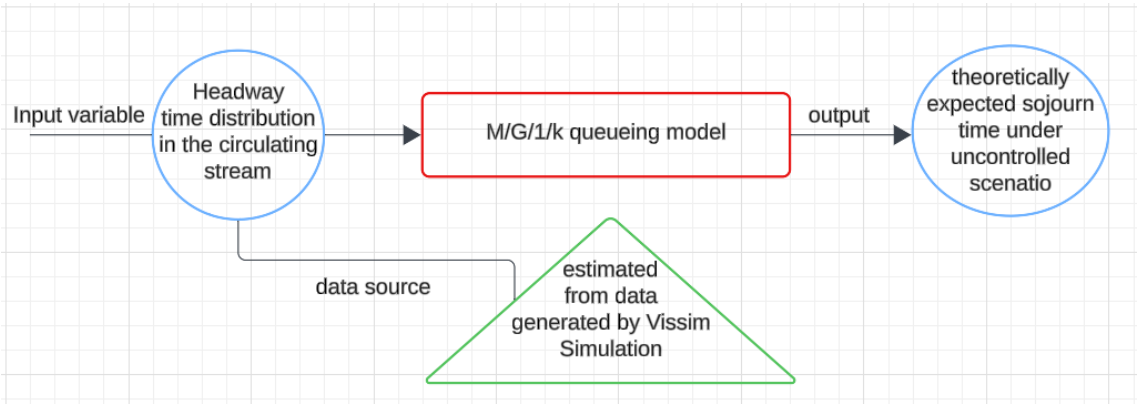

Figure 1.3: Explanation of Research Question 3.

These research questions will guide the development of the microscopic control model, the queueing analysis, and the performance evaluations that are central to this study.

1.4. Scope of Research

This research focuses on optimizing the efficiency of single-lane roundabouts through the integration of CAVs. The scope of this study is defined by the following key aspects:

1. **Modeling Focus**:

   The primary focus of this study is to evaluate the efficiency of single-lane roundabouts influenced by CAVs. The research builds upon the development of two main models: a microscopic control model and an $M/G/1/k$ queueing model. The microscopic control model seeks to reduce the total sojourn time of all vehicles within the controlled area as well as to enhance the driving experience. In contrast, the $M/G/1/k$ queueing model aims to determine the theoretical expected sojourn time under human-driven scenarios. These models incorporate key variables, including vehicle speed, acceleration, sojourn time, critical gaps, and follow-up times.

2. **Comparison**:

   The research will also compare the performance of CAV-controlled roundabouts with those operating under human-driven conditions. By developing theoretical queueing models for the human-driven scenario and comparing the theoretical sojourn time to those gained by the CAV-controlled model, the study will aim to highlight the efficiency improved through automation and connectivity.

3. **Data Sources and Assumptions**:

   The data used in this research will rely on simulation data, primarily from the VISSIM traffic simulation software, to estimate key parameters such as vehicle headway times in the circulating stream, waiting times in the entry line, and sojourn times from entering the control zone to merging into

the roundabout. This is a possible way because results by Vissim is calibrated and validated well for years. These simulations will serve as a basis for estimating the headway time distribution and expected sojourn time under a human-driven scenario.

4. **Exclusions**:

   This research will not address the broader implications of autonomous vehicles outside of the context of roundabout efficiency. Specifically, the integration of CAVs in other traffic environments, such as intersections or urban streets, will not be part of the scope. Additionally, the study will not focus on the societal, legal, or ethical aspects of CAV implementation, as it is solely concerned with roundabout efficiency optimization.

By focusing on the microscopic control model for single-lane roundabouts, the study seeks to provide insights into the specific benefits that CAVs can bring to this type of traffic control infrastructure, offering a detailed analysis of how CAVs can work together to improve efficiency in roundabout systems.

1.5. Main Results

This study presents a comprehensive investigation into the optimization of single-lane roundabouts for CAVs using a microscopic control model. Additionally, it outlines a systematic procedure for deriving the theoretical expected sojourn time through queueing theory analysis. The main results are summarized as follows:

1. **Efficiency Improvements through Microscopic Control Models:** The efficiency improvement achieved by the microscopic control model is calculated by dividing the absolute difference between the controlled mean sojourn time and the uncontrolled mean sojourn time by the uncontrolled mean sojourn time. Empirical improvements are based on the uncontrolled mean sojourn times generated using VISSIM data, while theoretical improvements are derived from the sojourn times calculated through the $M/G/1/k$ queueing model.
   - The microscopic control model significantly reduces the expected sojourn time for vehicles entering the roundabout. Compared to uncontrolled scenarios derived from VISSIM simulations, the control model improves the empirical efficiency of a single-lane roundabout by 26%, 80%, 91%, and 90% under arrival rates of 200, 400, 600, and $800pcu/h$ per leg, respectively. These findings closely align with theoretical predictions of efficiency improvements of 18%, 78%, 89%, and 90% under the same conditions.
   - This efficiency gain highlights the potential of integrating CAV-specific control zones into modern traffic systems, effectively reducing congestion and enhancing overall throughput.
2. **Performance of CAV-Controlled Scenarios vs. Human-Driven Scenarios:**
   - The M/G/1/k queueing model accurately predicts sojourn times for human-driven scenarios, which serve as a baseline for comparison.
   - Under high traffic volumes, the control model outperforms the human-driven baseline by maintaining steady throughput and avoiding blockages, even at an arrival rate of $800pcu/h$ per leg.
3. **Comfort Optimization:** The control model also successfully minimizes acceleration fluctuations, providing a smoother driving experience for CAV passengers while maintaining efficient traffic flow.
4. **Pressure Test Outcomes:**
   - The control model successfully withstands extreme arrival rates of $1200pcu/h$ per leg, maintaining a zero probability of blocking new vehicles from entering the control zone. This is a significant improvement compared to the theoretical probability of 0.45 under uncontrolled scenarios.
   - This resilience underscores the robustness of the optimization approach, even in high-demand conditions.
5. **Validation through Simulation and Theoretical Analysis:**

- The alignment between simulation results and theoretical predictions confirms the reliability of the proposed $M/G/1/k$ queueing model to calculate the expected sojourn time.
- Both the controlled and uncontrolled scenarios were evaluated using the same input arrival rates, ensuring comparability and accuracy.

These results provide a strong foundation for further research and practical implementation of CAV-controlled roundabouts, emphasizing their role in advancing smart traffic management systems.

1.6. Significance of the Research

The significance of this research lies in its potential to provide a deeper understanding of how CAVs can enhance the efficiency of single-lane roundabouts, a critical component of modern transportation infrastructure. As urbanization increases and traffic congestion becomes more prevalent, roundabouts offer a promising solution for improving traffic flow. However, their efficiency can be greatly affected by factors such as vehicle behavior, human-driven decision-making, and traffic dynamics.

By focusing on the optimization of roundabout operations through the control of CAVs, this research addresses several key issues:

1. **Improving Traffic Flow and Reducing Congestion**:

   The study seeks to develop methods for optimizing traffic flow within single-lane roundabouts. By minimizing sojourn times, this research can potentially alleviate congestion, especially during peak traffic hours. Efficient roundabout operations could contribute to reducing overall sojourn times, improving mobility, and enhancing the experience for all road users.

2. **Advancing the Integration of CAVs in Traffic Systems**:

   With the rise of autonomous vehicles, this research offers valuable insights into how CAVs can be integrated into existing traffic control systems. The models developed in this study could serve as a foundation for further research on the broader application of CAVs in various traffic scenarios, including intersections, highways, and turbo-roundabouts. Understanding the behavior of CAVs within a controlled environment in a single-lane roundabout can inform the design and implementation of future autonomous systems.

3. **Contributing to Smart Traffic Management Systems**:

   The findings of this research could contribute to the development of smart traffic management systems that leverage CAVs for real-time traffic control and optimization. By incorporating automated decision-making, such systems can dynamically adjust to changing traffic conditions, potentially improving efficiency, safety, and sustainability. This research could lay the groundwork for the deployment of such systems in roundabouts, which could then be expanded to other traffic management scenarios.

4. **Providing Policy and Design Recommendations**:

   The outcomes of this research can inform policymakers, traffic engineers, and urban planners about the benefits and challenges of deploying CAVs in roundabout systems. By demonstrating the potential for enhanced traffic flow, this study may encourage further investment in connected and automated vehicle technologies. Additionally, the findings could guide the design of more efficient roundabouts, particularly in areas with high traffic volume, to accommodate the future needs of transportation systems.

In summary, this research not only aims to improve roundabout efficiency but also contributes to the larger conversation about the future of transportation, the role of automation, and how intelligent systems can be employed to address the challenges of modern traffic management.

1.7. Structure of the Thesis

This thesis is organized into seven chapters, with each chapter addressing a distinct aspect of the research on single-lane roundabouts for CAVs.

1. **Introduction**: This is the introductory chapter, which provides the background, context, and motivation for the study, introducing the significance of roundabouts, especially single-lane roundabouts, and the potential benefits of CAVs. It defines the problem statement, formulates the research questions, outlines the research scope, and summarizes the main results and significance of the study.
2. **Literature Study**: This chapter reviews existing models and research related to traffic flow in roundabouts, including queueing models, driving behaviors, and parameter estimations of headway time. It identifies knowledge gaps and establishes the foundation for the models and methodologies developed in this thesis.
3. **Methodology**: This chapter describes the method constructed in the study. It explains the steps taken to construct and validate the microscopic control model and the queueing model, as well as the procedures for comparing controlled and uncontrolled scenarios.
4. **Model Construction**: Being the core chapter of our research, this chapter first explains the development of the microscopic control model for CAVs, which aims to minimize the sojourn time and maximize the driving experience, followed by developing a theoretical $M/G/1/k$ queueing model for calculating the expected sojourn time under human-driven conditions. To the end, it will introduce the values of parameters used in these two models. It includes assumptions, optimization modelling, parameter definitions, and some necessary mathematical derivation and proofs.
5. **Headway Time Data Analysis**: This chapter analyzes headway time distributions and parameter estimations using simulation data. It evaluates the statistical fit of various models to ensure reliable input for the queueing analysis.
6. **Model Evaluation**: The evaluation chapter compares the efficiency and robustness of the control model against uncontrolled scenarios using both theoretical and simulation data. It also includes stress tests to assess the performance of the control model under high traffic volumes.
7. **Discussions**: This final chapter synthesizes the achievements, acknowledges the limitations, and proposes directions for future research. It connects the findings to broader implications for traffic management and CAV integration.

Each chapter builds upon the previous one, creating a cohesive narrative that leads to the final conclusions and recommendations for the application of CAVs in single-lane roundabout systems.

2

Literature Study

2.1. Queueing Models Related to Roundabout

Flannery et al. [13] introduced a significant advancement in analyzing single-lane roundabouts in the United States by utilizing queueing models based on renewal theory. In contrast to earlier methods, such as those used in the US Highway Capacity Manual (HCM 2000), which relied on gap acceptance models developed in Australia and limited US-specific field data, this approach addressed critical limitations related to accuracy and applicability, especially given the unique driving behaviors observed in the US. The study developed an innovative analytical model capable of calculating both the mean and variance of service times for vehicles within the circulating stream, independent of the time headway distribution. These service time metrics were then incorporated into an $M/G/1$ queueing framework to estimate key metrics such as average delay and queue length under stable traffic conditions.

While our approach for modeling expected sojourn times under human-driven conditions utilizes the $M/G/1/k$ queueing system, the method for deriving the mean and variance of service times is adapted from Flannery's $M/G/1$ queueing model, as detailed in Sec.4.2.1. Additionally, Flannery's study validated its model through field data collected from six single-lane roundabout sites across the US, showcasing strong performance in light to moderate traffic conditions. This research not only provides a robust analytical tool for evaluating roundabout performance but also serves as a foundation for future studies focusing on multi-lane roundabouts within the US context.

The study from Flannery et al. presents a comprehensive approach to developing a delay estimation model for single-lane roundabouts in the United States, utilizing queueing theory with a focus on the M/G/1 queue model[12]. A new model, being an advancement over previous methods in [13], is validated through direct comparison with field-measured delays and contrasts with earlier queuing models, particularly focusing on the queuing length, service time, and its variance for vehicles at roundabout approaches. The data, derived from six different single-lane roundabouts across the U.S., enabled the formulation of a model that closely mirrors real-world traffic conditions. Notably, the study reveals that the new model surpasses the Troutbeck model[31][32][2] in accurately predicting system delays, especially under conditions of increasing conflicting flows, with a mean absolute deviation from field data of 1.27 seconds and a maximum of 6.95 seconds in 43 tested scenarios.

The difference between the two models lies in their methodologies. Flannery's model explicitly calculates the first and second moments of service time (hence variance) using renewal theory and integrates these into an M/G/1 queueing framework, accommodating an unknown (or general) headway distribution. In contrast, the Troutbeck model assumes service time equals the inverse of the approach capacity, with either deterministic or exponential distributions, neglecting observed variability. Furthermore, while Flannery et al.'s model incorporates realistic queue dynamics and sensitivity to increasing conflicting flows, the Troutbeck model uses a simpler approach with assumptions that lead to insensitivity to traffic conditions. These methodological advancements make the Flannery et al. model more accurate and adaptable under diverse real-world conditions.

However, the research acknowledges discrepancies due to assumptions of stop-go vehicle movement and instantaneous service in the queuing model, alongside the use of a lognormal distribution for headway representation. These insights not only enhance the accuracy of delay estimation for single-lane roundabouts but also lay the groundwork for ongoing improvements in traffic modeling and intersection design.

2.2. Comfortable Driving Acceleration/Deceleration

K. Nandi, Chakraborty, and Vaz studied the optimization of driving strategies for electric vehicles (EVs), focusing on the efficient use of stored battery energy and enhancing driving comfort[25]. Their research employs Multi-Objective Optimization (MOO) to address the conflicting goals of minimizing energy consumption and acceleration duration while optimizing comfort, primarily measured by jerk. A key finding of their study is that comfortable acceleration varies across different speed zones. Specifically, for velocities in the range of $0-35km/h$ and $0-55km/h$, the comfortable accelerations are determined to be $1.03m/s^2$ and $1.02m/s^2$ respectively. The study introduces two multi-objective optimization problems (MOOPs): one considering jerk as a constraint and the other focusing on minimizing jerk. The latter approach was found more effective for establishing a Comfortable Optimal Driving Strategy (CODS). This led to the identification of a Comfortable Optimal Driving Zone (CODZ), a novel concept in EV driving dynamics. Their work marks a significant contribution to EV technology, highlighting the importance of integrating multiple objectives, such as efficiency and comfort, to improve the overall driving experience.

In the field of autonomous vehicle development, significant strides have been made towards enhancing passenger comfort, a crucial aspect of the success and acceptance of self-driving shuttle services. Prior research has extensively focused on the mechanical and technological aspects of autonomous vehicles, highlighting the importance of controlling vehicle dynamics, such as acceleration and jerk, to ensure passenger comfort. A study has been established by Bae, Moon, and Seo that the comfort threshold for acceleration lies between 0.9 to $1.47m/s^2$[3]. This benchmark is instrumental in designing vehicle control strategies that prioritize smooth and comfortable transit experiences. Investigations have also delved into human factors, emphasizing the need to align technological advancements with human-machine interface (HMI) considerations to cater to varied personal preferences and perceptions of comfort. Furthermore, research has underscored the significance of adopting optimal velocity planning methods that balance time efficiency, stability, and comfort, particularly in the context of public transit vehicles like shuttle buses that operate on predefined routes. The comparative analysis of these control strategies against conventional methods in real-time, software-in-the-loop (SIL) environments has provided valuable insights into their efficacy in enhancing passenger comfort while maintaining safety standards. This holistic approach to studying both the technical and human aspects of autonomous vehicle operation is pivotal in advancing the field towards more passenger-centric and comfortable self-driving experiences.

Moon and Yi[24] conducted a research that significantly contributes to the understanding of vehicle adaptive cruise control systems, particularly in terms of aligning these systems with human driving behaviors for enhanced comfort and safety. Central to their findings is the identification of the braking deceleration comfort zone, which is determined to be within $-2m/s^2$ based on extensive human manual driving tests. This insight is crucial for developing adaptive cruise control algorithms that not only align with human perceptions of comfort but also ensure safety in various driving conditions. Furthermore, their research establishes the limits of acceleration and deceleration for such systems, with maximum acceleration capped at $3.07m/s^2$ and maximum deceleration at $-5.08m/s^2$. These parameters are critical in ensuring that the adaptive cruise control systems can respond effectively in different traffic scenarios while maintaining a driving experience that feels natural and safe to human drivers. Moon and Yi's work thus lays a foundational basis for future advancements in vehicle automation, particularly in enhancing driver acceptance and trust in such systems.

When driving around a roundabout or any curve, the lateral acceleration of the vehicle generates a centripetal force that allows the vehicle to follow the curved path instead of moving in a straight line. In physics, this centripetal force produced by the vehicle's lateral acceleration is necessary to change the vehicle's direction of motion, allowing it to move along a curved path. Thus, centripetal acceleration is also referred to as lateral acceleration. The magnitude and direction of this force determine the

vehicle's stability and comfort on curves.

In the study of acceleration analysis, Nidzamuddin Md. Yusof et al[38]. analyzed the preferred lateral accelerations for different automated driving styles, categorized as assertive and defensive. They discovered that lateral acceleration ranged from $0.42g$ to $0.54g$ for assertive driving and from $0.14g$ to $0.33g$ for defensive driving, where g represents gravitational acceleration. The findings highlighted that drivers tend to be more comfortable with the defensive driving style in automated vehicles. To analyse the lateral acceleration more precisely, Jin Xu et al.[34] conducted an experimental study in Sichuan Province, China. They established comfort thresholds as follows: drivers feel comfortable if $0\,m/s^2 < a_y$(lateral acceleration$) < 1.8\,m/s^2$; experience relative comfort between $1.8\,m/s^2 < a_y < 3.6\,m/s^2$; feel discomfort when $3.6\,m/s^2 < a_y < 5.0\,m/s^2$; and find it unbearable when $a_y > 5\,m/s^2$.

2.3. Driving Behaviour and Related Parameters in Single-lane Roudabouts

When a driver wants to perform actions like turning, merging, following, or crossing, he or she has to estimate the time or space interval to make sure the gap is large enough to make decisions safely. The Gap Acceptance Theory[18], introduced by Hein Botma, can reasonably explain the logic behind drivers' behavior. For a single-lane roundabout, the theory describes how drivers decide whether to merge into the circulating stream based on the time distance (or time gap) between consecutive vehicles already in the roundabout. The key parameters that influence people's driving behavior in a single-lane roundabout are critical gap t_C and follow-on time t_F[14].

The critical gap t_C represents the threshold of the time interval between two consecutive vehicles in the circulating stream that an entering driver perceives as sufficient to enter safely. For drivers travelling in a single-lane roundabout, it is the value used by them at the entry line to decide whether to proceed into the circulating flow. If the available time gap in the circulating stream is not less than t_C, drivers will accept the gap and merge into the roundabout. Otherwise, they will wait.

The follow-on time t_F refers to the time interval between successive vehicles entering a traffic stream (such as a single-lane roundabout) when the entering vehicles are following each other closely. In other words, it is the smallest time required for a vehicle to follow the one in front of it into the circulating traffic stream once the former has cleared.

The graphical representations of t_C and t_F are shown in Fig.2.1. It should be noted that t_C represents the time required by the first vehicle on the leg of the roundabout to make a decision to safely enter the circulating stream. However, t_F denotes the time needed for subsequent vehicles to follow the first vehicle into the circulating traffic.

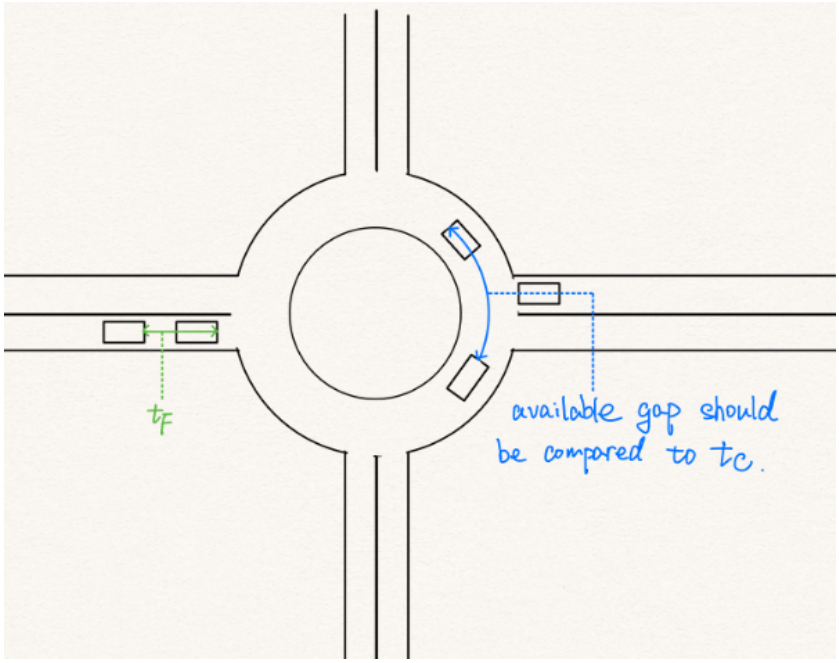

Figure 2.1: Concept of follow-on time and critical gap.

2.4. Microscopic Optimization Models in Single-lane Roundabouts for CAVs

There are only limited references that explore the microscopic control for connected and automated vehicles (CAVs) in single-lane roundabouts. However, the work by Ali Danesh et al.[9] provides valuable insights and serves as a significant reference in this area. The study focuses on optimizing roundabout control in environments fully populated by CAVs. The authors propose a two-phase optimization mechanism. In the first phase, the delay time of the arrival to the entry line is minimized by a mixed-integer linear programming. The second stage uses these optimal times to further optimize individual vehicle trajectories through non-linear programming, focusing on minimizing acceleration fluctuations for fuel efficiency and comfort. The model ensures vehicles traverse the roundabout without stopping and provides consistent throughput and reduced delay under various traffic scenarios. Sensitivity analyses reveal the influence of control zone length and roundabout size on system performance, emphasizing the model's adaptability to real-world geometric and demand variations.This paper inspires the implementation of two-phase optimization, enabling both the computation of optimal sojourn times and precise trajectory planning for individual vehicles.

However, the paper has several limitations and observations worth noting. Firstly, the first-phase optimization does not account for the critical gap, a key factor influencing vehicle merging behavior at roundabouts. Secondly, in its analysis of conflict points—locations where vehicle trajectories intersect, posing collision risks—the model considers only scenarios where vehicles on the same approach reach the conflict point first, neglecting the reverse situation. Additionally, the global optimization performed each time a vehicle enters the control zone recalculates trajectories for all vehicles in the zone, significantly increasing computational complexity and posing challenges for real-time implementation. Finally, while the paper provides a detailed flowchart, the absence of open-source code limits reproducibility and practical application, as implementing the algorithm based solely on the flowchart requires considerable effort and interpretation.

Based on our study of this paper, we adopted its optimization model as a foundation for solving our **Research Question 1** (See Sec.4.1 for the detailed reformulation) and reformulated its mathematical optimization framework. Notably, in implementing the code, we employed a local optimization approach. Specifically, whenever a new vehicle arrives at the control zone, we optimize its sojourn time and trajectory based on the information of vehicles that already exists inside the control zone, and the

optimized data is stored as attributes of the vehicle in Python language. Importantly, when subsequent vehicles enter the control zone, we do not re-optimize the vehicles that have already been optimized (See Appendix A). This method significantly reduces computational overhead compared to the original reference[9].

2.5. Headway Time Distribution and Parameter Estimations

Headway time, often referred to simply as"headway," is a critical concept in civil engineering and traffic engineering. In the context of a circulating stream, such as vehicles in a roundabout or traffic moving inside a circular route, headway time is defined as the time interval between the passage of the front of one vehicle and the front of the next vehicle, as observed from a fixed point.

Headway time distribution is a crucial element in the field of traffic flow. It serves as the foundation for capacity analysis, gap acceptance studies, intersection traffic control, and traffic simulation. Particularly for traffic flow, the headway time distribution and its computer simulation implementation are crucial for the simulation capabilities of traffic systems. Based on different traffic characteristics, researchers have proposed and verified many highly practical models, such as the exponential headway time distribution model for free flow conditions and the shifted exponential model. With the increase in road traffic load, to describe the corresponding patterns, models such as the Erlang distribution, lognormal distribution, and Cowan M3 distribution have been proposed[20].

2.5.1. Exponential Headway

The exponential headway time has a distribution function:

$$F(t) = 1 - e^{-\lambda t}, t > 0. \tag{2.1}$$

and density:

$$f(t) = \lambda e^{-\lambda t}, t > 0. \tag{2.2}$$

This distribution is widely used. However, it is often suitable for situations with low traffic volumes[28]: for two-way two-lane roads with traffic volumes not exceeding 400 vehicles per hour; for one-way two-lane roads with traffic volumes not exceeding 800 vehicles per hour, and in situations where there are no traffic management facilities within 1 kilometer of the observation point in the oncoming direction.

When modeling the headway time distribution for single-lane traffic flow using the exponential distribution, it inaccurately predicts a higher probability of smaller headway times than what is observed in reality. To address this issue, the shifted exponential distribution is employed. This distribution assumes that the minimum headway time cannot be less than a specified value t_M (minimum headway time). The distribution function for shifted exponential is:

$$F(t) = 1 - e^{-\lambda(t-t_M)}, \ t > t_M, \tag{2.3}$$

and the density function is:

$$f(t) = \lambda e^{-\lambda(t-t_M)}, \ t > t_M. \tag{2.4}$$

Zhang et al.[39] utilized the Kolmogorov-Smirnov (KS) test statistic along with 2-D plots to evaluate and reflect the extent of fitness of their models to the roadway data. While each model demonstrated some level of practicality, the test results indicated that the shifted exponential distribution model best fits the traffic flow data on urban highways.

The maximal likelihood estimators (MLE) for λ and t_M are quite simple to derive, so we omit the derivation. Based on identically independent observations t_1,t_2,...,t_n, the estimators are:

$$\hat{t}_M = t_{(1)} = \min\{t_1, t_2, ..., t_n\} \tag{2.5}$$

$$\hat{\lambda} = \frac{n}{\sum_{i=1}^{n}(t_i - t_{(1)})} \tag{2.6}$$

2.5.2. M3 Headway

Research has shown that in more congested traffic conditions, some vehicles tend to form platoon formations. To address this phenomenon, Cowan introduced the M3 distribution model[37]. This model posits that vehicles exist in two states: a segment of the vehicles travels in platoon formations, while the remainder moves under free-flow conditions. The distribution function for this model is as follows:

$$F(t) = \left(1 - \alpha e^{-\lambda(t-t_M)}\right) u(t - t_M), \tag{2.7}$$

where

$$u(t - t_M) = \begin{cases} 1 & \text{if } t \geq t_M \\ 0 & \text{if } t < t_M \end{cases}, \tag{2.8}$$

and:

- $\alpha \in (0, 1]$ is the proportion of free vehicles((non-clustered traffic).
- $t_M \in \mathbb{R}$ is the minimum headway time maintained between vehicles when they are traveling in platoon formations.
- $\lambda > 0$ is a parameter.

The density of the M3 distribution is:

$$f(t) = (1 - \alpha)\delta(t - t_M) + \alpha\lambda e^{-\lambda(t-t_M)} u(t - t_M), \tag{2.9}$$

where $\delta(t - t_M)$ is the Dirac delta function:

$$\delta(t - t_M) = \begin{cases} \infty & \text{if } t = t_M \\ 0 & \text{otherwise} \end{cases}, \tag{2.10}$$

with

$$\int_0^\infty \delta(t - t_M)dt = 1. \tag{2.11}$$

The proposal of the M3 distribution model has drew the attention of many researchers and has been cited in numerous important articles. The model contains many parameters, making estimation relatively difficult. Researchers have conducted extensive studies on this. Luttinen provided the maximum likelihood estimators (MLE) for the parameters t_M, λ, and α without derivation[21]. Here we complete the steps of how to find the MLE for it. Since the density in Equation (2.9) approaches infinity when $t = t_M$, it poses a challenge for finding the MLE. Therefore, we redefine the density in the context of Measure Theory to address this issue. Let

- $l :=$Lebesgue measure on $\mathbb{R}$, corresponding to the continuous part of the distribution.
- $\nu_0 :=$point mass measure, which means there is a discrete component at $t = t_M$
- $\mu := l + \nu_0$ is the combined measure, which includes both the continuous and discrete parts.

Then the density function of M3 distribution is:

$$f(t) = \frac{dF}{d\mu}(t) = \lambda\alpha e^{-\lambda(t-t_M)} \mathbb{1}_{(t_M,\infty)}(t) + (1 - \alpha)\mathbb{1}_{\{t_M\}}(t). \tag{2.12}$$

One can verify that:

$$\begin{aligned} \int_{t_M}^\infty f(t)d\mu(t) &= \int_{t_M}^\infty f(t)d(l + \nu_0)(t) \\ &= \int_{t_M}^\infty f(t)dl(t) + \int_{t_M}^\infty f(t)d\nu_0(t) \\ &= \int_{t_M}^\infty \lambda\alpha e^{-\lambda(t-t_M)}dt + f(t_M) \\ &= \alpha \int_0^\infty \lambda e^{-\lambda u}du + (1 - \alpha) \\ &= \alpha \cdot 1 + (1 - \alpha) \\ &= 1 \end{aligned} \tag{2.13}$$

In the third equality, we use the fact that the point mass at $t = t_M$ contributes only at that single point. The fourth equality is obtained by changing the variable $u = t - t_M$. The fifth equality holds because the total probability of an exponential distribution is 1.

Based on identically independently distributed observations of headway times $t_i's$, where $i = 1, 2, ..., n$, the likelihood function is:

$$\begin{aligned}\mathcal{L}(\alpha, t_M, \lambda \mid t_1, t_2, ..., t_n) &= \prod_{i=1}^{n} \Big((1-\alpha)\mathbb{1}_{\{t_i = t_M\}}(t_i) + \alpha\lambda e^{\lambda(t-t_M)}\mathbb{1}_{\{t_i > t_M\}}(t_i) \Big) \\ &= \begin{cases} 0 & \text{if } \exists i \text{ such that } t_i < t_M \\ \prod_{i:t_i=t_M}(1-\alpha)\prod_{i:t_i>t_M}\Big(\alpha\lambda e^{-\lambda(t_i-t_M)}\Big) > 0 & \text{if } t_i \geq t_M \ \forall i = 1, 2, ..., n \end{cases}\end{aligned} \tag{2.14}$$

Hence the MLE for t_M is:

$$\hat{t}_M = t_{(1)} = \min\{t_1, t_2, ..., t_n\} \tag{2.15}$$

The log-likelihood function is:

$$\begin{aligned}\ell(\alpha, t_M, \lambda \mid t_1, t_2, ...t_n) &= \log\Big(\prod_{i=1}^{n}\big(f(t_i)\big)\Big) \\ &= \sum_{i:t_i=t_M}\log(1-\alpha) + \sum_{i:t_i>t_M}\Big(\log\big(\alpha\lambda e^{-\lambda(t_i-t_M)}\big)\Big) \\ &= \sum_{i:t_i=t_M}\log(1-\alpha) + \sum_{i:t_i>t_M}\Big(\log(\alpha)+\log(\lambda)-\lambda(t_i-t_M)\Big)\end{aligned} \tag{2.16}$$

Then the partial derivative of $\ell(\cdot)$ with respect to λ is:

$$\begin{aligned}\frac{\partial\ell(\alpha, t_M, \lambda \mid t_1, t_2, ...t_n)}{\partial\lambda} &= \frac{\partial}{\partial\lambda}\sum_{i:t_i>t_M}\Big(\log(\lambda)-\lambda(t_i-t_M)\Big) \\ &= N_{t_i>t_M}(\frac{1}{\lambda}+t_M) - \sum_{i:t_i>t_M} t_i,\end{aligned} \tag{2.17}$$

where

$$N_{t_i>t_M} := \text{the number of observations having values bigger than } t_M. \tag{2.18}$$

Setting the above partial derivative to be zero, one could obtain:

$$N_{t_i>t_M}(\frac{1}{\lambda}+t_M) = \sum_{i:t_i>t_M} t_i \tag{2.19}$$

Hence

$$N_{t_i>t_M}\frac{1}{\lambda} = \sum_{i:t_i>t_M}\Big(t_i - t_M\Big), \tag{2.20}$$

which implies

$$\hat{\lambda} = \frac{N_{t_i>\hat{t}_M}}{\sum_{i:t_i>\hat{t}_M}\Big(t_i-\hat{t}_M\Big)} = \frac{1}{\bar{t}_g - \hat{t}_M} = \frac{1}{\bar{t}_g - t_{(1)}}, \tag{2.21}$$

where

$$\bar{t}_g = \frac{1}{N_{t_i>\hat{t}_M}}\sum_{i:t_i>\hat{t}_M} t_i \tag{2.22}$$

is the average of observations having values greater than $\hat{t}_M$. One can check that the second-order partial derivative of $\ell(\cdot)$ is $-N_{t_i>t_M}\frac{1}{\lambda^2}$, which is smaller than zero for all values of λ. This ensures that $\ell(\cdot)$ is maximized at $\lambda = \hat{\lambda}$, i.e. $\hat{\lambda}$ in Eq.(2.21) is the MLE for λ.

The partial derivative of $\ell(\cdot)$ with respect to α is:

$$\begin{aligned}\frac{\partial \ell(\alpha, t_M, \lambda \mid t_1, t_2, ...t_n)}{\partial \alpha} &= \frac{\partial}{\partial \alpha}\Big(\sum_{i:t_i=t_M}\log(1-\alpha) + \sum_{t_i>t_M}\log(\alpha)\Big) \\ &= -\sum_{i:t_i=t_M}\frac{1}{1-\alpha} + \sum_{i:t_i>t_M}\frac{1}{\alpha}\end{aligned}. \tag{2.23}$$

Let the above partial derivative be zero, we can obtain:

$$N_{t_i>t_M}\frac{1}{\alpha} = N_{t_i=t_M}\frac{1}{1-\alpha}, \tag{2.24}$$

which implies

$$N_{t_i>t_M} = \big(N_{t_i=t_M} + N_{t_i>t_M}\big)\alpha. \tag{2.25}$$

Hence the MLE of α is:

$$\hat{\alpha} = \frac{N_{t_i>\hat{t}_M}}{N_{t_i\geq\hat{t}_M}} = \frac{N_{t_i>\hat{t}_M}}{n} = \frac{N_{t_i>t_{(1)}}}{n}. \tag{2.26}$$

It can be easily verified that the second-order partial derivative of $l(\cdot)$ with respect to α is:

$$-N_{t_i=t_M}\frac{1}{(1-\alpha)^2} - N_{t_i>t_M}\frac{1}{\alpha^2} < 0. \tag{2.27}$$

Hence indeed $\hat{\alpha}$ in Eq.(2.26) is the global maximum and is the MLE of α.

Additionally, researchers have analyzed the relationship between traffic flow rate $q\ pcu/s$ and the parameter α. The 2000 edition of the Highway Capacity Manual from the United States[6] provides the relationship as follows:

$$\alpha = e^{-\beta t_M q}, \tag{2.28}$$

where β is a parameter and for its values, please see Tab2.1.

	$t_M\ (s)$	β
Single Lane	1.5	0.6
Two Lanes	0.5	0.5
Three Lanes or More	0.5	0.8

Table 2.1: Values of t_M and β.

2.5.3. $Erlang-k$ Headway

The $Erlang-k(\lambda)$ distribution is another commonly used headway time distribution. It is the sum of independent random variables having a common exponential distribution with mean $\frac{1}{\lambda}$. The distribution function is:

$$F(t) = 1 - \sum_{j=0}^{k-1}\frac{(\lambda t)^j}{j!}e^{-\lambda t},\ t>0. \tag{2.29}$$

and the density is:

$$f(t) = \lambda\frac{(\lambda t)^{k-1}}{(k-1)!}e^{-\lambda t},\ t>0, \tag{2.30}$$

Let $T \sim Erlang - k(\lambda)$, and $X_1, X_2, ..., X_d \overset{\text{i.i.d}}{\sim} Exp(\lambda)$, then the mean and variance of T are:

$$\mathbb{E}(T) = \mathbb{E}\Big(\sum_{i=1}^{k} X_i\Big) = \sum_{i=1}^{k} \mathbb{E}(X_i) = \frac{k}{\lambda}, \tag{2.31}$$

$$\mathbb{V}ar(T) = \mathbb{V}ar\Big(\sum_{i=1}^{k} X_i\Big) \overset{\text{IND}}{=} \sum_{i=1}^{k} \mathbb{V}ar(X_i) = \frac{k}{\lambda^2}. \tag{2.32}$$

The parameter λ is called the scale parameter, and k is called the shape parameter. As k takes on different values, different distribution functions can be obtained. Therefore, the Erlang-k distribution has a wide range of applications. Specifically, when $k = 1$, Eq.(2.29) corresponds to the case where the headway time follows an exponential distribution. Studies have shown that as the value of k increases, it indicates that traffic becomes more congested and the randomness of driver behavior decreases[10].

For vehicles traveling on the same lane, the headway time cannot be less than the minimum headway time. Therefore, it is necessary to modify the model in Eq.(2.29) and introduce the shifted Erlang-k distribution. The distribution function of shifted Erlang-k is:

$$F(t) = 1 - \sum_{j=0}^{k-1} \frac{\lambda^j (t - t_M)^j}{j!} e^{-\lambda(t - t_M)},\ t > t_M, \tag{2.33}$$

and the density function is:

$$f(t) = \lambda \frac{\lambda^{k-1}(t - t_M)^{k-1}}{(k-1)!} e^{-\lambda(t - t_M)},\ t > t_M. \tag{2.34}$$

Based on i.i.d observations $t_1, t_2, ...t_n$, the likelihood function and the log-likelihood function are:

$$\mathcal{L}(t_M, \lambda, k \mid t_1, t_2, ..., t_n) = \prod_{i=1}^{n} \lambda \frac{\lambda^{k-1}(t_i - t_M)^{k-1}}{(k-1)!} e^{-\lambda(t_i - t_M)} \tag{2.35}$$

$$\ell(t_M, \lambda, k \mid t_1, t_2, ..., t_n) = \sum_{i=1}^{n} \Big(k \log(\lambda) + (k-1)\log(t_i - t_M) - \lambda(t_i - t_M) - \log\big((k-1)!\big) \Big) \tag{2.36}$$

One can estimate t_M by using a similar argument in Sec.2.5.2 and get

$$\hat{t}_M = t_{(1)} \tag{2.37}$$

To obtain the MLE of λ, one can let

$$\frac{\partial \ell(t_M, \lambda, k \mid t_1, t_2, ...t_n)}{\partial \lambda} = 0 \tag{2.38}$$

and get:

$$\hat{\lambda}_j = \frac{n\hat{k}_j}{\sum_{i=1}^{n}(t_i - t_{(1)})} \tag{2.39}$$

for each value of k_j. Since k is discrete (k is an positive integer), we cannot take the partial derivative of $\ell(\cdot)$ with respect to k to get the MLE of k. In practice, if $k \in \{1, 2, 3, ...\}$, one can get the MLE of k and λ by finding the pairs (λ_j, k_j) that maximize the log-likelihood function $\ell(\cdot)$:

$$(\hat{\lambda}, \hat{k}) = \underset{\substack{(\lambda_j, k_j) \\ j \in \{1,2,3,...\}}}{\operatorname{argmax}}\ \ell(t_{(1)}, \lambda_j, k_j \mid t_1, t_2, \ldots, t_n) \tag{2.40}$$

In practice, the Method of Moment Estimator (MM) can also be applied. The expectation and variance of a shifted $Erlang - k(\lambda)$ random variable T are:

$$\mathbb{E}(T) = \frac{k}{\lambda} + t_M \tag{2.41}$$

$$\mathbb{V}ar(T) = \frac{k}{\lambda^2} \tag{2.42}$$

Given the sample mean and variance:

$$\bar{t} = \frac{1}{n}\sum_{i=1}^{n} t_i \tag{2.43}$$

$$s^2 = \frac{1}{n-1}\sum_{i=1}^{n}(t_i - \bar{t})^2 \tag{2.44}$$

as well as the estimator of t_M, equating the expectation and variance to the sample mean and variance, one can get:

$$\begin{cases} \bar{t} = \dfrac{k_{MM}}{\lambda_{MM}} + t_{(1)} \\ s^2 = \dfrac{k_{MM}}{\lambda_{MM}^2} \end{cases}, \tag{2.45}$$

where k_{MM} and λ_{MM} are Method of Moment Estimators. Solving the above system for λ_{MM} and k_{MM}, the estimators are:

$$\begin{cases} \lambda_{MM} = \dfrac{\bar{t} - t_{(1)}}{s^2} \\ k_{MM} = \dfrac{\left(\bar{t} - t_{(1)}\right)^2}{s^2} \end{cases} \tag{2.46}$$

The k_{MM} in Eq. (2.46) may not be an integer. To obtain the estimator, one can get the profile estimator $\hat{k}$ by minimizing the sum of the following squared difference:

$$(\hat{\lambda}, \hat{k}) = \underset{\lambda=\lambda_{MM}, k\in\mathbb{Z}^+}{\operatorname{argmin}} \left\{ \left(\frac{k}{\lambda} + t_{(1)} - \bar{t} \right)^2 + \left(\frac{k}{\lambda^2} - s^2 \right)^2 \right\} \tag{2.47}$$

Note that if $k \in \mathbb{R}^+$, then the Erlang distribution becomes the Gamma distribution. The MLE of λ and k can be obtained by solving the system:

$$\begin{cases} \hat{\lambda} = \dfrac{n\hat{k}}{\sum_{i=1}^{n}(t_i - t_{(1)})} \\ \psi(\hat{k}) = log(\hat{\lambda}) + \dfrac{1}{n}\displaystyle\sum_{i=1}^{n} log(t_i - t_{(1)}) \end{cases}, \tag{2.48}$$

where $\psi(\cdot)$ is the digamma function defined as:

$$\psi(k) = \frac{d}{dk}\log\Gamma(k) = \frac{\Gamma'(k)}{\Gamma(k)} \tag{2.49}$$

The second equation in system2.48 does not have a closed-form solution. One can solve it by numerical root-finding techniques like the Newton-Raphson method or other optimization algorithms provided by libraries such as Scipy in Python.

2.5.4. Lognormal Headway

In moderate to high traffic volumes, where the interaction between vehicles becomes significant but not extremely congested, the variability in headway times can be captured well by the lognormal distribution. This distribution can be particularly useful in conditions where traffic is neither in free flow nor in complete stop-and-go congestion, but rather in a mixed state where some variability in headway times is expected[35]. The distribution function is:

$$F(t) = \Phi\Big(\frac{logt - \mu}{\sigma}\Big),\ t > 0, \tag{2.50}$$

where $\Phi(\cdot)$ is the cdf of standard normal distribution. The density function is:

$$f(t) = \frac{1}{t\sigma\sqrt{2\pi}} exp\Big(-\frac{(logt - \mu)^2}{2\sigma^2}\Big),\ t > 0. \tag{2.51}$$

Assume that the observations are independent and identically distributed. Let $t_i' = logt_i$ for $i = 1, 2, ..., n$, then t_i' follows a normal distribution. The MLE are:

$$\hat{\mu} = \frac{1}{n}\sum_{i=1}^{n} t_i', \tag{2.52}$$

$$\hat{\sigma}^2 = \frac{1}{n}\sum_{i=1}^{n}(t_i' - \hat{\mu})^2, \tag{2.53}$$

and the Method of Moment Estimators are:

$$MM(\mu) = \frac{1}{n}\sum_{i=1}^{n} t_i', \tag{2.54}$$

$$MM(\sigma^2) = \frac{1}{n-1}\sum_{i=1}^{n}\Big(t_i' - \sum_{i=1}^{n} t_i'\Big)^2. \tag{2.55}$$

Typically, one can first perform a logarithmic transformation on the observations, and then conduct a distribution assumption test and goodness-of-fit test on the transformed data.

2.6. Model Selection Criterion

When multiple statistical models with varying numbers of parameters are fitted to a dataset, model selection can be performed using the Akaike Information Criterion (AIC) or the Bayesian Information Criterion (BIC).

AIC

The Akaike Information Criterion (AIC), introduced by Hirotugu Akaike [1], is a widely used criterion for model selection. It evaluates the relative quality of models by balancing goodness-of-fit with model complexity. AIC aims to identify the model that best describes the data, striking a balance between maximizing the likelihood and minimizing the number of parameters. The formula for AIC is as follows:

$$\mathsf{AIC} = 2m - 2\log(L_{\mathsf{max}}), \tag{2.56}$$

where m is the number of estimated parameters in the model, and L_{max} is the maximum value of the likelihood function for the model.

AIC considers both the likelihood and the number of parameters to balance model performance with complexity. It encourages the selection of models that fit the data well while avoiding excessive complexity. This approach mitigates the risk of overfitting and helps prevent the model from capturing noise or irrelevant patterns in the dataset.

BIC

The Bayesian Information Criterion (BIC), proposed by Gideon Schwarz [29], is a model selection criterion similar to AIC that assesses both model fit and complexity. Unlike AIC, BIC imposes a stricter penalty for model complexity. The formula for BIC is as follows:

$$\text{BIC} = \log(n)m - 2\log(L_{\text{max}}). \tag{2.57}$$

In the above equation, m and L_{max} retain the same definitions as in AIC, whereas n represents the sample size. The $\log(n)$ term in BIC imposes a stricter penalty for model complexity compared to AIC, as the penalty grows logarithmically with the sample size. Notably, when $n > e^2$, BIC penalizes complex models more significantly than AIC.

AIC or BIC?

The behavior of AIC and BIC with respect to sample size significantly influences their model selection outcomes. AIC's penalty for model complexity remains constant regardless of sample size, which means that as the sample size increases, AIC may still favor more complex models if they provide a better fit to the data. In contrast, BIC's penalty for complexity increases with the sample size, making it more conservative. As a result, BIC tends to prefer simpler models, particularly in large datasets, due to its stronger penalty for model complexity. This difference in behavior means that BIC is more likely to select simpler models compared to AIC, especially when dealing with large amounts of data.

When selecting between AIC and BIC, the choice depends on the objectives of model evaluation and the characteristics of the dataset. AIC is best utilized when the primary focus is on maximizing predictive accuracy and when working with smaller sample sizes. Its relatively mild penalty for model complexity allows for greater flexibility in capturing complex patterns within the data, making it suitable for exploratory analysis and scenarios where a detailed understanding of the data is sought. Conversely, BIC is more appropriate when the goal is to prefer simpler models, particularly in large datasets. BIC imposes a stricter penalty for model complexity, which increases with sample size, thus favoring more parsimonious models as the data volume grows. This makes BIC a more conservative choice in ensuring model generalizability and preventing the risk of overfitting. In summary, AIC is advantageous for models where predictive accuracy is prioritized, especially for data with a small sample size, while BIC is preferable when simplicity and model parsimony are critical, especially with larger datasets.

3

Methodology

In this part, the method of how to conduct this research is explained. As stated in Ch.1, the three research questions in this thesis are:

1. **Given the arrival speed to the control zone, how to control each vehicle inside the control zone to maximize the efficiency of a single-lane roundabout and the driving experience of each driver?**
2. **How to quantify the efficiency improved by controlling all CAVs within the control zone microscopically?**
3. **Under human-driven conditions (uncontrolled scenario), what is the theoretical expected sojourn time for vehicles from entering the control zone to merging into the roundabout on each leg?**

To answer **Research Question 1**, a control model will be constructed in Sec.4.1. The first objective aims to minimize the total sojourn time for all vehicles on all legs from entering the control zone to merging into the roundabout, while the second objective focuses on minimizing the acceleration fluctuation for each individual vehicle. A natural question is how to quantify the efficiency improved, leading to the formulation of **Research Question 2**. A straightforward approach to quantifying the efficiency improved by the control model is to compare the sojourn time from the control model with the theoretical value under human driving conditions, which is the reason for proposing **Research Question 3**.

To address **Research Question 3**, an $M/G/1/k$ queuing model is developed in Sec.4.2 to calculate the expected sojourn time, defined as the time a vehicle takes from entering the control zone to merging into the roundabout. In this model, M represents the Markovian (or memoryless) property of the arrival process; G denotes a general distribution for the service time; 1 indicates a single server in the system; and k specifies the system's capacity, meaning the number of vehicles cannot exceed k. It should be noted that the server can be modeled as the first vehicle at the roundabout's entry line. To simplify this concept, imagine a person standing at the entrance of each leg of the roundabout, directing whether the first vehicle should enter immediately or wait. Calculating the expected sojourn time requires the coefficient of variation of the service time. Since service time data is difficult to obtain in real-world scenarios and can only be estimated from software simulation, the coefficient of variation of the service time can instead be derived from the distribution of headway times. Therefore, a parametric test to determine the headway time distribution will be conducted in Ch.5. To verify the accuracy of the calculated sojourn time, in Sec.6.1, we will compare it to the values obtained from an uncontrolled scenario in the Vissim simulation across different arrival rates (λ_1, λ_2, λ_3, and λ_4 pcu/h).

Research Question 2 is answered from three different perspectives:

- Comparing the sojourn time obtained from the control model to the one from the Vissim simulation: across different arrival rates, we will first plot the histograms of the sojourn time for both the control model and the Vissim simulation and compare them. Secondly, we will compare the descriptive statistics of the sojourn obtained from the control method to the one from the Vissim simulation.

This will be explained in Sec.6.2. It should be noted that to make the above two sojourn times comparable, the input data of the control model is from the Vissim simulation. In other words, for each vehicle, the speed and time of entering the control zone, and the exit are the same for both scenarios.

- Comparing the average sojourn time from control models to theoretical value: in Sec.6.3, the average sojourn time from the control model will be compared to the expected sojourn time from the $M/G/1/k$ queueing model across different arrival rates.
- Pressure Test (See Sec.6.4): In real-world human driving conditions, a control zone does not exist at a separate entity. A leg of a roundabout may connect to other roads or traffic facilities, with many vehicles intending to enter the roundabout. All roads connected to this leg can be seen as potential sources of vehicles entering the roundabout. Therefore, we can model a single-lane roundabout as an $M/G/1$ queueing model, meaning that the arrival process is Markovian, the service time has a general distribution, there is one server, and the system capacity is infinite. In queueing theory terminology, the $/\infty$ after 1 is typically omitted.

  To conduct a stress test, we first use the $M/G/1$ queueing model to calculate the probability that the control zone is full at an arrival rate of $\lambda_{\max}$ pcu/h. Additionally, at this arrival rate, we will determine the probability that the control zone is full under the controlled scenario. It should be noted that the optimization model includes constraints to prevent queues; therefore, the probability in the controlled scenario means under the extreme arrival rate, the probability that the control model will fail. Finally, we will compare these two probabilities. In [26], researchers pointed out that the maximum arrival rate on each leg of a normal single-lane roundabout was between 1000 and $1200pcu/h$. In our research, we will choose $\lambda_{\max}$ to be $1200pcu/h$.

  In the $M/G/1$ queueing model, we will use the Laplace–Stieltjes transform of the service time distribution, $F_B(t)$, to obtain the probability generating function (PGF) of the number of vehicles in the system, denoted by $P_L(z)$. By the Strong Law of Large Numbers, empirical service time data can be utilized. Next, we can then find the desired probability by making use of the $P_L(z)$.

  In the controlled scenario (optimization), we will record the number of vehicles on each leg every 0.1 second. The required probability is then estimated by the fraction of time during which any of the control zone legs exceeds its capacity.

The big pictures of this thesis is presented in Figs.3.1,3.2, and 3.3.

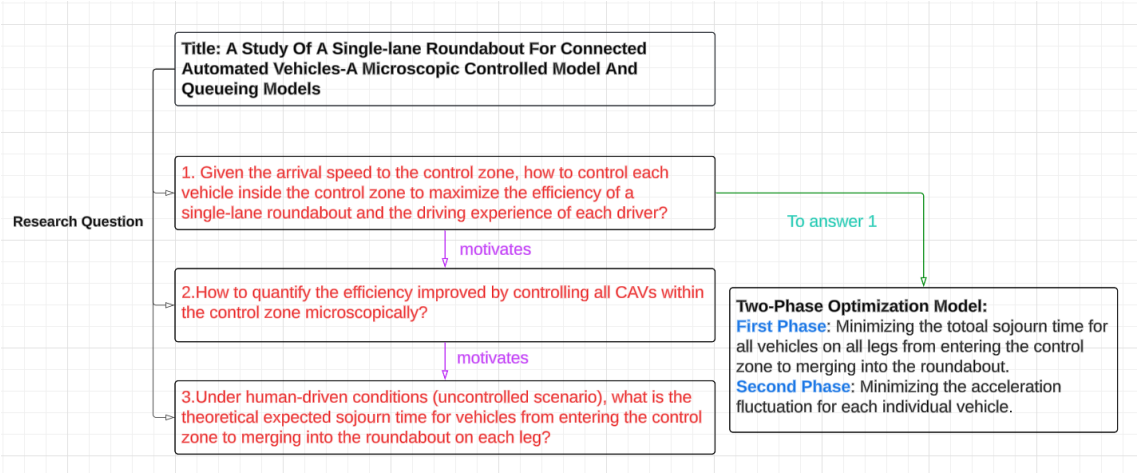

Figure 3.1: Big picture 1: Research Questions and how to answer 1.

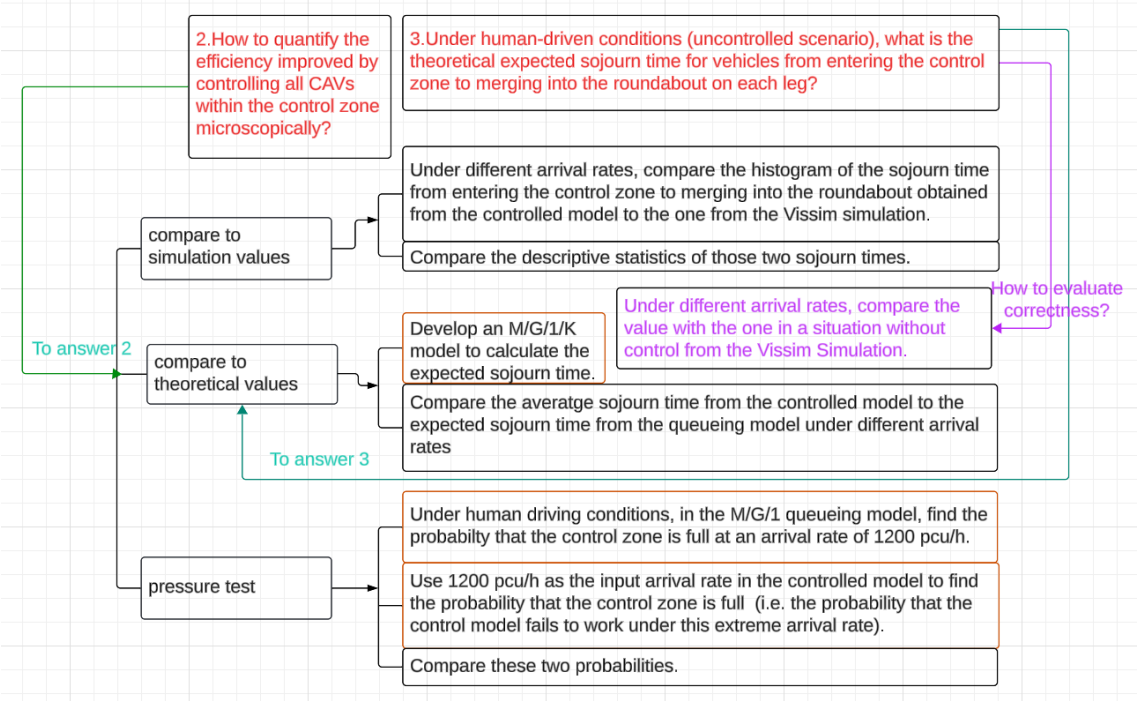

Figure 3.2: Big Picture 2: How to answer Research Questions 2 and 3.

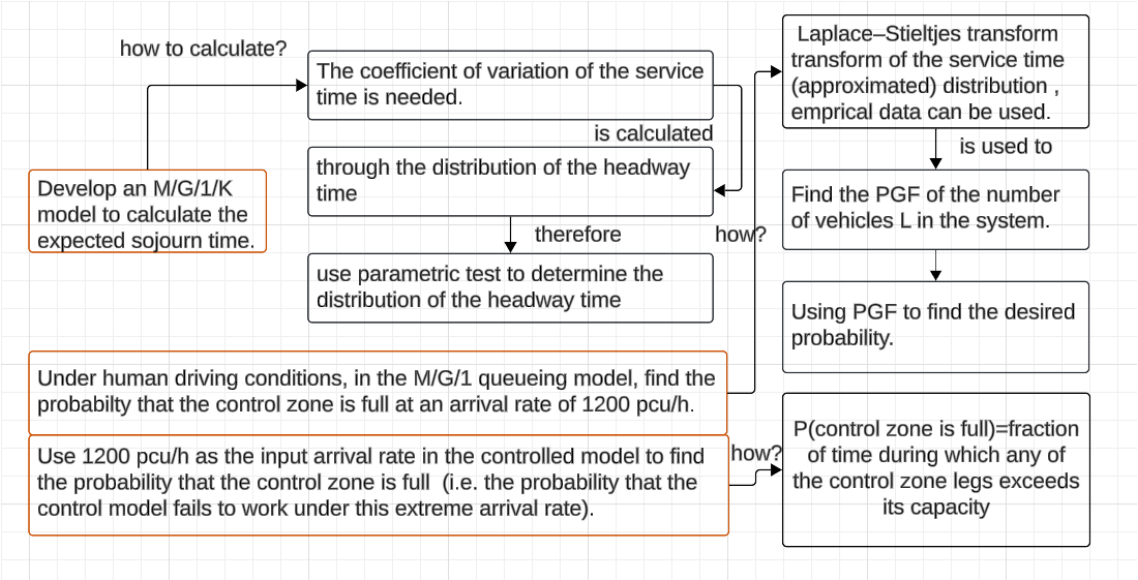

Figure 3.3: Big Picture 3: how to calculate the expected sojourn time and blocking probabilities.

4

Model Construction

4.1. Single-lane Roundabout Microscopic Control Model

In this section, we will construct a microscopic control model for individual vehicles at the microscopic level to enhance the efficiency of a single-lane roundabout. The microscopic level refers to determining the acceleration or cruising speed for each individual vehicle at specific time intervals. In other words, it involves deciding at what time and with what acceleration or speed each vehicle should be directed to travel.

The structure of this section and the interconnections between its subsections are illustrated in Fig.4.1. In Sec.4.1.1, the necessary assumptions for the control model are introduced. Next, the boundary of the arrival time for individual vehicles, which serves as one of the constraints for the optimization, is discussed in Sec.4.1.2 as a background knowledge.

Upon a vehicle's entry into the control zone, an optimization control process is initiated (see Fig.4.2). The control model is divided into two optimization phases. In the first phase, the objective is to determine the optimal sojourn time for each vehicle that enters the control zone at each leg of a single-lane roundabout, using Mixed Integer Optimization techniques. This process is introduced in Sec.4.1.3. It should be noted that the first phase optimization only determines the optimal sojourn time for each vehicle but does not provide a microscopic control method. This is why the second phase of optimization is necessary.

Once the optimal arrival sojourn is determined, it is used in the second phase of the optimization. The goal of the second phase is to ensure a comfortable driving experience by minimizing acceleration fluctuations, thereby providing a smoother journey for drivers. The second phase of optimization not only ensures driving comfort but also determines the specific time intervals at which each vehicle should maintain a particular cruising speed or acceleration, thus achieving the overall objective of this section.

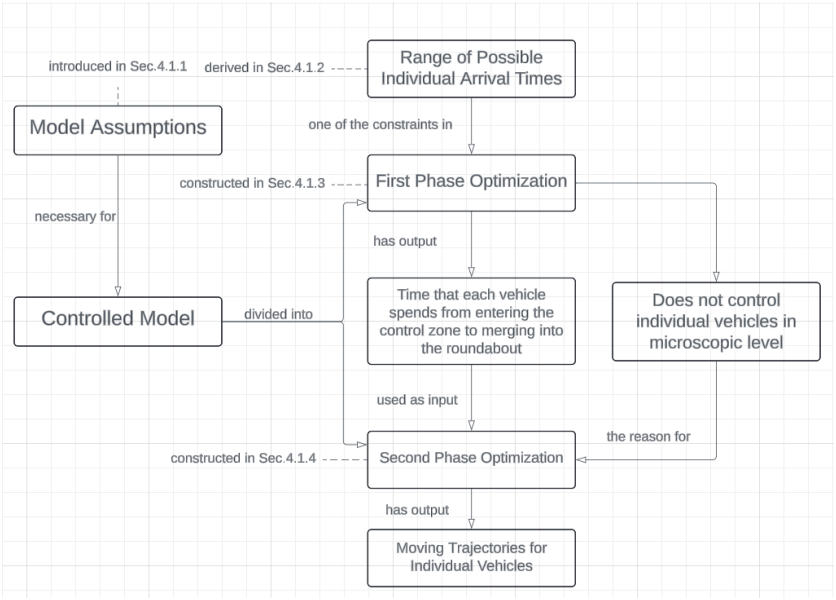

Figure 4.1: Organization of Sec.4.1.

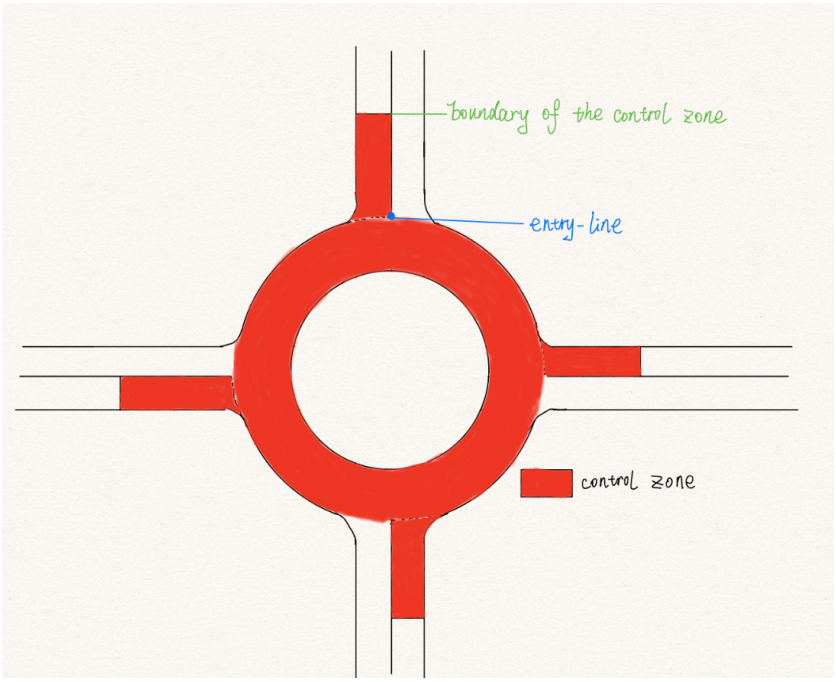

Figure 4.2: Conceptual figure of control zone and entry line of a single-lane roundabout.

4.1.1. Model Assumptions

Our model operates within an Automated Guided Vehicles (AVG) environment for CAVs, where all vehicles are interconnected within the control zone. This means that incoming vehicles entering the control zone can obtain necessary information about the vehicles already present in the zone. This information includes the predicted sojourn time at the entry line and the speed of each vehicle at any given moment. A central controller then issues commands to each vehicle, directing it to accelerate, cruise, or decelerate within a specified time period. These commands are executed by the onboard computer in each vehicle. When vehicles accelerate or decelerate, they follow a uniformly accelerated linear motion. We also assume that all CAVs are seamlessly interconnected, ensuring instantaneous signal and information transmission without any delays.

In each leg of the single-lane roundabout, the maximum speed limit is v_{max}, the maximum acceleration limit is a_{max}, and the minimum acceleration limit is a_{min}, which is negative. To ensure smoother vehicle operation within the roundabout, we assume that vehicles reach the roundabout's internal maximum speed limit v_r before entering. It is also assumed that vehicles maintain this speed v_r while traveling inside the roundabout until they exit. To prevent collisions between consecutive vehicles on each leg, a constant safety distance d_{safe} is maintained. .

Moreover, the distance from the boundary of the control zone to the entry line is assumed to be uniform across all legs of the roundabout, and is denoted by x_0. This assumption simplifies the model by ensuring that each vehicle, regardless of the leg it enters from, has to travel the same distance before reaching the entry line. This uniformity is crucial for maintaining consistency in the timing calculations and ensures that the control strategies applied to each vehicle are comparable.

Besides, for all legs, vehicles arrive at the control zone following a Poisson Process with the same rate λ. Here, λ is a general notation. When simulating with different arrival rates, we use the values λ_1, λ_2, λ_3, and λ_4.

Additionally, all vehicles are assumed to be of the same size, with a length VL. This standardization in vehicle dimensions is important for maintaining a uniform safety distance d_{safe} between vehicles, which helps in preventing collisions and ensuring smooth traffic flow. The assumption of identical vehicle sizes also simplifies the modeling of vehicle dynamics and control algorithms, as it eliminates the need to account for variations in vehicle length that could otherwise complicate the timing and spacing calculations within the control zone.

On top of that, when vehicles enter the control zone, it is assumed that they experience free flow until they reach the roundabout. This means that there may be multiple vehicles traveling within the control zone at the same time, but none of them will come to a stop. Consequently, the number of vehicles within the control zone on each leg will not exceed its capacity C_l, which can be calculated as $\lfloor \frac{x_0}{VL+d_{\text{safe}}} \rfloor$.

Furthermore, we assume that the radius r of the roundabout is measured to the midpoint of the roadway inside the roundabout. Although the paths of vehicles within the roundabout might slightly deviate from a perfect arc, we assume that vehicles follow a path that lies on a perfect circle. This simplification helps in modeling and ensures that the trajectory calculations remain manageable while accurately reflecting the dynamics within the roundabout.

4.1.2. Range of Possible Individual Arrival Times

In this section, we will determine the range of arrival times to the entry line for each individual vehicle by calculating the lower and upper bounds of the arrival time. Let i denote the index of vehicles, j denote the index of the leg of the roundabout, and let $n_j \in \mathbb{N}$ represent the total number of vehicles on leg j, where $i \in \{1, 2, 3, \ldots, n_j\}$ and $j \in \{1, 2, 3, 4\}$. Let $A_{i,j}^{\text{min}}$ and $A_{i,j}^{\text{max}}$ represent the minimum and maximum arrival times of vehicle i from leg j to the entry line. By definition, these boundary times can be expressed in terms of the speed limit on the leg v_{max}, the speed limit inside the roundabout v_r, maximum acceleration limit a_{max}, minimum acceleration limit a_{min}, and the initial speed of vehicle i entering the control zone, denoted as $v_{i,0}$.

Let S_i^j denote the time that vehicle i sojourns traveling from the boundary of the control zone to the entry line of the roundabout on leg j, where $i \in \{1, 2, 3, \ldots, n_j\}$, $j \in \{1, 2, 3, 4\}$, and $n_j \in \mathbb{N}$. According to C. Yu et al. [36], the time that vehicle i arrive to the entry line of the roundabout from leg j, i.e., $t_{i,0} + S_i^j$, is bounded by $A_{i,j}^{\text{min}}$ and $A_{i,j}^{\text{max}}$, where $t_{i,0}$ represents the time at which vehicle i reaches the boundary of the control zone. That is,

$$A_{i,j}^{\text{min}} \leq t_{i,0} + S_i^j \leq A_{i,j}^{\text{max}}. \tag{4.1}$$

It should be noted that in order to determine $A_{i,j}^{\text{min}}$ and $A_{i,j}^{\text{max}}$, it is essential to distinguish between cases based on whether the vehicle can reach the maximum speed v_{max} on the leg during its journey from the boundary of the control zone to the entry line. (See cases (a) and (b) in Fig.4.3, where x_0 is the radius of the control zone).

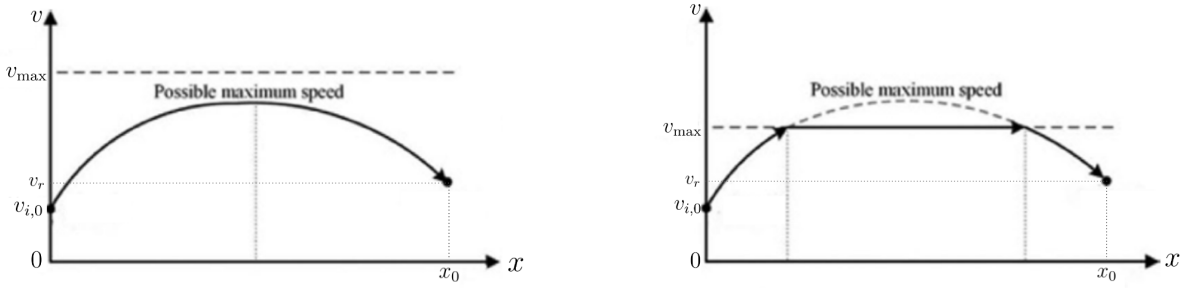

(a) The Vehicle Does Not Reach The Maximal Speed.

(b) The Vehicle Reaches The Maximal Speed.

Figure 4.3: Two cases during vehicle's journey to the entry line, modified based on[9].

Boundary Values in Case (a)

Since Uniformly accelerated linear motion is assumed, case (a) in Fig.4.3 can be represented as

$$\frac{(v_{\max})^2-(v_{i,0})^2}{2a_{\max}}+\frac{(v_{\max})^2-(v_r)^2}{2|a_{\min}|}>x_0. \tag{4.2}$$

In this case,

$$A_{i,j}^{\min}:=\frac{v'_{i,0}-v_{i,0}}{a_{\max}}+\frac{v'_{i,0}-v_r}{|a_{\min}|}, \tag{4.3}$$

where

$$v'_{i,0}=\sqrt{\frac{2a_{\max}|a_{\min}|x_0+|a_{\min}|(v_{i,0})^2+a_{\max}(v_r)^2}{a_{\max}+|a_{min}|}}. \tag{4.4}$$

The upper boundary in this case is:

$$A_{i,j}^{\max}:=\begin{cases}\infty & \text{if } x_0>\frac{(v_r)^2}{2a_{\max}} \text{ and } v_{i,0}<\sqrt{2x_0|a_{\min}|-\frac{(v_r)^2|a_{\min}|}{a_{\max}}}\\ \frac{v_{i,0}-\tilde{v}_{i,0}}{|a_{\min}|}+\frac{v_r-\tilde{v}_{i,0}}{a_{\max}} & \text{otherwise}\end{cases}, \tag{4.5}$$

where

$$\tilde{v}_{i,0}=\sqrt{\frac{a_{\max}(v_{i,0})^2+|a_{\min}|(v_r)^2-2a_{\max}|a_{\min}|}{a_{\max}+|a_{\min}|}}. \tag{4.6}$$

Boundary Values in Case (b)

Case (b) in Fig.4.3 is equivalent to

$$\frac{(v_{\max})^2-(v_{i,0})^2}{2a_{\max}}+\frac{(v_{\max})^2-(v_r)^2}{2|a_{\min}|}\leq x_0. \tag{4.7}$$

In this case, $A_{i,j}^{\min}$ is obtained when the vehicle uses the maximum acceleration $a_{\max}$ to reach the maximum speed $v_{\max}$. It then cruises at this speed for a certain time before decelerating with the minimum acceleration $a_{\min}$ to reach the speed v_r, i.e.

$$A_{i,j}^{\min}=t_a+t_c+t_d, \tag{4.8}$$

where t_a, t_c, and t_d represent the acceleration time, cruising time, and deceleration time respectively. The formulas of them are:

$$\begin{aligned}t_a&=\frac{v_{\max}-v_{i,0}}{a_{\max}}\\ t_c&=\frac{x_0-\frac{(v_{\max})^2-(v_{i,0})^2}{2a_{\max}}-\frac{(v_{\max})^2-(v_r)^2}{2|a_{\min}|}}{v_{\max}}.\\ t_d&=\frac{v_{\max}-v_r}{|a_{\min}|}\end{aligned} \tag{4.9}$$

However, $A_{i,j}^{\max}$ is the same as the one in case (a) (see Eq.(4.5) for detail).

4.1.3. First Phase Optimization

Objective Function

In our model, when vehicles arrive at the entry line of the roundabout, they are assumed to be traveling at the speed v_r. During their journey from entering the control zone to merging into the roundabout, they do not stop. Therefore, increasing the efficiency of the roundabout is equivalent to reducing the total sojourn time from the boundary of the control zone to the entry line of the roundabout. Consequently, the objective function of this optimization is defined as follows:

$$\text{Min} \sum_{j=1}^{4} \sum_{i=0}^{n_j} S_i^j, \tag{4.10}$$

where S_i^j is the time that vehicle i spends traveling from the boundary of the control zone to the entry line of the roundabout on leg j.

Background Information

Before constructing the constraints of this optimization, some concepts and notations are introduced. As shown in Fig.4.4, conflict points in a single-lane roundabout refer to the locations where vehicle paths intersect or merge, potentially leading to collisions or requiring vehicles to yield or stop to avoid accidents. Let set $C_j^{j'} = \{c_1, c_2, c_3, c_4\}$ be the set of conflict points for vehicles from leg j and j', where $j \neq j'$ and $j, j' \in \{1, 2, 3, 4\}$. Let $A_{i,j}^c$ be the time when vehicle i reaches the conflict point c from leg j, where $c \in C_j^{j'}$. Here we will give an example of how to calculate $A_{i,j}^c$. Recall that $t_{i,0}$ is the time at which vehicle i arrives at the boundary of the control zone. If vehicle 3 from leg 1 will exit the roundabout from leg 4, then

$$\begin{aligned} A_{3,4}^{c_1} &= t_{3,0} + S_3^1 \\ A_{3,4}^{c_2} &= t_{3,0} + S_3^1 + \frac{\frac{2\pi r}{4}}{v_r} \\ A_{3,4}^{c_3} &= t_{3,0} + S_3^1 + \frac{\frac{2\pi r}{2}}{v_r} \end{aligned}, \tag{4.11}$$

where r represents the radius of the circulatory lane inside the roundabout. For this particular vehicle, $A_{3,4}^{c_4}$ does not exist, since it leaves the roundabout from leg 4 before reaching the conflict point c_4.

On top of that, defining the following binary variable:

$$BI_{i,i'}^c = \begin{cases} 1 & \text{if vehicle } i \text{ reaches the conflict point } c \text{ prior to } i' \\ 0 & \text{otherwise} \end{cases}. \tag{4.12}$$

In Equation(4.12), vehicle i and i' are from different legs. Besides, denote the critical gap and follow-on time by t_C and t_F respectively.

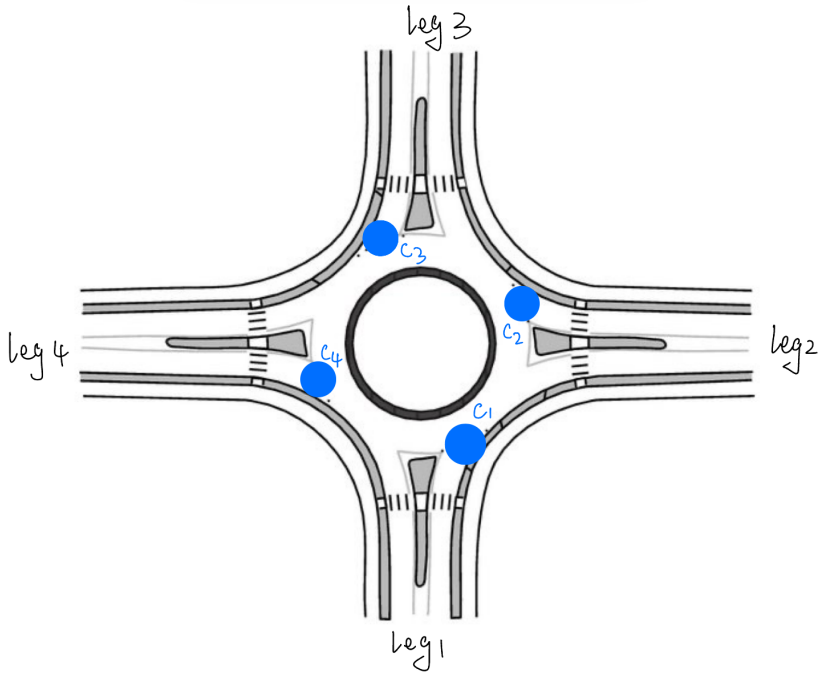

Figure 4.4: Conflict points in a single-lane roundabout, modified based on[9].

Constraints for the First Phase Optimization

Having the above variables defined, we can construct our constraints for the optimization problem (4.10) as follows:

$$A_{i,j}^{min} \leq t_{i,0} + S_i^j \leq A_{i,j}^{max}, \quad \forall i \in \{1, 2, \ldots, n_j\}, \quad j \in \{1, 2, 3, 4.\} \quad \text{(Arrival Time is Bounded)} \tag{4.13}$$

$$t_{i,0} + S_i^j + t_F \leq t_{i+1,0} + S_{i+1}^j, \quad \forall i \in \{1, 2, \ldots, n_j - 1\}, \quad j \in \{1, 2, 3, 4\}. \quad \text{(Follow-on Time is Considered)} \tag{4.14}$$

$$BI_{i,i'}^c + BI_{i',i}^c = 1, \quad \text{(By Definition of Binary Variables)}$$
$$\forall c \in C_j^{j'}, \quad i \in \{1, 2, \ldots, n_j\}, \quad i' \in \{1, 2, \ldots, n_j'\},$$
$$j \neq j', \quad j, j' \in \{1, 2, 3, 4\}. \tag{4.15}$$

$$A_{i,j}^c + t_C \leq A_{i',j'}^c, \quad \text{(Collision is Avoided)}$$
$$\forall c \in C_j^{j'}, \quad i \in \{1, 2, \ldots, n_j\}, \quad i' \in \{1, 2, \ldots, n_j'\},$$
$$j \neq j', \quad j, j' \in \{1, 2, 3, 4\}, \quad BI_{i,i'}^c = 1 \tag{4.16}$$

$$A_{i',j'}^c + t_C \leq A_{i,j}^c, \quad \text{(Collision is Avoided)}$$
$$\forall c \in C_j^{j'}, \quad i \in \{1, 2, \ldots, n_j\}, \quad i' \in \{1, 2, \ldots, n_j'\},$$
$$j \neq j', \quad j, j' \in \{1, 2, 3, 4\}, \quad BI_{i,i'}^c = 0 \tag{4.17}$$

Constraint (4.13) ensures that the time at which vehicle i reaches the entry line of the single-lane roundabout from leg j is bounded by its minimal and maximal arrival times, as explained in Section

4.1.2. Constraint (4.14) ensures that when consecutive vehicles arrive at the entry line, there is at least a follow-on time between them. Constraint (4.15) implies that for vehicles i and i' crossing the same conflict point, either vehicle i reaches c first, or vehicle i' reaches c first. Constraint (4.16) ensures that there is no collision for vehicles reaching the same conflict point from different legs. This can be explained as follows: if vehicle i from leg j arrives at the conflict point c earlier than vehicle i' from leg j', then $BI^c_{i,i'} = 1$. Consequently, vehicle i' is only allowed to arrive at the conflict point after the critical gap time required by the merging behavior in the roundabout. Constraint (4.17) also ensures no collision at the conflict point but in a symmetric case where vehicle i' arrives at the conflict point c prior to vehicle i.

4.1.4. Second Phase Optimization

The output of the First Phase Optimization is the time that individual vehicle spends from the control boundary to the entry line (S_i^j), i.e. what we define as the sojourn time. Therefore, for each individual vehicle, we can get the time at which it arrives at the entry line, i.e. $t_{i,0} + S_i^j$. Using the sojourn time S_i^j as the input for the Second Phase Optimization, we can construct our model for the optimization. As suggested by Mandava et al. [22] and Feng et al. [11], the trajectory of individual vehicles can be divided into three segments:

1. Starting with an initial speed $v_{i,0}$ upon entering the control zone, vehicle i accelerates at a rate of $a_{i,1}$ to reach a cruising speed $v_{i,*}$. This acceleration occurs from $t_{i,0}$, the time at which vehicle i enters the control zone, until $t_{i,1}$, the time at which the vehicle reaches its cruising speed.
2. Vehicle i travels at the cruising speed $v_{i,*}$ from $t_{i,1}$ to $t_{i,2}$, at which point the vehicle will undergo another acceleration, denoted as $a_{i,2}$.
3. Vehicle i accelerates at $a_{i,2}$ from $t_{i,2}$ to $t_{i,0} + S_i^j$, at which point it reaches the speed v_r and enters the roundabout.

In principle, the trajectory (v-t plot) can be classified into four cases, determined by the signs of $a_{i,1}$ and $a_{i,2}$ (See Fig.4.5). For example, in the bottom-left part of Fig.4.5, the vehicle first accelerates from the time at which it enters the control zone until time $t_{i,1}$, reaching the cruising speed $v_{i,*}$. The vehicle then maintains this cruising speed until time $t_{i,2}$. Finally, it decelerates from $t_{i,2}$ until $t_{i,0} + S_i^j$, the time at which it enters the roundabout at speed v_r. It should be noted that if $t_{i,1} = t_{i,2}$, then the second segment does not exist.

Let $v_i(t)$ denote the speed of vehicle i at time t, and let $x_i(t)$ represent its position relative to the control boundary after it enters the control zone. At the next time step $t + \Delta t$, the speed and position can be determined iteratively:

$$v_i(t+\Delta t) = \begin{cases} v_i(t) + a_{i,1}\Delta t & \text{if } 0 \le t < t_{i,1} \\ v_{i,*} & \text{if } t_{i,1} \le t < t_{i,2} \\ v_i(t) + a_{i,2}\Delta t & \text{if } t_{i,2} \le t \le t_{i,0} + S_i^j \end{cases}. \tag{4.18}$$

$$x_i(t+\Delta t) = \begin{cases} x_i(t) + v_i(t)\Delta t + \frac{1}{2}a_{i,1}\Delta t^2 & \text{if } 0 \le t < t_{i,1} \\ x_i(t) + v_{i,*}\Delta t & \text{if } t_{i,1} \le t < t_{i,2} \\ x_i(t) + v_i\Delta t + \frac{1}{2}a_{i,2}\Delta t^2 & \text{if } t_{i,2} \le t \le t_{i,0} + S_i^j \end{cases}. \tag{4.19}$$

The goal of the Second Phase Optimization is to ensure a comfortable driving experience, which is equivalent to achieving a smoother trajectory with less abrupt acceleration changes. There are several approaches to performing this optimization. One can choose either Convex Optimization, with the objective function defined as the integral of the absolute value of the acceleration over the driving time, or Quadratic Optimization, where the objective function is the integral of the square of the acceleration over the driving time (see He et al.[16] for details). In this work, we use Convex Optimization with non-linear constraints to construct our models because we are implementing this in the Gurobi Optimizer, which is a software package that can be executed in Python. In Gurobi, Quadratic Optimization requires the addition of extra constraints, as quadratic expressions are treated as constraints, which increases computational complexity. Therefore, we opted for Convex Optimization. The objective function is:

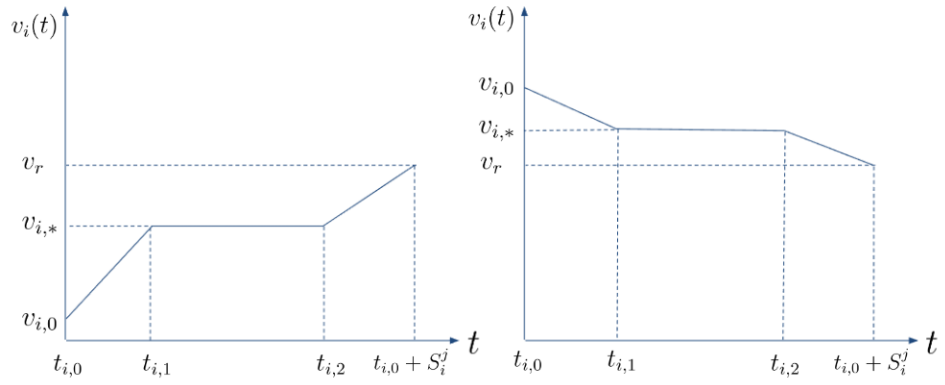

(a) Cases for $a_{i,1}$ and $a_{i,2}$ having the same sign.

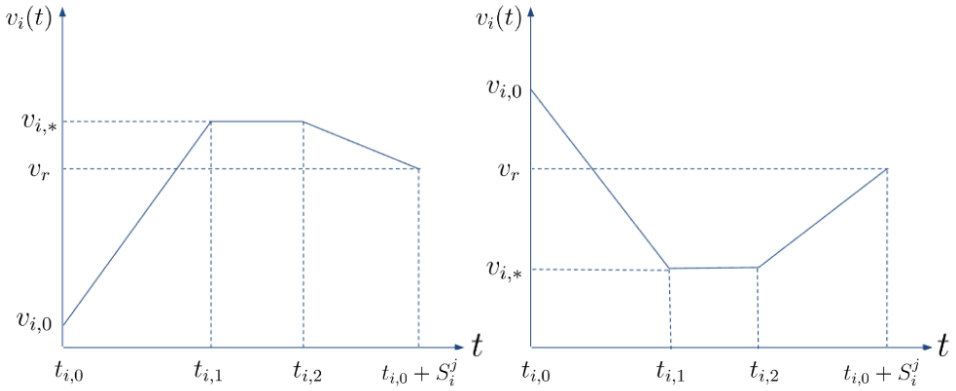

(b) Cases for $a_{i,1}$ and $a_{i,2}$ having different signs.

Figure 4.5: $v - t$ plots for vehicle i's trajectory.

$$\text{Minimize} \left(\int_{t_{i,0}}^{t_{i,1}} |a_{i,1}| dt + \int_{t_{i,2}}^{t_{i,0}+S_i^j} |a_{i,2}| \, dt \right), \tag{4.20}$$

subject to:

$$0 \leq v_{i,*} = v_{i,0} + a_{i,1}(t_{i,1} - t_{i,0}) \leq v_{\text{max}}, \quad \forall i \in \{1, 2, \ldots, n_j\}. \tag{4.21}$$

(Cruising Speed is Bounded)

$$v_r = v_{i,*} + a_{i,2}(t_{i,0} + S_i^j - t_{i,2}), \quad \forall i \in \{1, 2, \ldots, n_j\}, \quad j \in \{1, 2, 3, 4\}. \tag{4.22}$$

(Reaching Speed v_r When Entering the Roundabout)

$$\begin{aligned} x_0 = {} & v_{i,0}(t_{i,1} - t_{i,0}) + \frac{1}{2} a_{i,1}(t_{i,1} - t_{i,0})^2 + v_{i,*}(t_{i,2} - t_{i,1}) \\ & + v_{i,*}(t_{i,0} + S_i^j - t_{i,2}) + \frac{1}{2} a_{i,2}(t_{i,0} + S_i^j - t_{i,2})^2, \quad \forall i \in \{1, 2, \ldots, n_j\}, \quad j \in \{1, 2, 3, 4\}. \end{aligned} \tag{4.23}$$

(Total Travel Distance is x_0)

$$0 \leq t_{i,1} \leq t_{i,2} \leq t_{i,0} + S_i^j, \quad \forall i \in \{1, 2, \ldots, n_j\}, \quad j \in \{1, 2, 3, 4\}. \tag{4.24}$$

(The Three Segments are Odered)

$$a_{\text{min}} \leq a_{i,1} \leq a_{\text{max}}, \quad \forall i \in \{1, 2, \ldots, n_j\}. \tag{4.25}$$

($a_{i,1}$ is Bounded)

$$a_{\text{min}} \leq a_{i,2} \leq a_{\text{max}}, \quad \forall i \in \{1, 2, \ldots, n_j\}. \tag{4.26}$$

($a_{i,2}$ is Bounded)

$$x_i(t + \Delta t) - x_{i+1}(t + \Delta t) \geq d_{\text{safe}}, \quad \forall i \in \{0, 1, 2, \ldots, n_j\}, \quad j \in \{1, 2, 3, 4\}, \quad t \in (t_{i,0}, t_{i,0} + S_i^j). \tag{4.27}$$

(Collision is Avoided on the Leg)

Constraint (4.21) ensures that vehicle i will reach its cruising speed v_{i*} at $t_{i,1}$ by using acceleration $a_{i,1}$, and its cruising speed is bounded between 0 and the maximum speed limit v_{max} on the leg. Constraint (4.22) ensures that after the cruising segment, vehicle i will reach the speed v_r at time $t_{i,0} + S_i^j$ by using acceleration $a_{i,2}$. Constraint (4.23) ensures that, in total, vehicle i travels the distance x_0, i.e., the distance from the boundary of the control zone to the entry line, by following the three-segment trajectories mentioned above. Constraint (4.24) ensures the order of the different segments is followed, transitioning from segment 1 to segment 2 to segment 3. Constraints (4.25) and (4.26) ensure that $a_{i,1}$ and $a_{i,2}$ are bounded by the maximum and minimum acceleration limits on the leg. Constraint (4.27) ensures that there is a safety distance between consecutive vehicles, thereby preventing collisions on each leg. One should note that the output of the Second Phase Optimization is $a_{i,1}$, $t_{i,1}$, $v_{i,*}$, $t_{i,2}$, and $a_{i,2}$ for each individual vehicle i.

4.2. Queueing Model

To justify whether the microscopic control model in Section 4.1 enhances the efficiency of a single-lane roundabout, we will develop an $M/G/1/k$ queueing model to derive the theoretical expected sojourn time. The M denotes the Markovian or memoryless nature of the arrival process, which aligns with real-world scenarios where vehicles arrive at the roundabout according to a Poisson Process. In the context of this queueing model,"customers" are vehicles attempting to enter the roundabout. The G represents the general distribution of service times, reflecting the random time required for the first vehicle at the entry line to enter the roundabout. The 1 indicates the presence of a single server in the system. Although no physical server exists, one can imagine a person standing at the roundabout entrance, deciding vehicle entry based on traffic conditions. Lastly, the k represents the system's capacity, including the server, which in this case corresponds to the number of vehicles that can be accommodated within each leg of the control zone in our control model. An illustration of our queueing system is provided in Fig.4.6.

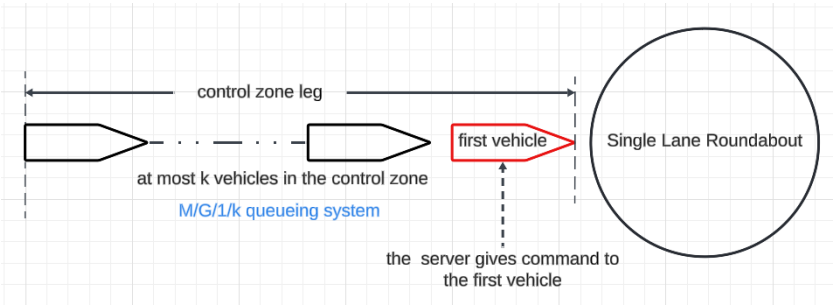

Figure 4.6: Illustration of the $M/G/1/k$ queueing system model.

The term"sojourn time" S in a queueing system refers to the total time a customer spends within the system. This time is the sum of the waiting time W in the queue and the service time B. In our model, it represents the time a vehicle takes to travel from entering the control zone to merging into the roundabout. The goal of this section is to theoretically derive an approximation for the expected sojourn time $\mathbb{E}(S)$. To achieve this, we need to determine the expected number of customers $\mathbb{E}(L)$ in the system. This can be done either purely theoretically using an embedded Markov Chain, provided the service time distribution function $F_B(t)$ is known, or by using an approximation formula (see Section 4.2.3). Once $\mathbb{E}(L)$ is determined, we can apply the well-known Little's Law, $\mathbb{E}(S) = \frac{\mathbb{E}(L)}{\lambda}$, where λ is the arrival rate of vehicles. The proof of Little's Law will be provided in Section 4.2.4. If we opt to use the approximation formula, the squared coefficient of variation of the service time C_s^2 is required. To calculate this, the first and second moments of the service time must be derived. It should be noted that even if the distribution function $F_B(t)$ is unavailable, the moments $\mathbb{E}(B)$ and $\mathbb{E}(B^2)$ can still be obtained from the circulating headway time distribution, which is often accessible through data. This process will be explained in Section 4.2.1. The structure of this section and the interconnections between its subsections are illustrated in Fig.4.7.

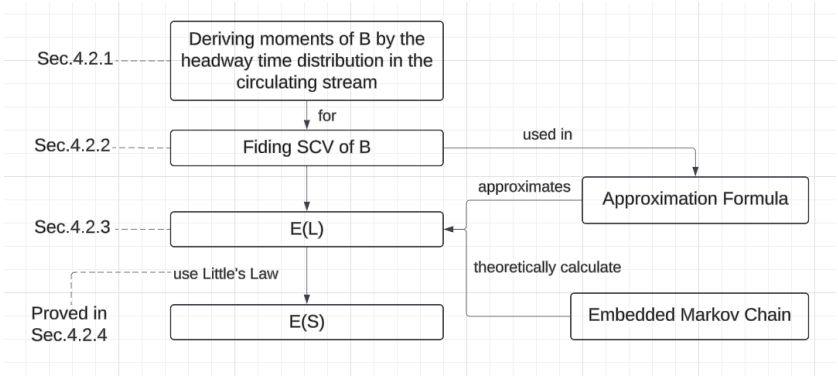

Figure 4.7: Organization of Sec.4.2.

4.2.1. Moments of the Service Time

In this section, we will derive the moments of service time in our $M/G/1/k$ model. To facilitate this derivation, we will first introduce some essential background information.

- Non-Delayed Renewal Process: A Non-Delayed Renewal Process is a counting process $N(t) :=$the number of events happening in $(0, t]$ with inter-arrival (inter-event) times $A_i \overset{\text{i.i.d}}{\sim} F_A(t)$.
- Delayed Process: A Delayed Process is a process in which the distribution for the first inter-arrival time A_1 is F_{A_1} distributed, while the sequence $\{A_n : n = 2, 3, 4, ...\}$ follows the distribution F_{A_n} independently. The relationship of the distribution function F_{A_1} (equilibrium distribution) and F_{A_n} is associated as:

$$F_{A_1}(t) = \frac{1}{a}\int_0^t \big(1 - F_{A_n}(u)\big)du, \text{ with } a = \mathbb{E}(A_n). \tag{4.28}$$

If the inter-arrival time in a Non-delayed Renewal Process follows an exponential distribution, then the process is a Poisson Process. A Delayed Process contains an Equilibrium Process with an equilibrium distribution function F_{A_1} associated with the distribution F_{A_n} (Eq.(4.28)) in the subsequent Non-Delayed Renewal Process. The relationship between the Non-Delayed Renewal Process and the Delayed Process is illustrated in Fig.4.8.

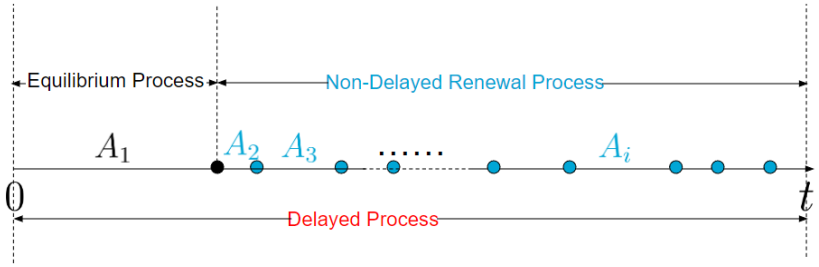

Figure 4.8: The relationship between Delayed Process and Non-delayed Renewal Process.

As suggested by Flannery et al.[13], when the first vehicle on the approach is trying to enter the roundabout, the arrival process of the circulating stream to the conflict point is assumed to be a Delayed Process, denoted as $\{C(t)\}$, with inter-arrival times $C_i(t)$, where $i = 1, 2, 3, \ldots$. One should note that the inter-arrival time in this Stochastic Process is essentially the same as the headway time, since the time between events of vehicles passing the same reference point is identical to the time gap between consecutive vehicles.

First Moment of the Service Time

Let F_{C_n} be the distribution function of the headway times for the circulating traffic inside the roundabout associated with the equilibrium distribution F_{C_1}; let $t_C \in \mathbb{R}$ be the critical gap for drivers arriving at the entry line of the roundabout seeking to join the circulatory stream; let $h \in \mathbb{R}$ be the mean headway time for the circulating stream under the distribution F_{C_n}; let the random variable B be the service time in our queueing model, which is the random time required for service for the vehicle in the first position at the entry line; let the random variable B_0 be the time that the first vehicle at the entry line has to wait under the Non-Delayed Renewal Process of the circulating stream; let the random variable C_1 be the first inter-event time under the equilibrium distribution F_{C_1} when the first vehicle is trying to enter the roundabout; and let the random variable C_2 be the second inter-event time under the Non-Delayed Renewal Process (it is the Non-Delayed part of $\{C(t)\}$).

Considering the situation in which the first vehicle on the approach is trying to enter the roundabout, if the time gap between the upcoming vehicle in the circulating stream and the conflict point is large enough (greater than t_C), then the first vehicle at the entry line can enter the roundabout immediately. Therefore, the conditional expectation of B given that $C_1 = t_1$ is $\mathbb{E}(B \mid C_1 = t_1) = 0$. However, if the gap is too small, the first vehicle on the approach needs to wait until the first vehicle in the circulating

stream crosses the conflict point, meaning the conditional expectation of B is $\mathbb{E}(B|C_1 = t_1) = t_1 + \mathbb{E}(B_0)$. Therefore,

$$\mathbb{E}(B|C_1 = t_1) = \begin{cases} t_1 + \mathbb{E}(B_0) & \text{if } t_1 \leq t_C \\ 0 & \text{if } t_1 > t_C \ . \end{cases} \tag{4.29}$$

Applying Tower Property to Eq.(4.29), we get

$$\begin{aligned} \mathbb{E}(B) &= \mathbb{E}\big(\mathbb{E}(B|C_1)\big) \\ &= \int_0^{t_C} \mathbb{E}(B|C_1 = t_1) dF_{C_1}(t_1) + \int_{t_C}^{\infty} 0 dF_{C_1}(t_1) \\ &= \int_0^{t_C} t_1 dF_{C_1}(t_1) + \mathbb{E}(B_0)\big(F_{C_1}(t_C) - F_{C_1}(0)\big) \\ &= \int_0^{t_C} t_1 dF_{C_1}(t_1) + \mathbb{E}(B_0) F_{C_1}(t_C). \end{aligned} \tag{4.30}$$

In Eq.(4.30), $\mathbb{E}(B_0)$ is unknown. Using a similar approach, by conditioning on the next inter-event time $C_2 = t_2$, if t_2 is greater than the critical gap t_C, then $\mathbb{E}(B_0 \mid C_2 = t_2)$ is zero, meaning the first vehicle on the approach does not have to wait after the first vehicle in the circulating stream passes through the conflict point. Otherwise, it has to wait again for the second vehicle in the circulating stream to cross the conflict point. To conclude,

$$\mathbb{E}(B_0|C_2 = t_2) = \begin{cases} t_2 + \mathbb{E}(B_0) & \text{if } t_2 \leq t_C \\ 0 & \text{if } t_2 > t_C \ . \end{cases} \tag{4.31}$$

Using the Tower Property in Eq.(4.31), we obtain the following result:

$$\begin{aligned} \mathbb{E}(B_0) &= \mathbb{E}\big(\mathbb{E}(B_0|C_2)\big) \\ &= \int_0^{t_C} \big(t_2 + \mathbb{E}(B_0)\big) dF_{C_n}(t_2) + \int_{t_C}^{\infty} 0 dF_{C_n}(t_2) \\ &= \int_0^{t_C} t_2 dF_{C_n}(t_2) + \mathbb{E}(B_0)\big(F_{C_n}(t_C) - F_{C_n}(0)\big) \\ &= \int_0^{t_C} t_2 dF_{C_n}(t_2) + \mathbb{E}(B_0) F_{C_n}(t_C). \end{aligned} \tag{4.32}$$

Simplifying Eq.(4.32), we get

$$\mathbb{E}(B_0) = \frac{\int_0^{t_C} t_2 dF_{C_n}(t_2)}{1 - F_{C_n}(t_C)}. \tag{4.33}$$

Substituting Eq.(4.33) into Eq.(4.30), we get

$$\mathbb{E}(B) = \int_0^{t_C} t_1 dF_{C_1}(t_1) + \frac{\int_0^{t_C} t_2 dF_{C_n}(t_2)}{1 - F_{C_n}(t_C)} F_{C_1}(t_C). \tag{4.34}$$

Recall the relationship between the equilibrium distribution and the inter-event distribution as stated in Eq.(4.28), in our case

$$F_{C_1}(t) = \frac{1}{h} \int_0^t (1 - F_{C_n}(u)) du, \tag{4.35}$$

where $h = \int_0^{\infty} \big(1 - F_{C_n}(u)\big) du$ is the expectation of the inter-event time (mean headway time) in the Non-Delayed part of the Delayed Process. Thus

$$dF_{C_1}(t_1) = \frac{1 - F_{C_n}(t_1)}{h} dt_1, \tag{4.36}$$

which can be derived by Eq.(4.35) by using the Fundamental Theorem of Calculus. Then the first part of the RHS in Eq.(4.34) can be calculated as:

$$\int_0^{t_C} t_1 dF_{C_1}(t_1) = \frac{1}{h}\int_0^{t_C} t_1\big(1 - F_{C_n}(t_1)\big)dt_1. \tag{4.37}$$

Using Eq.(4.35), we can also get

$$F_{C_1}(t_C) = \frac{1}{h}\int_0^{t_C} \big(1 - F_{C_n}(u)\big)du. \tag{4.38}$$

Plugging Eq.(4.37) and Eq.(4.38) into Eq.(4.34), we can get

$$\begin{aligned}
\mathbb{E}(B) &= \frac{1}{h}\int_0^{t_C} t_1\big(1 - F_{C_n}(t_1)\big)dt_1 + \frac{\int_0^{t_C} t_2 dF_{C_n}(t_2)}{1 - F_{C_n}(t_C)}\frac{1}{h}\int_0^{t_C}\big(1 - F_{C_n}(u)\big)du \\
&= \frac{1}{h}\Big(\int_0^{t_C} t_1\big(1 - F_{C_n}(t_1)\big)dt_1 + \frac{\int_0^{t_C} t_2 dF_{C_n}(t_2)}{1 - F_{C_n}(t_C)}\Big(t_C - \int_0^{t_C} F_{C_n}(u)du\Big)\Big) \\
&= \frac{1}{h}\Big(\frac{1}{2}(t_C)^2 - \int_0^{t_C} tF_{C_n}(t)dt + \big(1 - F_{C_n}(t_C)\big)^{-1}\Big(t_C - \int_0^{t_C} F_{C_n}(u)du\Big)\int_0^{t_C} t dF_{C_n}(t)\Big).
\end{aligned} \tag{4.39}$$

Second Moment of the Service Time

When the first vehicle on the approach tries to enter the roundabout, the circulating stream follows a Delayed Process. The service time B is zero if the first inter-event time of the circulating stream is sufficiently large. Otherwise, the first vehicle on the approach must wait for the first vehicle in the circulating stream to pass and then wait for an acceptable gap under the Non-Delayed Renewal Process of the circulating stream. Recall that

$$\mathbb{E}(B|C_1 = t_1) = \begin{cases} t_1 + \mathbb{E}(B_0) & \text{if } t_1 \le t_C \\ 0 & \text{if } t_1 > t_C\ . \end{cases} \tag{4.40}$$

Then the conditional second moment of B given $C_1 = t_1$is

$$\mathbb{E}(B^2 \mid C_1 = t_1) = \begin{cases} \mathbb{E}\big((B_0)^2\big) + 2t_1\mathbb{E}(B_0) + (t_1)^2 & \text{if } t_1 \le t_C \\ 0 & \text{if } t_1 > t_C\ . \end{cases} \tag{4.41}$$

By Eq.(4.31), the conditional second moment of B_0 given $C_2 = t_2$ is

$$\mathbb{E}\big((B_0)^2 \mid C_2 = t_2\big) = \begin{cases} \mathbb{E}\big((B_0)^2\big) + 2t_2\mathbb{E}(B_0) + (t_2)^2 & \text{if } t_2 \le t_C \\ 0 & \text{if } t_2 > t_C\ . \end{cases} \tag{4.42}$$

Applying Tower Property to Eq.(4.41), we get

$$\begin{aligned}
\mathbb{E}(B^2) &= \mathbb{E}\big(\mathbb{E}(B^2 \mid C_1)\big) \\
&= \int_0^{t_C} \mathbb{E}(B^2 \mid C_1 = t_1)dF_{C_1}(t_1) + \int_{t_C}^{\infty} 0 dF_{C_1}(t_1) \\
&= \int_0^{t_C} \big((t_1)^2 + 2t_1\mathbb{E}(B_0)\big)dF_{C_1}(t_1) + \int_0^{t_C} \mathbb{E}\big((B_0)^2\big)dF_{C_1}(t_1) \\
&= \int_0^{t_C} \big((t_1)^2 + 2t_1\mathbb{E}(B_0)\big)dF_{C_1}(t_1) + \mathbb{E}\big((B_0)^2\big)\big(F_{C_1}(t_C) - F_{C_1}(0)\big) \\
&= \int_0^{t_C} \big((t_1)^2 + 2t_1\mathbb{E}(B_0)\big)dF_{C_1}(t_1) + \mathbb{E}\big((B_0)^2\big)F_{C_1}(t_C).
\end{aligned} \tag{4.43}$$

Using a similar technique to Eq.(4.42),

$$\begin{aligned}\mathbb{E}\big((B_0)^2\big) &= \mathbb{E}\big(\mathbb{E}(B_0)^2 \mid C_2)\big)\\ &= \int_0^{t_C} \mathbb{E}\big((B_0)^2 \mid C_2 = t_2\big) dF_{C_n}(t_2) + \int_{t_C}^{\infty} 0 dF_{C_n}(t_2)\\ &= \int_0^{t_C} \big((t_2)^2 + 2t_2\mathbb{E}(B_0)\big) dF_{C_n}(t_2) + \int_0^{t_C} \mathbb{E}\big((B_0)^2\big) dF_{C_n}(t_2)\\ &= \int_0^{t_C} \big((t_2)^2 + 2t_2\mathbb{E}(B_0)\big) dF_{C_n}(t_2) + \mathbb{E}\big((B_0)^2\big)\big(F_{C_n}(t_C) - F_{C_n}(0)\big)\\ &= \int_0^{t_C} \big((t_2)^2 + 2t_2\mathbb{E}(B_0)\big) dF_{C_n}(t_2) + \mathbb{E}\big((B_0)^2\big) F_{C_n}(t_C).\end{aligned} \tag{4.44}$$

Simplifying Eq.(4.44), we can derive

$$\mathbb{E}\big((B_0)^2\big) = \big(1 - F_{C_n}(t_C)\big)^{-1} \int_0^{t_C} \big((t_2)^2 + 2t_2\mathbb{E}(B_0)\big) dF_{C_n}(t_2). \tag{4.45}$$

Substituting Eq.(4.45) into Eq.(4.43) yields

$$\mathbb{E}(B^2) = \int_0^{t_C} \big((t_1)^2 + 2t_1\mathbb{E}(B_0)\big) dF_{C_1}(t_1) + F_{C_1}(t_C)\big(1 - F_{C_n}(t_C)\big)^{-1} \int_0^{t_C} \big((t_2)^2 + 2t_2\mathbb{E}(B_0)\big) dF_{C_n}(t_2). \tag{4.46}$$

Making use of Eq.(4.36), the first integral involving t_1 in Eq.(4.46) is

$$\int_0^{t_C} (t_1)^2 dF_{C_1}(t_1) = \frac{1}{h} \int_0^{t_C} (t_1)^2 \big(1 - F_{C_n}(t_1)\big) dt_1, \tag{4.47}$$

and the second integral w.r.t. t_1 in Eq.(4.46) is

$$\int_0^{t_C} 2t_1\mathbb{E}(B_0) dF_{C_1}(t_1) = \frac{2\mathbb{E}(B_0)}{h} \int_0^{t_C} t_1\big(1 - F_{C_n}(t_1)\big) dt_1. \tag{4.48}$$

Thus

$$\int_0^{t_C} \big((t_1)^2 + 2t_1\mathbb{E}(B_0)\big) dF_{C_1}(t_1) = \frac{1}{h}\Big(\frac{1}{3}(t_C)^3 + \mathbb{E}(B_0)(t_C)^2 - \int_0^{t_C} \big(t^2 + 2t\mathbb{E}(B_0)\big) F_{C_n}(t) dt\Big). \tag{4.49}$$

Substituting Eq.(4.38) into the integral w.r.t t_2 in Eq.(4.46), we can obtain

$$\begin{aligned}&F_{C_1}(t_C)\big(1 - F_{C_n}(t_C)\big)^{-1} \int_0^{t_C} \big((t_2)^2 + 2t_2\mathbb{E}(B_0)\big) dF_{C_n}(t_2)\\ &= \frac{1}{h}\Big(\int_0^{t_C} \big(1 - F_{C_n}(u)\big) du\Big)\big(1 - F_{C_n}(t_C)\big)^{-1} \int_0^{t_C} \big((t_2)^2 + 2t_2\mathbb{E}(B_0)\big) dF_{C_n}(t_2)\\ &= \frac{1}{h}\Big(t_C - \int_0^{t_C} F_{C_n}(t) dt\Big)\big(1 - F_{C_n}(t_C)\big)^{-1}\Big(\int_0^{t_C} t^2 dF_{C_n}(t) + 2\mathbb{E}(B_0) \int_0^{t_C} t dF_{C_n}(t)\Big).\end{aligned} \tag{4.50}$$

Plugging Eq.(4.49) and Eq.(4.50) into Eq.(4.46), we can find the expression of the second moment of $\mathbb{E}(B^2)$:

$$\begin{aligned}&\mathbb{E}(B^2)\\ &= \frac{1}{h}\Big(\frac{1}{3}(t_C)^3 + \mathbb{E}(B_0)(t_C)^2 - \int_0^{t_C} \big(t^2 + 2t\mathbb{E}(B_0)\big) F_{C_n}(t) dt\Big)\\ &+ \frac{1}{h}\Big(t_C - \int_0^{t_C} F_{C_n}(t) dt\Big)\big(1 - F_{C_n}(t_C)\big)^{-1}\Big(\int_0^{t_C} t^2 dF_{C_n}(t) + 2\mathbb{E}(B_0) \int_0^{t_C} t dF_{C_n}(t)\Big),\end{aligned} \tag{4.51}$$

where $\mathbb{E}(B_0)$ was found in Eq.(4.33).

4.2.2. Squared Coefficient of Variation of the Service Time

According to the definition,

$$\mathbb{V}ar(B) = \mathbb{E}(B^2) - \big(\mathbb{E}(B)\big)^2. \tag{4.52}$$

Using the information of Eq.(4.39) and Eq.(4.51), the variance of the service time is

$$\begin{aligned}\mathbb{V}ar(B) &= \frac{1}{h}\Big(\frac{1}{3}(t_C)^3 + \mathbb{E}(B_0)(t_C)^2 - \int_0^{t_C}\big(t^2 + 2t\mathbb{E}(B_0)\big)F_{C_n}(t)dt\Big) \\ &+ \frac{1}{h}\Big(t_C - \int_0^{t_C} F_{C_n}(t)dt\big(1 - F_{C_n}(t_C)\big)^{-1}\Big)\Big(\int_0^{t_C} t^2 dF_{C_n}(t) + 2\mathbb{E}(B_0)\int_0^{t_C} t dF_{C_n}(t)\Big) \\ &- \left\{\frac{1}{h}\Big(\frac{1}{2}(t_C)^2 - \int_0^{t_C} tF_{C_n}(t)dt + \big(1 - F_{C_n}(t_C)\big)^{-1}\Big(t_C - \int_0^{t_C} F_{C_n}(u)du\Big)\int_0^{t_C} t dF_{C_n}(t)\Big)\right\}^2\end{aligned} \tag{4.53}$$

In an $M/G/1/K$ queue, the squared coefficient of variation (SCV) of the service time, denoted as C_s^2, plays a crucial role in determining the performance and behavior of the system. The SCV measures the relative variability of service times compared to their mean, influencing several key performance metrics. Higher C_s^2 indicates greater variability, typically resulting in longer waiting times, higher average queue lengths, and an increased probability of the system being full. This variability affects the overall stability and efficiency of the system. For instance, in systems with high C_s^2, the queue is more likely to experience significant fluctuations. Conversely, lower C_s^2 (indicating more consistent service times) generally leads to better performance, with shorter queues and reduced waiting times. Additionally, the expected system size is highly dependent on the SCV and is calculated differently depending on whether $C_s^2 \geq 1$ or not. The SCV can be expressed as follows:

$$C_s^2 = \frac{\mathbb{V}ar(B)}{\big(\mathbb{E}(B)\big)^2}, \tag{4.54}$$

where $\mathbb{V}ar(B)$ and $\mathbb{E}(B)$ has already been derived in Eq.(4.53) and Eq.(4.39) respectively.

4.2.3. Expected Number of Vehicles in the Approach

In this section, we will determine the expected number of vehicles in the queue, $\mathbb{E}(L_q)$, excluding the one currently being serviced, as well as the expected number of vehicles in the system, $\mathbb{E}(L)$, including the one in service. There are two methods to determine this. The first method provides an analytical solution by analyzing the Embedded Markov Chain, which requires the distribution function of the service time, $F_B(t)$. The second method approximates $\mathbb{E}(L_q)$ using the approximation formula proposed by Smith [30]. This method can be utilized if the squared coefficient of variation of the service time is known.

Embedded Markov Chain

Considering an $M/G/1/$ system, let L_k^d be the number of vehicles left behind after the kth vehicle departs the system (enters the roundabout), and let A_k be the number of vehicles that arrive during the service time of the kth vehicle. Then, at the next departure epoch,

$$L_{k+1}^d = \begin{cases} L_k^d - 1 + A_{k+1}, & \text{if } L_k^d > 0 \\ A_{k+1}, & \text{if } L_k^d = 0. \end{cases} \tag{4.55}$$

This is because if there are already some vehicles in the system after the kth vehicle departs, the number of vehicles left in the system after the departure of the $k+1$th vehicle is equal to the number of vehicles left after the kth departure minus one (since the $k+1$th vehicle itself leaves the system) plus the number of vehicles that enter the system during the service time of the $k+1$th vehicle. If there are no vehicles left in the system after the kth departure, then the number of vehicles left behind by the departure of the $k+1$th vehicle is exactly the same as the number of vehicles arriving during its service time.

The sequence $\{L_k^d\}_{k=0}^{\infty}$ forms a Discrete Time Markov Chain (DTMC) because, given the information of all the previous stages $L_k^d, L_{k-1}^d, L_{k-2}^d, \ldots$, the status of the next stage L_{k+1}^d is only dependent on the status of L_k^d. This Markov Chain is called an Embedded Markov Chain as we observe it at embedded time points, i.e., at the departure epochs.

The transition probability is this Embedded DTMC is

$$p_{i,j} = \mathbb{P}(L_{k+1}^d = j \mid L_d^k = i) \tag{4.56}$$

Let

$$\alpha_n := \mathbb{P}(\text{there are } n \text{ arrivals during a service time } B) \tag{4.57}$$

Given that the state is zero, there are no vehicles left after the departure of the kth vehicle, so the probability of having j vehicles in the system at the next departure epoch for the $k+1$th vehicle, $p_{0,j}$, is the probability that j vehicles arrive during its service time, i.e., a_j. For $j < i-1$, the transition probability $p_{i,j} = 0$, since at the next departure epoch, the lower bound for the state is $i-1$, meaning no vehicles arrive during the service time of the $k+1$th vehicle. For $j \geq i-1$, $p_{i,j}$ is the probability that exactly $j-i+1$ vehicles arrive during the service time of the $k+1$th vehicle, since the $k+1$th vehicle departs from the system itself. The above argument gives the transition probability matrix:

$$P_{M/G/1/} = \begin{pmatrix} \alpha_0 & \alpha_1 & \alpha_2 & \alpha_3 & \cdots \\ \alpha_0 & \alpha_1 & \alpha_2 & \alpha_3 & \cdots \\ 0 & \alpha_0 & \alpha_1 & \alpha_2 & \cdots \\ 0 & 0 & \alpha_0 & \alpha_1 & \cdots \\ \vdots & \vdots & \vdots & \vdots & \ddots \end{pmatrix}. \tag{4.58}$$

However, in an $M/G/1/k$ system, the capacity is limited to k (including the one in service). Therefore, the transition probability matrix must be truncated at level $k-1$. This is because, before a departure epoch, the system might be full, but after the departure epoch, the system can have at most $k-1$ vehicles. Thus, the transition probability matrix of the Embedded DTMC $\{L_k^d\}_{k=0}^{k-1}$ in an $M/G/1/k$ system is adjusted to:

$$P_{M/G/1/k} = \begin{pmatrix} \alpha_0 & \alpha_1 & \alpha_2 & \alpha_3 & \cdots & 1-\sum_{n=0}^{k-2}\alpha_n \\ \alpha_0 & \alpha_1 & \alpha_2 & \alpha_3 & \cdots & 1-\sum_{n=0}^{k-2}\alpha_n \\ 0 & \alpha_0 & \alpha_1 & \alpha_2 & \cdots & 1-\sum_{n=0}^{k-3}\alpha_n \\ 0 & 0 & \alpha_0 & \alpha_1 & \cdots & 1-\sum_{n=0}^{k-4}\alpha_n \\ \vdots & \vdots & \vdots & \vdots & \ddots & \vdots \\ 0 & 0 & 0 & 0 & \cdots & 1-\alpha_0 \end{pmatrix}, \tag{4.59}$$

with the transition probability

$$\begin{aligned} \alpha_n &= \mathbb{P}(\text{there are } n \text{ arrivals during a service time } B) \\ &= \int_0^{\infty} \mathbb{P}(\text{there are } n \text{ arrivals during a service time } B \mid B = t) dF_B(t) \\ &= \int_0^{\infty} \frac{e^{-\lambda t}(\lambda t)^n}{n!} dF_B(t), \end{aligned} \tag{4.60}$$

where the last equality follows from the fact that the Arrival Process is a Poisson Process with rate λ.

With the help of Balance Equation $\boldsymbol{\pi} P_{M/G/1/k} = \boldsymbol{\pi}$, where

$$\boldsymbol{\pi} = (\pi_o, \pi_1, ..., \pi_{k-1}) \tag{4.61}$$

represents the stationary probability vector, we can derive the following system of linear equations:

$$\pi_i = \begin{cases} \pi_0\alpha_i + \sum_{j=1}^{i+1}\pi_j\alpha_{i-j+1}, & i = (0,1,2,\ldots,k-2) \\ 1-\sum_{n=0}^{k-2}\pi_n, & i = k-1, \end{cases} \tag{4.62}$$

and solve for π_i, the probability of having i vehicles in the system where $i = 0, 1, ..., k-1$. Then the expected number of vehicles in the system is

$$\mathbb{E}(L) = \sum_{n=0}^{k-1} n\pi_n \tag{4.63}$$

and the expected number of vehicles in the queue (excluding the one in service) is

$$\begin{aligned} \mathbb{E}(L_q) &= \mathbb{E}(L) - \mathbb{E}(\text{number of vehicles in service}) \\ &= \sum_{n=0}^{k-1} n\pi_n - \rho, \end{aligned} \tag{4.64}$$

where $\rho = \lambda\mathbb{E}(B)$ is the utilization of the server, also representing the expected number of vehicles in service.

Approximation Formula

If the distribution function of the service time $F_B(t)$ is unknown, but the first moment $\mathbb{E}(B)$ and the squared coefficient of variation of the service time C_s^2 are known, the following approximation formula can be used:

First, one can approximate the blocking probability, which is the probability that a new vehicle enters the system and finds that the system is full, by:

$$p_k \approx \frac{\rho^{(\sqrt{\rho}C_s^2 - \sqrt{\rho} + 2k)/(2+\sqrt{\rho}C_s^2 - \sqrt{\rho})}(\rho - 1)}{\rho^{2(1+\sqrt{\rho}C_s^2 - \sqrt{\rho} + k)/(2+\sqrt{\rho}C_s^2 - \sqrt{\rho})} - 1}, \tag{4.65}$$

where ρ is the utilization of the system, defined by $\rho := \lambda\mathbb{E}(B)$, with λ being the arrival rate of vehicles.

Then, the expected number of vehicles in the system can be approximated by:

$$\mathbb{E}(L) \approx \begin{cases} \dfrac{\rho\left(\ln(1/\rho) + p_k \ln\left(p_k/(1-\rho+p_k\rho)\right) + p_k\ln(\rho)\right)\left(2 + \sqrt{\rho/e^{C_s^2}}C_s^2 - \sqrt{\rho/e^{C_s^2}}\right)}{2\ln(\rho)(\rho-1)} & C_s^2 \leq 1, \\ \dfrac{\rho\left(\ln(1/\rho) + p_k \ln\left(p_k/(1-\rho+p_k\rho)\right) + p_k\ln(\rho)\right)\left(2 + \sqrt{\rho/e}C_s^2 - \sqrt{\rho/e}\right)}{2\ln(\rho)(\rho-1)} & 1 < C_s^2. \end{cases} \tag{4.66}$$

Finally, the expected number of vehicles in the queue can be found by:

$$\mathbb{E}(L_q) = \mathbb{E}(L) - \rho, \tag{4.67}$$

as indicated in Eq.(4.64).

4.2.4. Little's Law

Once the expected number of vehicles $\mathbb{E}(L)$ in the system is known, the expected sojourn time $\mathbb{E}(S)$ can be determined using Little's Law. Little's Law, first proposed by Cobham [8], is stated as follows:

Theorem 1 (Little's Law)**.** *In a queueing system, let $\mathbb{E}(L)$ denote the expected number of customers in the system, including the one in service, $\mathbb{E}(S)$ the expected sojourn time of a customer (which includes both the expected waiting time in the queue and the expected service time), and λ the average arrival rate to the system. If the system is stable, meaning there exists a steady state, then*

$$\mathbb{E}(L) = \lambda\mathbb{E}(S). \tag{4.68}$$

Proof. Firstly, we define the following:

- $L(t) :=$ the number of customer in the system at time t.

- S_i :=the time that customer i spends in the system.
- T_i := the arrival time of customer i to the system.
- $N(t)$:= the number of customers that have arrived in the system up to time t
- D_i := the departure time of customer i from the system.

The expected number of customers in the system is:

$$\mathbb{E}(L) = \lim_{t\to\infty} \frac{1}{t} \int_0^t L(u)du. \tag{4.69}$$

The expected sojourn time of a customer can be expressed by:

$$\mathbb{E}(S) = \lim_{t\to\infty} \frac{1}{N(t)} \sum_{i=1}^{N(t)} S_i, \tag{4.70}$$

and the average arrival rate to the system can be calculated as:

$$\lambda = \lim_{t\to\infty} \frac{N(t)}{t}. \tag{4.71}$$

The limits in Eq.(4.69), (4.70), and (4.71) exist and are finite. They can be derived immediately by the Ergotic Theorem for strictly Stochastic Process ([7], pp 465 and 551).

Secondly, we can find the expression of $L(u)$ given a fixed u. At time u, customer i is in the system if and only if it arrives at or before u and leaves after u, meaning $T_i \leq u < D_i$. Let $\mathbb{1}\{\cdot\}$ be the indicator function, then $L(u)$ can be written by:

$$L(u) = \sum_{i:T_i\leq u} \mathbb{1}\{D_i > u\}. \tag{4.72}$$

Since the departure time of customer i is

$$D_i = S_i + T_i, \tag{4.73}$$

Eq.(4.72) can be written as:

$$L(u) = \sum_{i:T_i\leq u} \mathbb{1}\{T_i + S_i > u\} = \sum_{i:T_i\leq u} \mathbb{1}\{S_i > u - T_i\}. \tag{4.74}$$

Therefore,

$$\begin{aligned}
&\int_0^t L(u)du \\
&= \int_0^t \Big\{ \sum_{i:T_i\leq u} \mathbb{1}\{S_i > u - T_i\}\Big\}du = \int_0^t \Big\{ \sum_{i:T_i\leq t} \mathbb{1}\{S_i > u - T_i\}\Big\}du \\
&= \sum_{i:T_i\leq t} \Big\{ \int_{T_i}^t \mathbb{1}\{S_i > u - T_i\}du\Big\} = \sum_{i:T_i\leq t} \Big\{ \int_0^{t-T_i} \mathbb{1}\{S_i > s\}ds\Big\} \\
&= \sum_{i:T_i\leq t} \min\{S_i, t - T_i\}.
\end{aligned} \tag{4.75}$$

In Eq.(4.75), the second equality holds because we integrate over u from 0 to t, allowing us to change the sum from $i : T_i \leq u$ to $i : T_i \leq t$. Each item i starts contributing to the sum from its arrival time T_i and continues contributing until time t. When we change the order of summation and integration, we recognize that the integral for each item i should only consider the time period from its arrival time T_i to the end of the interval t. Therefore, the integration over time u runs from T_i to t, which explains why the third equality holds. The fourth equality utilizes the change of variable $s = u - T_i$. The indicator

function $\mathbb{1}\{S_i > s\} = 1$ if $s < S_i$, meaning $\int_0^{t-T_i} \mathbb{1}\{S_i > s\}\, ds$ is the length of the interval $(0, S_i)$ or $(0, t - T_i)$, depending on whether $S_i \geq t - T_i$ or not. Thus the final equality holds.

Thirdly, the boundary of $\int_0^t L(u)du$ can be derived. The upper bound can be obtained immediately:

$$\int_0^t L(u)du = \sum_{i:T_i \leq t} \min\{S_i, t - T_i\} \leq \sum_{i:T_i \leq t} S_i \leq \sum_{i=1}^{N(t)} S_i. \tag{4.76}$$

To obtain the lower bound, we can split the sum into two cases: the first case is the sum over indices in which customers arrive and depart before time t, and the second case is the sum over indices in which customers arrive before t but leaves after t. Therefore,

$$\begin{aligned}
&\int_0^t L(u)du = \sum_{i:T_i \leq t} \min\{S_i, t - T_i\} \\
&= \sum_{i:T_i \leq t, D_i \leq t} \min\{S_i, t - T_i\} + \sum_{i:T_i \leq t, D_i > t} \min\{S_i, t - T_i\} \\
&= \sum_{i:T_i \leq t, D_i \leq t} S_i + \sum_{i:T_i \leq t, D_i > t} (t - T_i) \\
&\geq \sum_{i:T_i \leq t, D_i \leq t} S_i \\
&= \sum_{i:D_i \leq t} S_i,
\end{aligned} \tag{4.77}$$

where the third equality is reasoned by $D_i = T_i + S_i$, and the final inequality holds because we sum over fewer indices. Combing the inequality in (4.76) and (4.77), we can obtain

$$\sum_{i:D_i \leq t} S_i \leq \int_0^t L(u)du \leq \sum_{i=1}^{N(t)} S_i. \tag{4.78}$$

Next, multiplying the right part of the inequality in (4.78) by $\frac{1}{t}$ and taking the limit as $t \to \infty$, we can derive the following RHS.

$$\begin{aligned}
&\lim_{t\to\infty} \frac{1}{t} \int_0^t L(u)du = \mathbb{E}(L) \\
&\leq \lim_{t\to\infty} \frac{1}{t} \sum_{i=1}^{N(t)} S_i \\
&= \lim_{t\to\infty} \Big\{ \Big(\frac{N(t)}{t} \Big) \Big(\frac{1}{N(t)} \sum_{i=1}^{N(t)} S_i \Big) \Big\} \\
&= \lambda \mathbb{E}(S).
\end{aligned} \tag{4.79}$$

Finally, we can obtain the LHS by using a similar manner:

$$\begin{aligned}
&\lambda \mathbb{E}(S) \\
&= \lim_{t\to\infty} \Big\{ \Big(\frac{N(t)}{t} \Big) \Big(\frac{1}{N(t)} \sum_{i=1}^{N(t)} S_i \Big) \Big\} \\
&= \lim_{t\to\infty} \frac{1}{t} \sum_{i=1}^{N(t)} S_i = \lim_{t\to\infty} \frac{1}{t} \sum_{i:D_i \leq t} S_i \\
&\leq \lim_{t\to\infty} \frac{1}{t} \int_0^t L(u)du = \mathbb{E}(L).
\end{aligned} \tag{4.80}$$

Hence $\lambda \mathbb{E}(S) \leq \mathbb{E}(L) \leq \lambda \mathbb{E}(S)$. This implies $\lambda \mathbb{E}(S) = \mathbb{E}(L)$ and proves the theorem. □

To determine the expected waiting time for a vehicle in the queue, $\mathbb{E}(W)$, using the expected number of vehicles in the approach, $\mathbb{E}(L_q)$, one should apply the alternative version of Little's Law.

Theorem 2 (Alternative Version of Little's Law)**.** *In a queueing system, let $\mathbb{E}(L_q)$ denote the expected number of customers in the queue, excluding the one in service, $\mathbb{E}(W)$ the expected waiting time of a customer until he or she get served, and λ the average arrival rate to the system. If the system is stable, meaning there exists a steady state, then*

$$\mathbb{E}(L_q) = \lambda \mathbb{E}(W). \tag{4.81}$$

Proof. Let B denote the service time in a queueing system. Then $\rho := \lambda \mathbb{E}(B)$ is the utilization of the system, hence representing the probability that the server is busy. Moreover

$$\rho = 1 \cdot \rho + 0 \cdot (1 - \rho) \tag{4.82}$$

is also the expected number of customers in service. By Little's Law

$$\mathbb{E}(L) = \lambda \mathbb{E}(S). \tag{4.83}$$

Subtracting ρ in both sides, we can get

$$\begin{aligned} \mathbb{E}(L_q) &= \mathbb{E}(L) - \rho \\ &= \lambda \mathbb{E}(S) - \rho \\ &= \lambda \mathbb{E}(S) - \lambda \mathbb{E}(B) \\ &= \lambda (\mathbb{E}(S) - \mathbb{E}(B)) \\ &= \lambda \mathbb{E}(W), \end{aligned} \tag{4.84}$$

where we use the fact that sojourn time is the sum of waiting time and service time. □

4.3. Parameter Values

The values of the parameters to be used in the control model and the $M/G/1/k$ queueing model are presented in Tabs. 4.1 and 4.2. It should be noted that, in the $M/G/1/k$ queueing model, when deriving the expected sojourn time $\mathbb{E}(S)$, we use the notation λ to represent the arrival rate on each leg as a general notation. However, when calculating $\mathbb{E}(S)$ at different arrival rates, the values of λ_1, λ_2, λ_3, and λ_4 will be used.

Parameter	Definition	Value	Reference
λ_1	arrival rate on all legs	$200pcu/h$	[19]
λ_2	arrival rate on all legs	$400pcu/h$	[19]
λ_3	arrival rate on all legs	$600pcu/h$	[19]
λ_4	arrival rate on all legs	$800pcu/h$	[19]
a_{max}	maximal acceleration on all legs	$3.6m/s^2$	Default Values from Vissim
a_{min}	minimal acceleration on all legs	$-3.6m/s^2$	Default Values from Vissim
v_{max}	maximal speed on all legs	$50km/h$	Speed Limit Rules in Dutch Cities
v_r	maximal speed on the circulating road	$30km/h$	Speed Limit Rules in Dutch Cities
d_{safe}	safety distance	$2m$	Default Values from Vissim
x_0	control zone distance on all legs	$100m$	Designated
t_F	follow-on time	$1.12s$	[15]
t_C	critical gap	$2.24s$	[15]
VL	vehicle length	$4.76m$	Default Values from Vissim
C_L	leg capacity within the control zone	17	$\lfloor \frac{x_0}{VL+d_{\text{safe}}} \rfloor$
Δt	time step	$0.1s$	Designated

Table 4.1: Parameter values in the control model.

Parameter	Definition	Value	Reference
λ_1	arrival rate on all legs	$200pcu/h$	[19]
λ_2	arrival rate on all legs	$400pcu/h$	[19]
λ_3	arrival rate on all legs	$600pcu/h$	[19]
λ_4	arrival rate on all legs	$800pcu/h$	[19]
t_C	critical gap	$3.15s$	[15]
k	system capacity	17	The Same as C_L

Table 4.2: Parameter values in the $M/G/1/k$ queueing model.

5

Headway Time Data Analysis

To approximate the expected sojourn time in our $M/G/1/k$ queueing model, which represents the average time a vehicle spends traveling from entering the control zone to merging into the roundabout, we first approximate the blocking probability p_k using Eq. (4.65). Then, we use Eq. (4.66) to estimate the expected number of vehicles in the system, $\mathbb{E}(L)$. Finally, by applying Little's Law, we calculate the expected sojourn time, $\mathbb{E}(S)$, as:

$$\mathbb{E}(S) = \frac{\mathbb{E}(L)}{\lambda},$$

where λ is the arrival rate of vehicles. The key element in this approximation is the coefficient of variation of the service time, which can be calculated using the first and second moments of the service time. These moments can be estimated empirically from the service time data. It should be noted that in the simulation software, the service time can only be estimated by subtracting the time when the vehicle's tail crosses the entry line from the time when the vehicle's head crosses the entry line, and further subtracting the time obtained by dividing the vehicle length by the speed at which it enters the roundabout. However, in realistic driving scenarios, not all vehicles enter the roundabout at a constant speed (some vehicles might accelerate or decelerate to enter the roundabout), making this estimation less accurate. Nevertheless, as discussed in Sec.4.2, even if the service time is not explicitly known, these moments can still be obtained from the distribution of the headway time within the roundabout (see Eqs.(4.39) and (4.51)). Therefore, the goal of this section is to determine the distribution and its parameters for the headway time in the circulating stream.

5.1. Data Sources

Vissim, developed by the PTV Group, stands for **"Verkehr In Städten-Simulation"**, which translates to **"Traffic In Cities-Simulation"** in English. It is a comprehensive and widely used microscopic traffic simulation software that simulates and analyzes various types of traffic flow, including urban streets, highways, intersections, and roundabouts.

The headway time data in the circulating stream of a single-lane roundabout was derived from Vissim simulations to model the scenario of human-driven vehicles entering and exiting a single-lane roundabout. In this simulation, vehicles arrive at each leg according to a Poisson Process with rates of 200, 400, 600, and $800pcu/h$, respectively, over a duration of 3600 seconds. It should be noted that he distribution of headway time in the circulating stream is evidently highly dependent on the arrival rate. Higher arrival rates tend to result in shorter headway times, and vice versa. The difference in each arrival rate is set at $200pcu/h$. This is because, when analyzing the distribution of circulating headway times, Li et al.[19] classified the headway time distribution in increments of $200pcu/h$ and observed that each $200pcu/h$ increase could result in significant differences in the distribution or its parameters. In

other words, with each $200pcu/h$ increase in the arrival rate, either the distribution of the headway time changes or the parameters within the same parametric distribution family are altered.

The maximum arrival rate of $800pcu/h$ per leg was chosen because, at this rate, by 2000 seconds of simulation time, the number of vehicles within the control zone on the right leg reaches its capacity. This capacity represents the maximum number of vehicles that can travel on the leg of the control zone while maintaining a safe distance between each other, given by:

$$C_l = \left\lfloor \frac{x_0}{L + d_{\text{safe}}} \right\rfloor = 17,$$

if $x_0 = 100$, $L = 4.76$, and $d_{\text{safe}} = 2$ meters.

5.2. Distributions of the Circulating Stream Headway Time

To find an appropriate distribution that fits the circulating headway time data, we will begin by creating histograms to provide an initial estimate. Next, we will calculate the descriptive statistics for the data, followed by determining the estimators based on different classes of distributions (shifted exponential, Erlang-k, M3, and lognormal). Additionally, we will conduct a Kolmogorov-Smirnov (K-S) test to evaluate the goodness of fit for each distribution. If more than one distribution fits the data set, we will calculate the AIC or BIC values to determine the best-fitting distribution.

5.2.1. Histograms and Descriptive Statistics

To provide an initial estimate of the distribution of circulating stream headway times under different arrival rates, we plot the corresponding histograms and analyze the potential distribution types. The histograms are presented in Figs.5.1 and 5.2. The shapes of the histograms for arrival rates at 200 and $400pcu/h$ appear to resemble shifted exponential distributions, whereas those for arrival rates at 600 and $800pcu/h$ exhibit a lognormal-like shape. However, distinguishing between the density shapes of the M3 and shifted Erlang-k distributions is not straightforward. To further determine the most appropriate distributions, we will perform the Kolmogorov-Smirnov (K-S) tests. It should be noted that the power of the K-S test depends on the number of observations. If the distribution under the null hypothesis of the K-S test does not exactly match the data distribution, the p-value will converge to 0 as the number of observations approaches infinity. However, the number of observations for these arrival rates is not too large, with a maximum of 368, making the K-S test a feasible choice in our case.

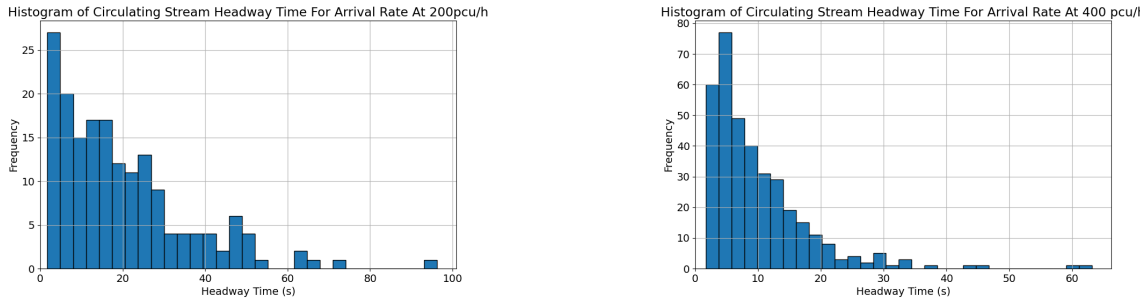

(a) $200pcu/h$ **(b)** $400pcu/h$

Figure 5.1: Histogram of the circulating stream headway time for arrival rates at 200 and $400pcu/h$.

The descriptive statistics for the circulating stream headway time at various arrival rates are shown in Table 5.1. These statistics highlight important trends in vehicle behavior. As the arrival rate increases, the number of observations rises accordingly, ranging from 175 at $200pcu/h$ to 368 at $800pcu/h$. This increase reflects the higher frequency of vehicles passing through the system as traffic volumes grow. However, at arrival rates of 400, 600, and $800pcu/h$, the count values remain relatively stable, indicating that the roundabout may have reached its capacity. Based on the observation from Vissim simulation, this suggests that the legs of the roundabout are likely saturated at these arrival rates, and the number

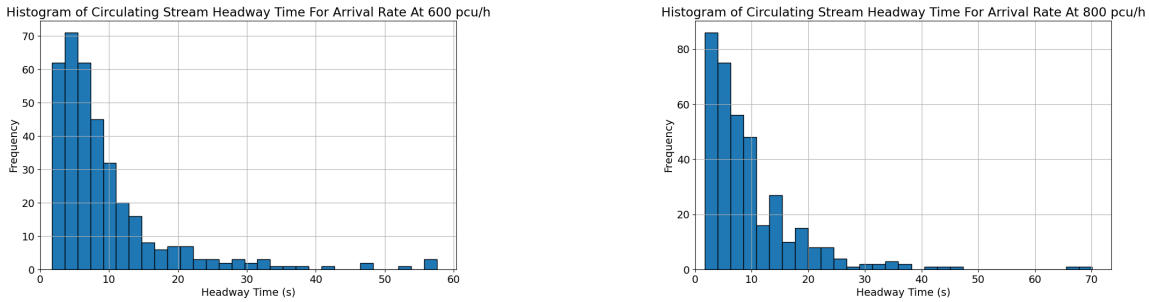

(a) $600pcu/h$ **(b)** $800pcu/h$

Figure 5.2: Histogram of the circulating stream headway time for arrival rates at 600 and $800pcu/h$.

Arrival Rate (pcu/h)	**200**	**400**	**600**	**800**
Count	175	362	362	368
Mean (s)	19.84	9.94	9.51	9.64
Std (s)	16.10	8.15	8.89	8.72
Min (s)	1.71	1.70	1.71	1.71
Q1 (s)	7.33	4.41	4.31	4.16
Q2 (s)	15.99	7.57	6.92	7.00
Q3 (s)	26.35	13.02	10.92	12.57
Max (s)	96.18	63.16	57.58	70.09

Table 5.1: Descriptive statistics of the circulating stream headway time at different arrival rates.

of vehicles entering the roundabout has reached the roundabout's capacity (referring to how many vehicles the roundabout can handle per unit time).

The mean headway time decreases as the arrival rate increases. For instance, at $200pcu/h$, the mean is 19.84 seconds, while at $800pcu/h$, it drops to 9.64 seconds. This aligns with the expectation that as traffic volume increases, the time intervals between consecutive vehicles reduce. However, at an arrival rate of $800pcu/h$, the mean is slightly higher than that at $600pcu/h$, where the mean is 9.51 seconds. This increase could be attributed to the presence of outliers, as indicated by the higher maximum value observed at $800pcu/h$ compared to $600pcu/h$.

The standard deviation of headway time also shows a decreasing trend as the arrival rate increases. For instance, it drops from 16.10 seconds at $200pcu/h$ to 8.72 seconds at $800pcu/h$. This reduction in variability can be explained by the fact that with more vehicles circulating in the roundabout, the freedom of movement for each individual vehicle decreases, leading to more consistent headway times. Additionally, at arrival rates of 400, 600, and $800pcu/h$, the standard deviation values are relatively close (8.15, 8.89, and 8.72 seconds, respectively). This suggests that at these arrival rates, the headway time becomes less variable, reflecting a more stable and consistent flow of traffic within the roundabout.

The minimum headway time remains relatively stable across all arrival rates, with values ranging from 1.70 to 1.71 seconds, indicating that the shortest time intervals between consecutive vehicles do not change significantly as traffic increases. Quartile values, however, show a clear decreasing trend. The first quartile (Q1) drops from 7.33 seconds at $200pcu/h$ to 4.16 seconds at $800pcu/h$, while the median (Q2) decreases from 15.99 seconds to 7.00 seconds over the same range, reflecting shorter intervals between vehicles as traffic volumes grow. Similarly, the third quartile (Q3) declines from 26.35 seconds at $200pcu/h$ to 12.57 seconds at $800pcu/h$. These consistent reductions in quartile values indicate that as arrival rates increase, headway time becomes shorter and more compressed, reflecting a denser flow of traffic through the roundabout. This observation is quite natural, as higher arrival rates typically lead to increased traffic density, thereby reducing the gaps between vehicles. As more vehicles attempt to enter the roundabout, the available space between consecutive cars decreases, resulting in shorter headway times.

The maximum headway time shows notable fluctuations across different arrival rates. At $200pcu/h$,

the maximum headway time is 96.18 seconds, significantly higher than the values observed at other arrival rates. This large gap likely reflects the lower traffic density, where fewer vehicles pass through the system, leading to longer intervals between consecutive vehicles. As the arrival rate increases, the maximum headway time decreases, reaching 57.58 seconds at $600pcu/h$. However, an interesting observation is made at $800pcu/h$, where the maximum headway time rises slightly to 70.09 seconds. This increase, despite the higher arrival rate, could be attributed to the extended periods of vehicles' queueing time at the legs of the roundabout. The instability of the maximum headway time is natural, given that maximum values are particularly sensitive to outliers and unusual traffic conditions, which can be influenced by driver behavior, temporary delays, or other random factors. Consequently, maximum headway times tend to be less consistent compared to average or quartile measures.

5.2.2. Maximum Likelihood Estimators

After analyzing the datasets and their descriptive statistics in Section 5.2.1, this section focuses on determining the Maximum Likelihood Estimators (MLE) of the circulating stream headway time for each arrival rate (200, 400, 600, and $800pcu/h$). These estimators will be calculated under the assumptions that the headway time follows shifted exponential, M3, Erlang-k, and lognormal distributions respectively.

An important assumption in calculating the MLE is that the data is independently and identically distributed (i.i.d). The headway time in the circulating stream is defined as the time interval between the point at which one vehicle passes a specific reference point inside the roundabout and when the next vehicle passes the same reference point. In a situation that the traffic situation is not too crowded inside the roundabout, if we have three vehicles inside the roundabout, we can observe two headway times, t_1 and t_2. In principle, t_1 is influenced by the behavior of the second vehicle, while t_2 largely depends on the third vehicle. Thus, the circulating headway times can be considered approximately i.i.d. if the traffic condition inside the roundabout is not too crowded, making the calculation of MLE a feasible approach in our situation.

Assuming A Shifted Exponential Distribution

As discussed in Section 2.5, if the headway time follows a shifted exponential distribution, we can utilize Equations (2.5) and (2.6) to calculate the estimators. Under the assumption that the headway time is shifted exponentially distributed, the cumulative distribution function and density function are given by:

$$F(t) = 1 - e^{-\lambda(t-t_M)}, \quad t > t_M, \tag{5.1}$$

$$f(t) = \lambda e^{-\lambda(t-t_M)}, \; t > t_M. \tag{5.2}$$

Examples of the shifted exponential density functions with different parameters are presented in Fig.5.3. The estimated values of $\hat{t}_M$ for various arrival rates are 1.71, 1.70, 1.71, and 1.71, respectively. The estimated values of $\hat{\lambda}$ for these stream rates are 0.0552, 0.1214, 0.1281, and 0.1260, respectively.

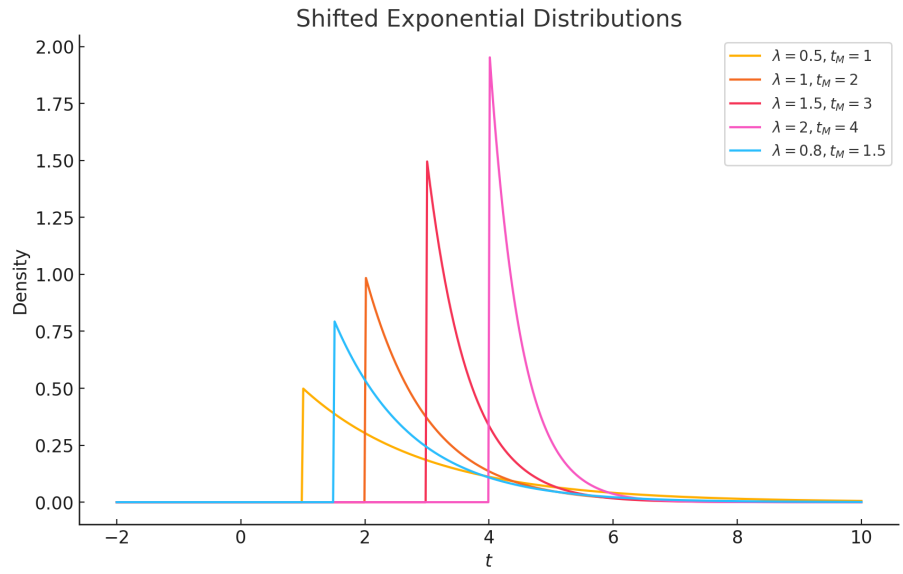

Figure 5.3: Examples of shifted exponential density functions with different parameters.

Assuming an M3 Distribution

If the headway time follows an M3 distribution, it is defined by the distribution function:

$$F(t) = \left(1 - \alpha e^{-\lambda(t-t_M)}\right) u(t - t_M), \tag{5.3}$$

where the unit step function $u(t - t_M)$ is given by:

$$u(t - t_M) = \begin{cases} 1 & \text{if } t \geq t_M, \\ 0 & \text{if } t < t_M. \end{cases} \tag{5.4}$$

Then density function of this distribution is defined as:

$$f(t) = (1 - \alpha)\delta(t - t_M) + \alpha\lambda e^{-\lambda(t-t_M)} u(t - t_M), \tag{5.5}$$

where $\delta(t - t_M)$ is the Dirac delta function:

$$\delta(t - t_M) = \begin{cases} \infty & \text{if } t = t_M \\ 0 & \text{otherwise} \end{cases}, \tag{5.6}$$

with

$$\int_0^\infty \delta(t - t_M)dt = 1. \tag{5.7}$$

Here:

- $\alpha \in (0, 1]$ is the proportion of free vehicles((non-clustered traffic).
- $t_M \in \mathbb{R}$ is the minimum headway time maintained between vehicles when they are traveling in platoon formations.
- $\lambda > 0$ is a parameter.

To avoid the trouble caused by the Dirac delta function, the alternative form of the M3 density is expressed as:

$$f(t) = \frac{dF}{d\mu}(t) = \lambda\alpha e^{-\lambda(t-t_M)} \mathbb{1}_{(t_M,\infty)}(t) + (1 - \alpha)\mathbb{1}_{\{t_M\}}(t). \tag{5.8}$$

Fig.5.4 shows some examples of the density functions of M3 distributions with different parameters. It should be noted that The density functions of the M3 distribution and the shifted exponential distribution look similar because they share a similar mathematical structure. Both involve an exponential decay starting at a threshold t_M. The difference is that the M3 distribution adds a scaling factor α to the exponential decay.

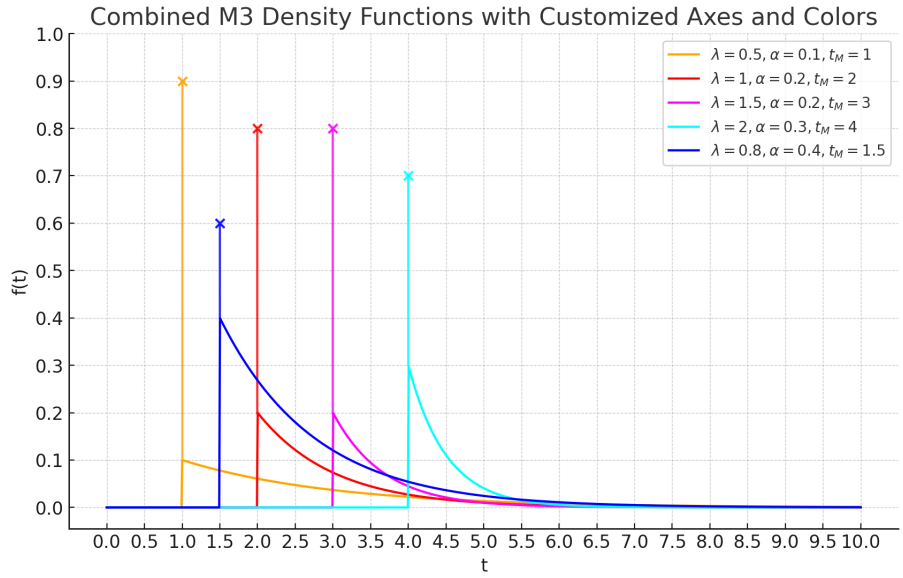

Figure 5.4: Examples of M3 density functions with different parameters.

To estimate t_M, one can either apply the Maximum Likelihood Estimation (MLE) method as in Equation (2.15) or refer to Table 2.1. The parameter λ can be estimated using the MLE method as in Equation (2.21). To estimate α, one can use either the MLE method described in Equation (2.26) or the relationship:

$$\alpha = e^{-\beta t_M q}, \tag{5.9}$$

where q is the flow rate in pcu/s, and β can be found in Table 2.1. For simplicity, we restrict ourselves to the MLE method. The estimated values of $\hat{t}_M$ for various arrival rates are 1.71, 1.70, 1.71, and 1.71, respectively. The estimated values of $\hat{\lambda}$ are 0.0548, 0.1177, 0.1235, and 0.1216, respectively. The estimated values of $\hat{\alpha}$ are 0.9943, 0.9696, 0.9641, and 0.9647, respectively.

Assuming a Shifted Erlang-k Distribution

If the headway time follows a shifted Erlang-k distribution, then distribution and density functions are described by:

$$F(t) = 1 - \sum_{j=0}^{k-1} \frac{\lambda^j (t - t_M)^j}{j!} e^{-\lambda(t - t_M)}, \quad t > t_M, \tag{5.10}$$

$$f(t) = \lambda \frac{(\lambda t)^{k-1}}{(k-1)!} e^{-\lambda t}, \; t > 0, \tag{5.11}$$

Examples of the density functions of this distribution can be seen in Fig.5.5.

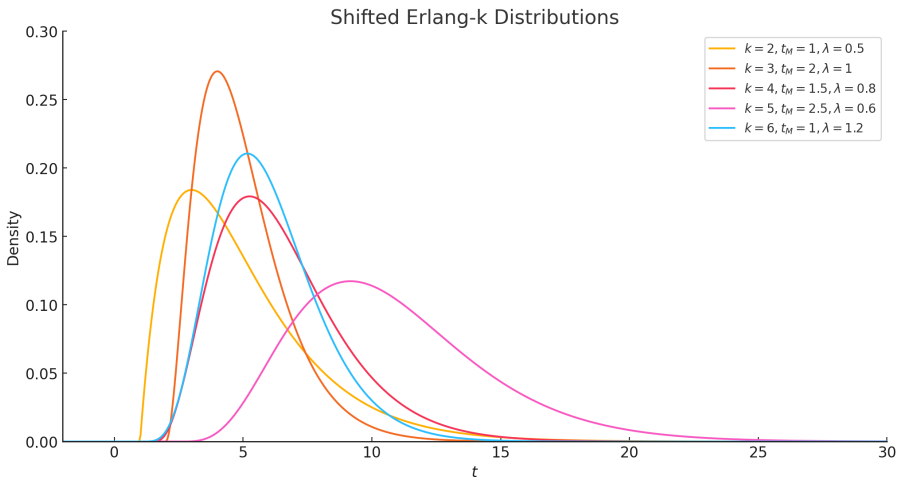

Figure 5.5: Examples of shifted Erlang-k density functions with different parameters.

The parameter t_M can be estimated using the MLE method described in Equation (2.37). To estimate $(\hat{\lambda}, \hat{k})$, one can either use the MLE method as described in Equation (2.40) or the following described estimator:

$$(\hat{\lambda}, \hat{k}) = \underset{\lambda=\lambda_{MM}, k\in\mathbb{Z}^+}{\operatorname{argmin}} \left\{ \left(\frac{k}{\lambda} + t_{(1)} - \bar{t} \right)^2 + \left(\frac{k}{\lambda^2} - s^2 \right)^2 \right\}, \tag{5.12}$$

where

$$\lambda_{MM} = \frac{\bar{t} - t_{(1)}}{s^2} \tag{5.13}$$

is the Method of Moments estimator. In practice, the value of k is typically 2 or 3 [5].

Using the MLE method and restricting k to $k \in \{1, 2, 3\}$, the estimated values of $\hat{t}_M$ for various flow rates are 1.71, 1.70, 1.71, and 1.71, respectively. The estimated values of $(\hat{\lambda}, \hat{k})$ for these flow rates are $(0.0552, 1)$, $(0.1214, 1)$, $(0.1281, 1)$, and $(0.1260, 1)$, respectively.

Assuming a Lognormal Distribution

If the headway time follows a lognormal distribution, the distribution function is given by:

$$F(t) = \Phi\left(\frac{\log t - \mu}{\sigma} \right), \quad t > 0, \tag{5.14}$$

where $\Phi(\cdot)$ denotes the cumulative distribution function (cdf) of the standard normal distribution. The density function of lognormal is given by:

$$f(t) = \frac{1}{t\sigma\sqrt{2\pi}} exp\Big(- \frac{(logt - \mu)^2}{2\sigma^2} \Big), \; t > 0. \tag{5.15}$$

Some examples of the density functions following Lognormal distributions with different parameters are presented in Fig.5.6.

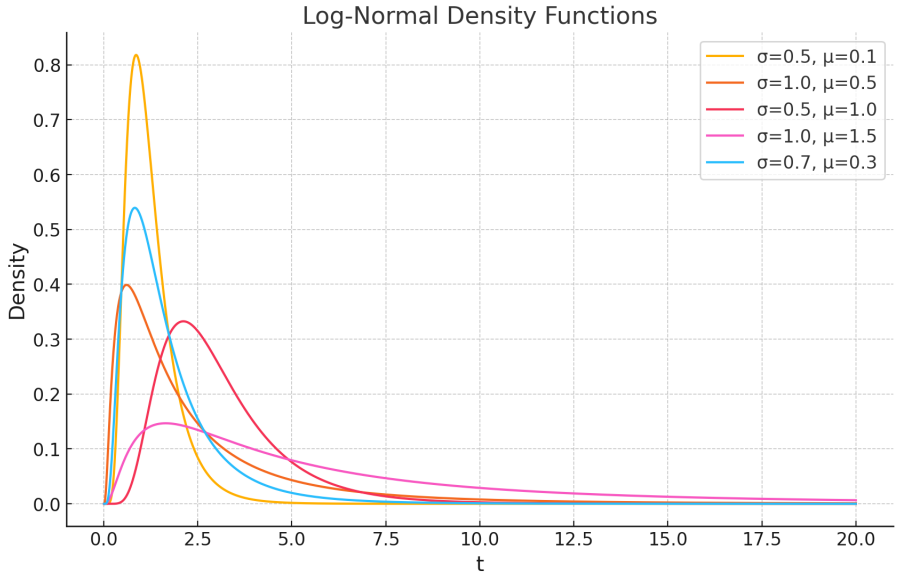

Figure 5.6: Examples of lognormal density functions with different parameters.

The estimators $(\hat{\mu}, \hat{\sigma}^2)$ can be obtained using either the Maximum Likelihood Estimation (MLE) method, as described in Equations (2.52) and (2.53), or the Method of Moments (MM) method, as described in Equations (2.54) and (2.55).

Using the MLE method, the estimators $(\hat{\mu}, \hat{\sigma}^2)$ for different circulating flow rates are found to be $(2.6347, 0.8162)$, $(2.0306, 0.5298)$, $(1.9584, 0.5495)$, and $(1.9659, 0.5841)$, respectively.

Summary of the Estimators

A summary of the Maximum Likelihood Estimators (MLEs) for circulating headway time under different distribution assumptions at various arrival rates is presented in Tab.5.2. First, the estimator $\hat{t}_M$ under the shifted exponential, M3, and shifted Erlang-k distributions is identical, being the minimum value of the observed data. This explains why $\hat{t}_M$ is the same across these distributions for the same arrival rates.

Furthermore, the estimators $\hat{k}$ under the shifted Erlang-k distribution are equal to 1 for all arrival rates. Notably, the other two estimators, $\hat{t}_M$ and $\hat{\lambda}$, are identical to those under the shifted exponential distribution. This occurs because when $k = 1$, the shifted Erlang distribution simplifies to the shifted exponential distribution.

Additionally, in the M3 distribution, the values of $\hat{\alpha}$ is close to 1 for all arrival rates. It is important to note that when $\alpha = 1$, all vehicles move freely (without clustering), and the headway time follows a shifted exponential distribution, or equivalently, a shifted Erlang-1 distribution, as shown in Eq.(5.3). This explains why, for the same arrival rates, the values of $\hat{\lambda}$ under the M3 distribution are similar to those under the shifted exponential and shifted Erlang-1 distributions.

Moreover, for arrival rates of 400, 600, and $800pcu/h$, the estimators are quite similar within the same distribution. This may be due to the fact that for arrival rates greater than $400pcu/h$, at least one leg of the roundabout becomes saturated, leading to the roundabout reaching its capacity. As a result, the situation of vehicles inside the roundabout or the time gaps between consecutive vehicles remains relatively stable. On top of that, for the same arrival rate, the similarity in estimator values between the shifted exponential, M3 with α close to 1, and shifted Erlang-1 distributions supports the correctness of the MLEs.

However, comparing the estimators from the lognormal distribution with those from the shifted exponential, M3, or shifted Erlang-k distributions is not meaningful, as the density function of the lognormal distribution does not have a clear relationship with those of the other three distributions. It is not immediately evident whether the circulating headway time follows a lognormal distribution for a given arrival

rate. Therefore, a Goodness-of-Fit test will be necessary for further analysis.

	Arrival Rate (pcu/h)			
Assumed Distribution and Parameters	**200**	**400**	**600**	**800**
Shifted Exponential				
$(\hat{t}_M, \hat{\lambda})$	$(1.71, 0.0552)$	$(1.70, 0.1214)$	$(1.71, 0.1281)$	$(1.71, 0.1260)$
M3				
$(\hat{t}_M, \hat{\lambda}, \hat{\alpha})$	$(1.71, 0.0548, 0.9943)$	$(1.70, 0.1177, 0.9696)$	$(1.71, 0.1235, 0.9641)$	$(1.71, 0.1216, 0.9647)$
Shifted Erlang-k				
$(\hat{t}_M, \hat{\lambda}, \hat{k})$	$(1.71, 0.0552, 1)$	$(1.70, 0.1214, 1)$	$(1.71, 0.1281, 1)$	$(1.71, 0.1260, 1)$
Lognormal				
$(\hat{\mu}, \hat{\sigma}^2)$	$(2.6347, 0.8162)$	$(2.0306, 0.5298)$	$(1.9584, 0.5495)$	$(1.9659, 0.5841)$

Table 5.2: Maximum Likelihood Estimators for circulating headway time under different distribution assumptions at various arrival rates.

5.2.3. Goodness of Fit Test

After obtaining the estimators for the circulating headway time under different distribution assumptions at various arrival rates (see Tab.5.2), we can now perform the well-known Kolmogorov-Smirnov (K-S) goodness-of-fit test to determine which distribution best fits the circulating headway time.

The K-S test is a non-parametric test that compares the empirical cumulative distribution function (CDF) of a sample with a hypothesized distribution. The test assesses whether the sample data follows the hypothesized distribution. Recall that the shifted Erlang-k distribution simplifies to the shifted exponential distribution when $k = 1$. Since, for our data, given that the data is shifted Erlang-k distributed, the estimator $\hat{k}$ is 1 across all arrival rates, we will focus the test on determining whether the circulating headway time data follows the shifted exponential, M3, or lognormal distribution for each arrival rate.

Hypothesis

Given a set of independent and identically distributed (i.i.d) observations $t_1, t_2, \ldots, t_n$, the three groups of null hypotheses H_0 and the alternative hypothesis H_1 are:

$$\begin{cases} H_0^{SE} : F \in \mathcal{F}^{SE} = \{F_\theta : \theta \in \Theta\} \\ H_1^{SE} : F \notin \mathcal{F}^{SE} = \{F_\theta : \theta \in \Theta\} \end{cases}, \text{ with } F_\theta(t) = F_{t_M,\lambda}(t) \tag{5.16}$$

$$\begin{cases} H_0^{M} : F \in \mathcal{F}^{M} = \{F_\theta : \theta \in \Theta\} \\ H_1^{M} : F \notin \mathcal{F}^{M} = \{F_\theta : \theta \in \Theta\} \end{cases}, \text{ with } F_\theta(t) = F_{t_M,\lambda,\alpha}(t) \tag{5.17}$$

$$\begin{cases} H_0^{LN} : F \in \mathcal{F}^{LN} = \{F_\theta : \theta \in \Theta\} \\ H_1^{LN} : F \notin \mathcal{F}^{LN} = \{F_\theta : \theta \in \Theta\} \end{cases}, \text{ with } F_\theta(t) = F_{\mu,\sigma^2}(t), \tag{5.18}$$

where the F denote the distribution function of the observations, and SE, M, LN in Eqs.(5.16), (5.17), and (5.18) represent shifted exponential, M3, and lognormal distribution, adapted to the composite hypotheses setting, respectively.

Test Statistic

The test statistic for the K-S tests for the three groups of hypotheses is defined as the infinity norm of the difference between the ecdf $F_n(t)$ (empirical cumulative distribution function) of the sample data and the hypothesized cdf $F_{\hat{\theta}}(t)$. Let KS^{SE}, KS^{M}, and KS^{LN} be the test statistic for the hypothesis test in Eqs.(5.16). (5.17), (5.18), respectively. Then

$$KS^{SE} := \|F_{\hat{\theta}} - F_n\|_\infty = \sup_t |F_{\hat{t}_M,\hat{\lambda}}(t) - F_n(t)|, \tag{5.19}$$

$$KS^{M} := \|F_{\hat{\theta}} - F_n\|_\infty = \sup_t |F_{\hat{t}_M,\hat{\lambda},\hat{\alpha}}(t) - F_n(t)|, \tag{5.20}$$

$$KS^{LN} := \|F_{\hat{\theta}} - F_n\|_\infty = \sup_t |F_{\hat{\mu},\hat{\sigma}^2}(t) - F_n(t)|, \tag{5.21}$$

where $\hat{\theta}$ represents the MLE of the parameter θ based on our sample, and $F_{\hat{\theta}}$ is the CDF with the estimated parameter $\hat{\theta}$. Specifically, for the shifted exponential, M3, and lognormal distributions, the parameter θ corresponds to (t_M, λ), (t_M, λ, α), and (μ, σ^2), respectively, and the MLE $\hat{\theta}$ corresponds to $(\hat{t}_M, \hat{\lambda})$, $(\hat{t}_M, \hat{\lambda}, \hat{\alpha})$, and $(\hat{\mu}, \hat{\sigma}^2)$, respectively. The values of $\hat{\theta}$ are provided in Tab.5.2.

Bootstrap Procedure for p-value Approximation

The p-value is approximated using a bootstrap procedure as follows:

1. **Compute the test statistic:**
   (a) Compute the MLE $\hat{\theta}$ based on the original data $t_1, t_2, \ldots, t_n$ for each type of distribution in the parametric family, which has already been done in Sec.5.2.2. (See Tab.5.2 for detail).
   (b) Compute the K-S test statistics $|F_{\hat{\theta}} - F_n\|_\infty$ in Eqs.(5.19) (5.20), and (5.21) (See Tab.5.3 for KS statistics in different distribution hypotheses).

Arrival Rate (pcu/h)	**200**	**400**	**600**	**800**
KS^{SE}	0.0604	0.0594	0.0628	0.0493
KS^{M}	0.0609	0.0779	0.0755	0.0496
KS^{LN}	0.0733	0.0325	0.0345	0.0320

Table 5.3: K-S Statistics for different types of distributions under different arrival rates.

   In Tab.5.3, for each arrival rate, the K-S statistics under the M3 distribution and the shifted exponential distribution do not have a big difference. This is because, for each arrival rate, the estimator $\hat{\alpha}$ under the M3 distribution is close to 1, the estimator $\hat{t}_M$ is identical to that in the shifted exponential distribution, and the estimator $\hat{\lambda}$ is similar to the one in the shifted exponential distribution. However, for arrival rates of 400, 600, and $800pcu/h$, the K-S statistic for the lognormal distribution is much smaller than that for the M3 or shifted exponential distributions. This suggests that the approximated p-value (which will be explained later) for the lognormal distribution may be larger than that for the other two distributions.
2. **Generate bootstrap samples and compute bootstrap test statistics:** For $j = 1$ to B ($B = 10,000$):
   (a) Draw a bootstrap sample $t'_1, t'_2, \ldots, t'_n$ from the distribution $F_{\hat{\theta}}$. In particular, the bootstrap sample is drawn from the shifted exponential, M3, and lognormal distribution, for the hypothesis tests in (5.16), (5.17), and (5.18), respectively.
   (b) Compute the MLE $\hat{\theta}'$ based on the bootstrap sample drawn from each distribution.
   (c) Compute the K-S statistic for the bootstrap sample:

$$KS_j^{SE'} = \|F_{\hat{\theta}'} - F_n^{SE'}\|_\infty, \tag{5.22}$$

$$KS_j^{M'} = \|F_{\hat{\theta}'} - F_n^{M'}\|_\infty, \tag{5.23}$$

$$KS_j^{LN'} = \|F_{\hat{\theta}'} - F_n^{LN'}\|_\infty, \tag{5.24}$$

where $F_n^{SE'}$, $F_n^{M'}$, and $F_n^{LN'}$ are the ECDFs of the bootstrap sample drawn from the exponential, M3, and lognormal distribution, respectively.

3. **Approximate the p-value:** The $p-$value for each hypothesis test is approximated by:

$$p^{SE} = \frac{1}{B}\sum_{j=1}^{B} \mathbb{1}\{KS_j^{SE'} \geq KS^{SE}\}, \tag{5.25}$$

$$p^{M} = \frac{1}{B}\sum_{j=1}^{B} \mathbb{1}\{KS_j^{M'} \geq KS^{M}\}, \tag{5.26}$$

$$p^{LN} = \frac{1}{B}\sum_{j=1}^{B} \mathbb{1}\{KS_j^{LN'} \geq KS^{LN}\}, \tag{5.27}$$

where $\mathbb{1}\{\cdot\}$ is the indicator function. The results are presented in Table 5.4. In this table, $N^{M3}_{KS'_j \geq KS}$, $N^{SEL}_{KS'_j \geq KS}$, and $N^{LN}_{KS'_j \geq KS}$ denote the number of bootstrap KS statistics that are greater than or equal to the KS statistic from the original data, under the M3, shifted Erlang-k, and lognormal distributions, respectively.

Arrival Rate (pcu/h)	**200**	**400**	**600**	**800**
p^{SE}	0.4176	0.1299	0.0950	0.2930
p^{M}	0.2351	0.0574	0.0662	0.5009
p^{LN}	0.2473	0.7940	0.7275	0.7947

Table 5.4: $p-$values of each hypothesis test under different arrival rates.

As discussed in Tab.5.3, for arrival rates of 400, 600, and $800pcu/h$, the p-value for the lognormal distribution is significantly larger compared to the shifted exponential or M3 distributions. This is because the K-S statistic for the lognormal distribution is considerably smaller than those for the other two distributions and the p-values are approximated by the fraction of K-S statistics from bootstrap samples that are not smaller than the K-S statistic obtained from the original data.

If we consider a significance level of 0.05, the results in Table 5.4 indicate that none of the null hypotheses in tests (5.16), (5.17), and (5.18) should be rejected. In other words, there is sufficient evidence to support the hypotheses that the circulating headway time follows a shifted exponential, M3, or lognormal distribution across all arrival rates should not be rejected. Therefore, we can proceed to select the best-fit distribution for the data across all arrival rates.

Model Selection

Our objective is to select the most accurate model (distribution) among the shifted exponential, M3, and lognormal distributions for the circulating headway time data across all arrival rates (200, 400, 600, and $800pcu/h$). To determine the best model, we will use either AIC or BIC. Both AIC and BIC quantify the quality of a model relative to others by balancing model complexity and maximum likelihood.

As discussed in Sec.2.6, AIC prioritizes predictive accuracy and generally favors more complex models, particularly when the sample size is relatively small, as it imposes a less stringent penalty for additional parameters compared to BIC. Conversely, BIC applies a stricter penalty for model complexity, favoring simpler models, and is particularly useful when the sample size is large. Given that the sample sizes

Arrival Rate (pcu/h)	**200**	**400**	**600**	**800**
AIC-SE	1368.15	2254.61	2215.83	2264.42
AIC-M3	1376.68	2308.41	2275.95	2324.56
AIC-LN	465.08	801.37	814.54	850.49

Table 5.5: AIC values of different distribution models for circulating headway time under different arrival rates.

for the headway time data at these arrival rates are 175, 362, 362, and 368, which are moderate in size, and considering our aim of selecting the best-fit model, we have chosen to use AIC for model selection.

Since we select the model with the smallest AIC value for the circulating headway time at each arrival rate under different models, Tab.5.5 suggests that the lognormal distribution fits the data best across all arrival rates.

The comparison between the histogram of headway time and the corresponding fitted model's density, with MLEs as parameters, is presented in Fig.5.7. It should be noted that in principle, other data (especially the real data) should be used to test our distributions' fitting statuses. Because of the unavailability of the real headway time data, we here use the same data to test the fitting conditions. The figure shows the empirical density of headway time for different arrival rates, overlaid with the fitted lognormal distribution for each case. Each subfigure compares the observed headway time data, displayed as green histograms representing the empirical density, with the theoretical lognormal probability density function (plotted as a blue line). To show how well the lognormal distribution fits the data, we take sub-Figs.5.7a and 5.7c as an example:

- In sub-Fig.5.7a, the fitted lognormal distribution with parameters as MLEs overall provides a good fit to the empirical density. However, some deviations are noticeable. For headway times less than 4 seconds and greater than 35 seconds, the lognormal distribution underestimates the density, predicting fewer very short and very long headway intervals than observed in the empirical data. Between 4 and 15 seconds, the lognormal distribution noticeably overestimates the density, indicating that the model predicts more frequent headway intervals in this range than are present in the actual data. This overestimation can be attributed to the sharper peak of the lognormal curve compared to the flatter empirical density in this region.
- In sub-Fig.5.7c, the fitted lognormal distribution provides a very fit overall, significantly better than in sub-Fig.5.7a. The fit is relatively accurate around the peak, with only very slight deviations observed. However, between 10 and 20 seconds, the lognormal distribution overestimates the density, predicting more headway intervals than the data in this range. In the far right tail, around 56 seconds, the lognormal distribution underestimates the density, failing to capture the larger headway time observed in the empirical data.

Arrival Rate (pcu/h)	**200**	**400**	**600**	**800**
Distribution	Lognormal	Lognormal	Lognormal	Lognormal
Parameter	$(\hat{\mu}, \hat{\sigma}^2)$=$(2.6347, 0.8162)$	$(\hat{\mu}, \hat{\sigma}^2)$= $(2.0306, 0.5298)$	$(\hat{\mu}, \hat{\sigma}^2)$= $(1.9584, 0.5495)$	$(\hat{\mu}, \hat{\sigma}^2)$= $(1.9659, 0.5841)$

Table 5.6: Fitting distributions for the circulating stream headway time at different arrival rates.

To conclude this section, the distribution models, among shifted exponential, M3, and lognormal distributions, that best fit the headway time data are summarized in Table 5.6.

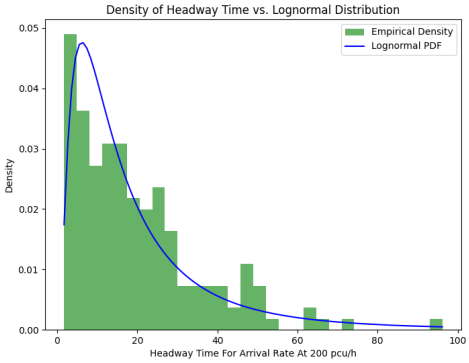

(a) $200pcu/h.$

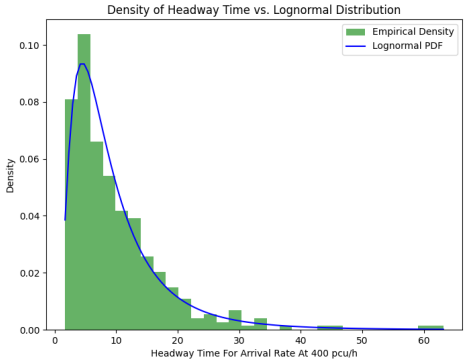

(b) $400pcu/h.$

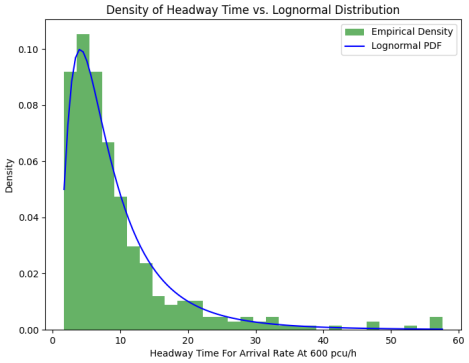

(c) $600pcu/h$

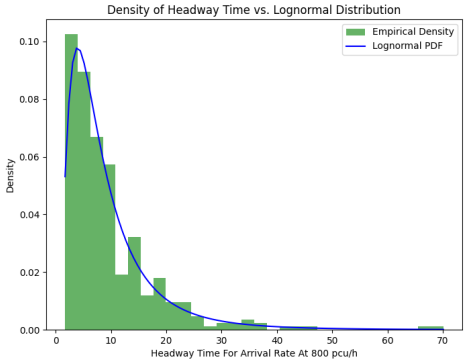

(d) $800pcu/h$

Figure 5.7: Empirical density of headway time vs. lognormal distribution for different arrival rates.

6

Model Evaluation

In the preceding chapters, we explored the mathematical optimization strategies for CAVs and the theoretical foundations for the expected sojourn time under human-driven conditions. Specifically, we developed a microscopic control model to optimize vehicle behavior within the control zone and derive the formulas for finding expected sojourn time under human-driven conditions within the frame of $M/G/1/k$ queueing system. These studies lay the groundwork for understanding how CAVs can be effectively controlled to enhance a single-lane roundabout's efficiency.

This chapter focuses on model evaluation to validate and quantify the proposed control and queueing models. We will conduct a comprehensive analysis involving multidimensional comparisons, including theoretical and observed average sojourn times, the sojourn times between the control model and empirical VISSIM simulation data, and the sojourn times between the control model and the theoretical $M/G/1/k$ queueing model. Additionally, stress tests are performed under high-pressure conditions.

Through these analyses, this chapter aims to provide deeper insights into the performance of the proposed model across various arrival rates and operational scenarios.

6.1. Evaluating the Correctness of the Expected Sojourn Time from the $M/G/1/k$ Queueing Model

In this section, to evaluate the accuracy of the theoretical sojourn time under an uncontrolled scenario with a control zone existing, which is related to **Research Question 3**, we will first calculate the numerical value of the expected sojourn time within the context of the $M/G/1/k$ Queueing Model across different arrival rates (200, 400, 600, and $800 pcu/h$). We will then compare the expected value to the average sojourn time from the Vissim simulation, which represents the simulated average sojourn time under human-driving conditions.

Calculating the Expected Sojourn Time under the $M/G/1/k$ Queueing Model

As derived in Chap. 4.2, knowing the headway time distribution in the circulating stream, analyzed in Chap. 5, allows us to calculate the expected sojourn time $\mathbb{E}(S)$ within the $M/G/1/k$ queueing model. The complete procedure for deriving $\mathbb{E}(S)$ from the headway time distribution in the circulating stream is illustrated in Fig. 6.1.

First, we can use Eqs. (4.39) and (4.53) to calculate the expectation and variance of the service time B, where t_C is chosen to be $3.15s$ based on Fortuijn and Salomons' research[15]. The squared coefficient of variation of the service time C_s^2 is then determined by its definition. Next, the blocking probability p_k is estimated using Eq. (4.65). Following this, the expected number of customers (vehicles) $\mathbb{E}(L)$ is approximated using Eq. (4.66). Finally, the expected sojourn time $\mathbb{E}(S)$ is obtained through Little's Law, as shown in Eq. (4.68).

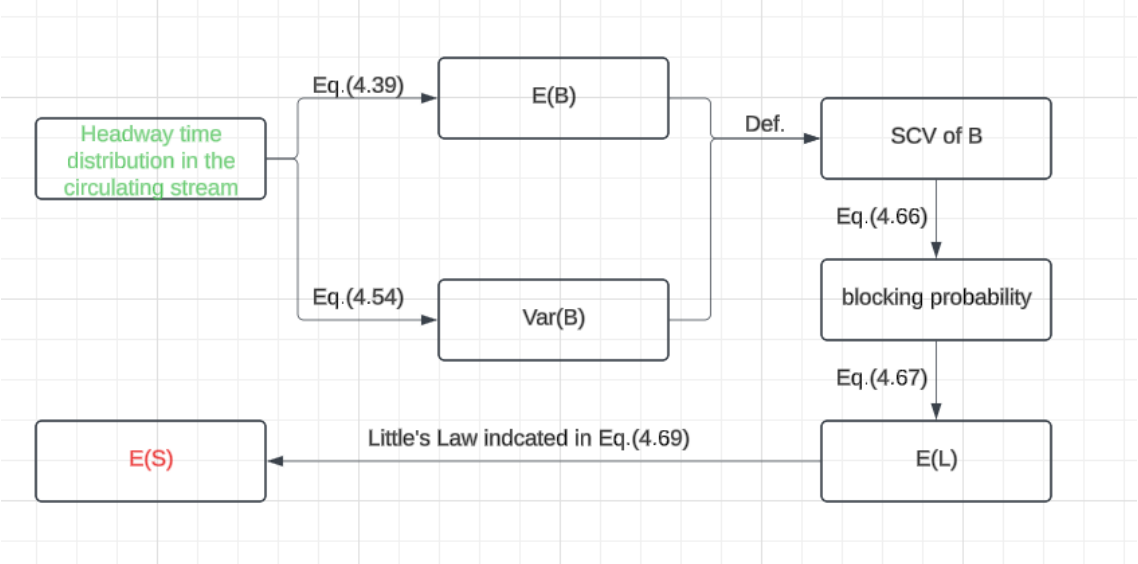

Figure 6.1: Procedure of finding the expected sojourn time.

Across different arrival rates, the numerical values of the above quantities are presented in Tab.6.1. The result can be interpreted as follows:

- $\mathbb{E}(B)$, p_k, $\mathbb{E}(L)$, and $\mathbb{E}(S)$ have an increasing trend as the arrival rate grows. This is reasonable, as higher arrival rates generally lead to more vehicles entering the system, resulting in longer service time, higher blocking probability (probability that an arriving vehicle finds the system is full), longer queues, greater congestion, and higher sojourn time.
- At an arrival rate of $200pcu/h$, $\mathbb{V}ar(B)$ is relatively small (2.17). This is because, at such a low arrival rate, most vehicles are in free-flow state, experiencing relatively consistent and shorter service time. However, when the arrival rate increases to 400, 600, and $800pcu/h$, $\mathbb{V}ar(B)$ rises to the values around 4. This is nearly double the value observed at $200pcu/h$ and can be attributed to the mixed traffic conditions at higher arrival rate. In the beginning, vehicles are in a free-flow state with very short service time. When congestion occurs, the service time becomes significantly large. This explanation aligns well with observations from the Vissim simulation.
- Interestingly, the values of $\mathbb{E}(S)$ under arrival rate 600 and $800pcu/h$ are nearly the same. This may be because, at an arrival rate of $600pcu/h$, the roundabout has already reached a heavily congested situation, almost reaching its limit for handling traffic. As a result, further increases in the arrival rate have less significant impact on $\mathbb{E}(S)$.
- C_s^2 decreases as the arrival rate grows. This trend may be attributed to the fact that, as the number of vehicles increases in the system, the variability in service times becomes relatively smaller compared to the overall scale of the service times. In other words, as congestion increases, service times tend to stabilize around longer durations, reducing the relative variability.

Arrival Rate (pcu/h)	$\mathbb{E}(B)$ (s)	$\mathbb{V}ar(B)$ (s^2)	C_s^2	p_k	$\mathbb{E}(L)$	$\mathbb{E}(S)$ (s)
200	0.51	2.17	8.34	0.01	1.47	26.54
400	0.97	4.03	4.28	0.06	10.58	95.18
600	1.21	4.18	2.88	0.50	34.49	206.92
800	1.73	4.22	1.40	0.54	47.33	213.00

Table 6.1: Numerical values of $\mathbb{E}(B)$, $\mathbb{V}ar(B)$, C_s^2, p_k, $\mathbb{E}(L)$, and $\mathbb{E}(S)$ across different arrival rates under $M/G/1/k$ queueing model.

Comparing $\mathbb{E}(S)$ from the Queueing Model to the One from Vissim Simulation

Let $Avg(S_V)$ denote the average sojourn time for vehicles from entering the control zone to merging into the roundabout in the Vissim simulation. To evaluate the accuracy of $\mathbb{E}(S)$ obtained from the $M/G/1/k$

queueing model, we compare these two values across different arrival rates. Tab.6.2 presents the numerical comparison, where $\frac{|Avg(S_V)-\mathbb{E}(S)|}{Avg_V(S)}$ indicates the extent to which $\mathbb{E}(S)$ deviates from $Avg(S_V)$.

Arrival Rate (pcu/h)	$\mathbb{E}(S)$ (s)	$Avg(S_V)(s)$	$\frac{\lvert Avg(S_V)-\mathbb{E}(S)\rvert}{Avg(S_V)}$
200	26.54	28.23	6%
400	95.18	106.94	11%
600	206.92	232.49	11%
800	213.00	231.52	8%

Table 6.2: Numerical comparison between $\mathbb{E}(S)$ and $Avg_V(S)$ across different arrival rates.

Two interesting results can be analyzed from the above table. Firstly, the values of $\mathbb{E}(S)$ are not exactly the same as $Avg(S_V)$. This discrepancy arises because, on the one hand, $Avg(S_V)$ is a simulation result, so it is not surprising that it differs from the theoretical results. On the other hand, the headway time distribution used in calculating $\mathbb{E}(B)$ and $\mathbb{V}ar(B)$ (Eqs. (4.39) and (4.53)) is an estimated distribution from statistical models rather than the exact distribution. Additionally, the formula for calculating $\mathbb{E}(L)$ (Eq. 4.66) is an approximation.

Secondly, for all arrival rates, $\mathbb{E}(S)$ is smaller than $Avg(S_V)$. This difference occurs because, in the Vissim simulation, the travel time S_V is recorded based on both the traffic situation on the leg and within the roundabout. In contrast, from the queueing perspective, the sojourn time for vehicle n is calculated using the following relationship:

$$S_n = \sum_{i=1}^{n} B_i, \tag{6.1}$$

where B_i only depends on the traffic situation inside the roundabout. Nevertheless, the maximal deviation is 11%, which is acceptable.

6.2. Comparison between Controlled Sojourn Time and Uncontrolled (Vissim) Sojourn Time

As introduced in Chap.3, to partially answer **Research Question 2** — that is, to evaluate the efficiency improvements provided by the control model — we will compare the histograms and descriptive statistics of the controlled sojourn time from the control model with the uncontrolled sojourn time from the Vissim simulation across different arrival rates (200, 400, 600, and $800pcu/h$). The empirical efficiency improvement provided by the control model is quantified by the following equation:

$$\text{efficiency improved} = \frac{\lvert \text{ mean uncontrolled sojourn time} - \text{mean controlled sojourn time } \rvert}{\text{mean uncontrolled sojourn time}}. \tag{6.2}$$

Comparison under an Arrival Rate of $200pcu/h$

At an arrival rate of $200pcu/h$, the histograms of the sojourn time under the control model and uncontrolled simulation are presented in Fig.6.5. As shown in Fig.6.2, the controlled sojourn time is narrowly distributed around a specific central value of roughly about 21s, indicating a high level of consistency and small variability in the controlled scenario. In contrast, the sojourn time from the uncontrolled scenario (Fig.6.3) exhibits a broader spread with a higher mean, suggesting more variability and higher overall sojourn time in the human-driving conditions.

The descriptive statistics of the sojourn time under controlled and uncontrolled scenarios at an arrival rate of $200pcu/h$ are presented in Tab. 6.3. The controlled sojourn time demonstrates remarkable consistency, with a mean of 20.97, an exceptionally small standard deviation of 0.03, and a narrow range from 20.92 to 21.08. This indicates that, as long as the optimization approach described in Sec. 4.1.3 has a feasible solution, all vehicles experience similar sojourn times under the controlled scenario, regardless of the traffic congestion conditions. Conversely, the sojourn time observed in the Vissim

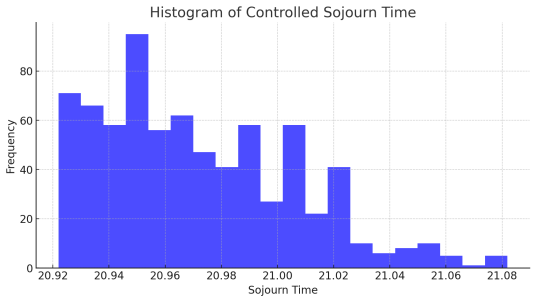

Figure 6.2: (a) Histogram of controlled sojourn time.

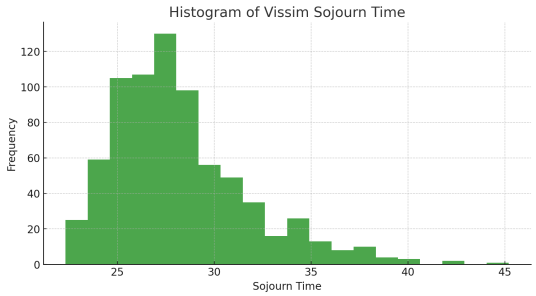

Figure 6.3: (b) Histogram of Vissim sojourn time.

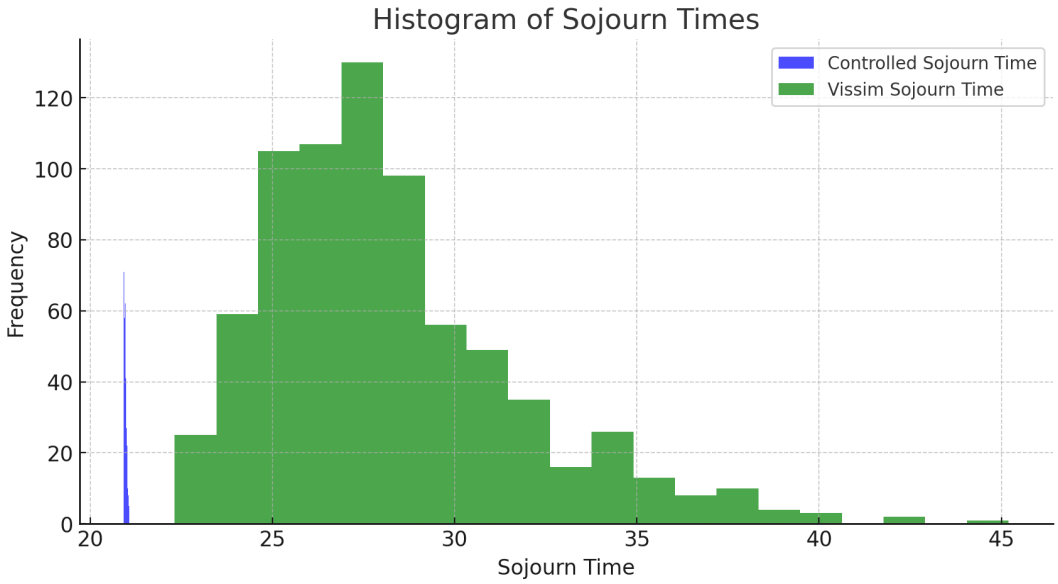

Figure 6.4: (c) Histogram of both controlled and Vissim sojourn time.

Figure 6.5: Histograms of sojourn Time under controlled and uncontrolled (Vissim) scenarios at an arrival rate of $200 pcu/h$.

Statistics	Controlled Sojourn Time	Uncontrolled Sojourn Time
Count	747	747
Mean (s)	20.97	28.23
STD (s)	0.03	3.50
Min (s)	20.92	22.32
Q1 (s)	20.94	25.75
Q2 (s)	20.96	27.62
Q3 (s)	21.00	29.88
Max (s)	21.08	45.20

Table 6.3: Descriptive statistics of the sojourn time under controlled and uncontrolled scenarios at an arrival rate of $200pcu/h$.

simulation exhibits significantly greater variability, with a mean of 28.23 and a standard deviation of 3.50, spanning a range from 22.32 to 45.20. This disparity arises because, at the start of the simulation, only a few vehicles occupy the control zone, resulting in shorter sojourn times. As time progresses and more vehicles attempt to enter the roundabout, the sojourn time increases significantly. Broadly speaking, the control model improves the roundabout's efficiency by approximately $\frac{28.23-20.97}{28.23} \approx 26\%$ under an arrival rate of $200pcu/h$.

Comparison under an Arrival Rate of $400pcu/h$

Fig. 6.9 illustrates notable differences in the sojourn time distributions under controlled and uncontrolled scenarios at an arrival rate of $400pcu/h$. The characteristics of these distributions are consistent with those described in the analysis for an arrival rate of $200pcu/h$. The disparity between the distributions indicates that the control model effectively mitigates delays, while the uncontrolled simulation exhibits greater variability due to increasing congestion over time.

Statistics	Controlled Sojourn Time	Uncontrolled Sojourn Time
Count	1448	1448
Mean (s)	20.91	106.94
STD (s)	0.22	75.28
Min (s)	20.80	24.68
Q1 (s)	20.83	44.00
Q2 (s)	20.86	78.76
Q3 (s)	20.89	151.38
Max (s)	22.64	416.43

Table 6.4: Descriptive statistics of the sojourn time under controlled and uncontrolled scenarios at an arrival rate of $400pcu/h$.

As shown in Tab.6.4, the disparity in the descriptive statistics between controlled and uncontrolled scenarios follows a similar pattern to that discussed for Table 6.3. This similarity arises because the underlying reasons behind the descriptive statistics are roughly the same as those discussed at an arrival rate of $200pcu/h$. It should be noted the control model improves the efficiency of the roundabout by 80% at an arrival rate of $400pcu/h$.

Comparison under an Arrival Rate of $600pcu/h$

The histograms of sojourn time under controlled and uncontrolled scenarios at an arrival rate of $600pcu/h$ are presented in Fig.6.13. As shown in Fig.6.10, the sojourn time is concentrated within a narrow interval, roughly from 21.30 to 23.25, with a higher frequency of values at the head and tail of the range. This suggests that the controlled sojourn time exhibits low variability. In contrast, the Vissim sojourn time, shown in Fig.6.11, spans a wider range. This broader spread may be attributed to increasing congestion over time at this arrival rate.

The descriptive statistics of the sojourn time under controlled and uncontrolled scenarios at an arrival rate of $600pcu/h$ are shown in Tab.6.5. The controlled sojourn time has a mean of 22.08 with a relatively low standard deviation of 0.71, indicating low variability in the sojourn times. The values range from a minimum of 21.32 to a maximum of 23.26, with the inter-quartile range (IQR) between 21.39 (Q1) and

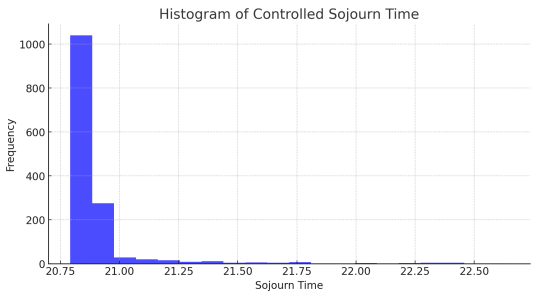

Figure 6.6: (a) Histogram of controlled sojourn time.

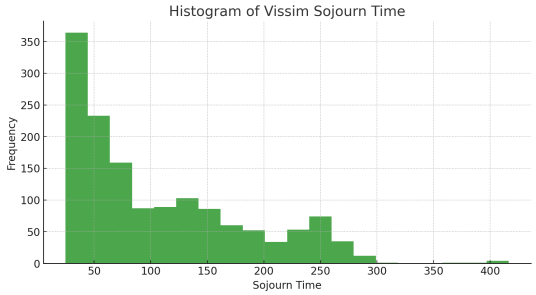

Figure 6.7: (b) histogram of Vissim sojourn time.

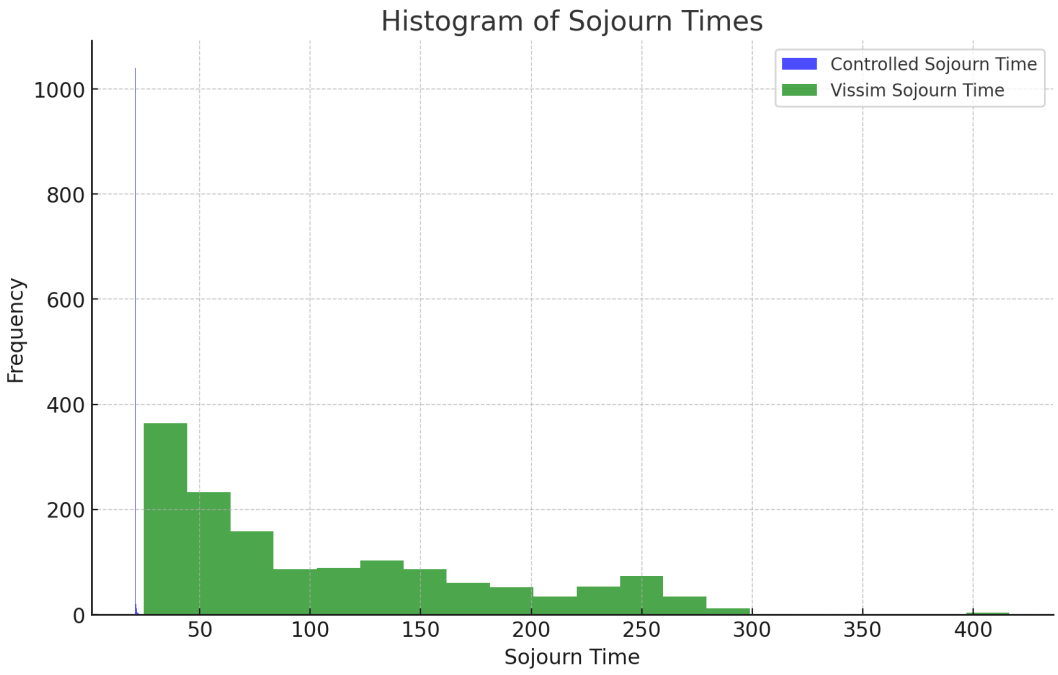

Figure 6.8: (c) Histogram of both controlled and Vissim sojourn time.

Figure 6.9: Histograms of sojourn time under controlled and uncontrolled (Vissim) scenarios at an arrival rate of $400 pcu/h$.

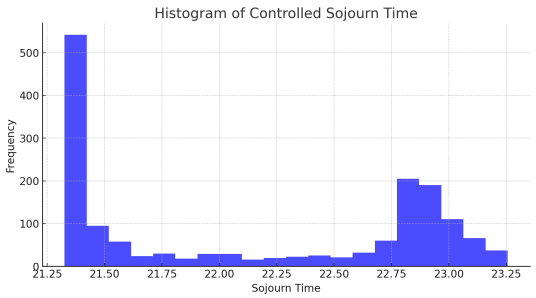

Figure 6.10: (a) Histogram of controlled sojourn time.

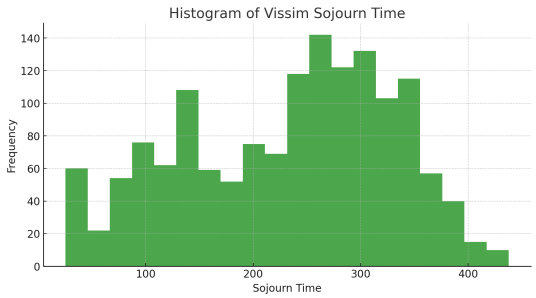

Figure 6.11: (b) Histogram of vissim sojourn time.

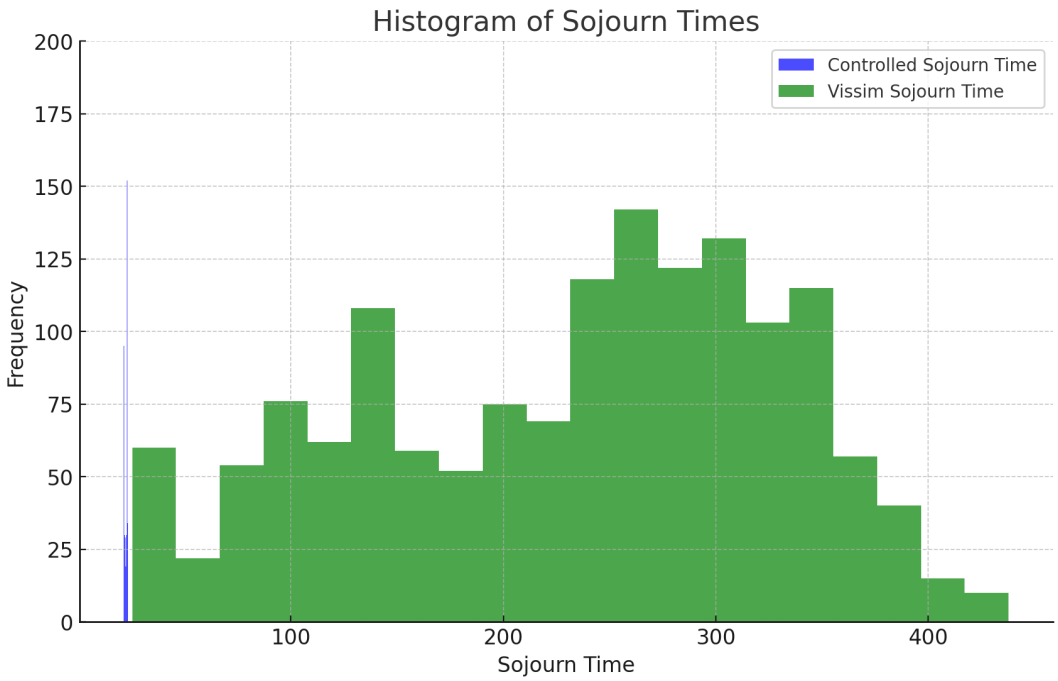

Figure 6.12: (c) Histogram of both controlled and Vissim sojourn time.

Figure 6.13: Histograms of sojourn time under controlled and uncontrolled (Vissim) scenarios at an arrival rate of $600 pcu/h$.

Statistics	Controlled Sojourn Time	Uncontrolled Sojourn Time
Count	1491	1491
Mean (s)	22.08	232.49
STD (s)	0.71	96.65
Min (s)	21.32	25.27
Q1 (s)	21.39	147.75
Q2 (s)	21.80	250.98
Q3 (s)	22.87	306.37
Max (s)	23.26	437.86

Table 6.5: Descriptive statistics of the sojourn time under controlled and uncontrolled scenarios at an arrival rate of $600pcu/h$.

22.87 (Q3). In contrast, the uncontrolled sojourn time exhibits much greater variability, with a mean of 232.49 and a much higher standard deviation of 96.65. The range of values is significantly broader, from a minimum of 25.27 to a maximum of 437.86, with an IQR spanning from 147.75 (Q1) to 306.37 (Q3). This indicates a much larger spread and higher uncertainty in the uncontrolled scenario, with a higher degree of congestion influencing the sojourn time. Notably, the efficiency of the roundabout at this arrival rate is improved at a level of 91% by the control model.

At an arrival rate of $600pcu/h$, the descriptive statistics of the controlled sojourn time are slightly higher than those at an arrival rate of $400pcu/h$. This suggests that the control model can still manage all vehicles efficiently at an arrival rate of $600pcu/h$. In contrast, the descriptive statistics (except for Count) of the uncontrolled sojourn time at this arrival rate are significantly larger than those at $400pcu/h$, with the mean doubling. This indicates that an increase of $200pcu/h$ in the arrival rate from $400pcu/h$ to $600pcu/h$ results in considerable traffic congestion in the uncontrolled scenario.

Comparison under an Arrival Rate of $800pcu/h$

The histograms and the descriptive statistics of the controlled and uncontrolled sojourn time at an arrival rate of $800pcu/h$ are presented in Fig.6.17 and Tab.6.6, respectively. At this arrival rate, the distribution and descriptive statistics of the uncontrolled sojourn time are quite similar to those under an arrival rate of $600pcu/h$. This suggests that an arrival rate of $600pcu/h$ is already quite high for the roundabout. In other words, an arrival rate of $600pcu/h$ already pushes the roundabout to its limit in handling traffic flows, meaning that traffic conditions will not change significantly when increasing the arrival rate from 600 to $800pcu/h$.

Similarly, at an arrival rate of $800pcu/h$, the distribution and descriptive statistics of the controlled sojourn time are nearly the same as those at an arrival rate of $600pcu/h$. This is because the input for the first phase optimization in the control model is collected from the traffic conditions of the Vissim simulation. If the traffic conditions are similar for arrival rates of 600 and $800pcu/h$, the output of the first phase optimization in the control model should not change significantly.

The patterns of the difference between the controlled and uncontrolled sojourn time histograms, as well as between the controlled and uncontrolled sojourn time descriptive statistics, at an arrival rate of $800pcu/h$ are similar to those observed at an arrival rate of $600pcu/h$, with the underlying reasons having been explained previously. The improved efficiency is also similar to that at an arrival rate of $600pcu/h$, at a level of approximately 90%.

Conclusion

After comparing the histograms and descriptive statistics of the controlled and emprically uncontrolled sojourn times (representing the sojourn time in human-driving conditions) across different arrival rates, we conclude the following:

- The control model can effectively mitigate traffic congestion across arrival rates from $200pcu/h$ to $800pcu/h$.
- The controld model significantly improves the efficiency of the single-lane roundabout, especially under high traffic volumes (high arrival rates). At arrival rates of 200, 400, 600, and $800pcu/h$, the efficiency of the roundabout is improved by the control model at a level of 26%, 80%, 91%, and

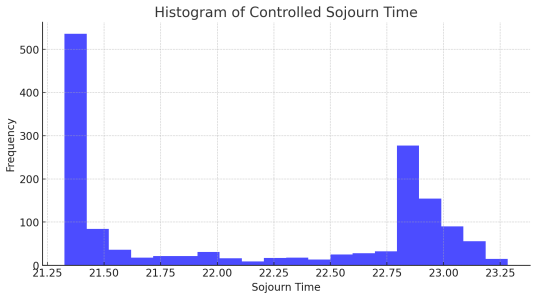

Figure 6.14: (a) Histogram of controlled sojourn time.

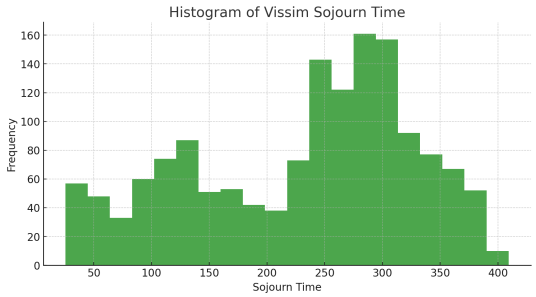

Figure 6.15: (b) histogram of Vissim sojourn time.

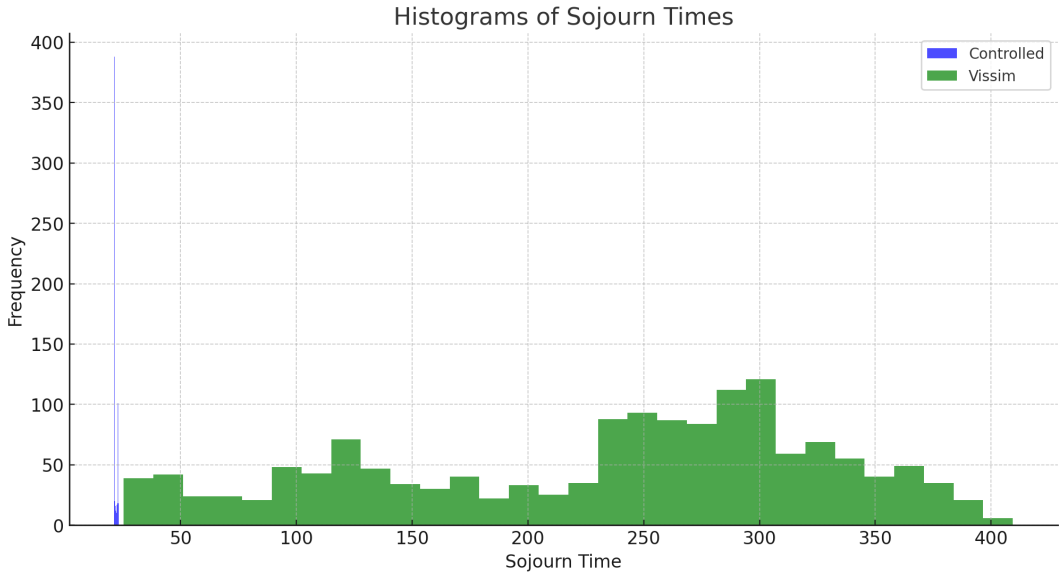

Figure 6.16: (c) Histogram of both controlled and Vissim sojourn time.

Figure 6.17: Histograms of sojourn time under controlled and uncontrolled (Vissim) scenarios at an arrival rate of $800 pcu/h$.

Statistics	Controlled Sojourn Time	Uncontrolled Sojourn Time
Count	1497	1497
Mean (s)	22.15	231.52
STD (s)	0.73	96.85
Min (s)	21.33	25.47
Q1 (s)	21.39	145.12
Q2 (s)	22.03	253.93
Q3 (s)	22.89	302.82
Max (s)	23.28	409.38

Table 6.6: Descriptive statistics of the sojourn time under controlled and uncontrolled scenarios at an arrival rate of $800pcu/h$.

90%, respectively.

6.3. Comparing the Average Traveling Time from the Optimization Model to the One from the $M/G/1/k$ Queueing Model

The theoretical efficiency improvement achieved by the control model can be quantified using a similar method as in Eq.(6.2). The difference is that, for calculating the theoretical efficiency improvement, we use the mean uncontrolled sojourn time from the $M/G/1/k$ queueing model, whereas the empirical efficiency improvement is based on the mean uncontrolled sojourn time from the VISSIM simulation.

Let $\mathbb{E}(S_c)$ denote the mean controlled sojourn time from the control model, and let $\mathbb{E}(S_{uc}^{qk})$ represent the mean uncontrolled sojourn time calculated from the $M/G/1/k$ queueing model. The comparison between the mean controlled and mean uncontrolled sojourn times, as well as the efficiency improvement, are presented in Table 6.7.

Arrival Rate (pcu/h)	$\mathbb{E}(S_c)$ (s)	$\mathbb{E}(S_{uc}^{qk})$ (s)	efficiency improved
200	20.97	25.64	18%
400	20.91	95.18	78%
600	22.08	206.92	89%
800	22.15	213.00	90%

Table 6.7: Comparison between the mean controlled sojourn time and the mean uncontrolled sojourn time from the $M/G/1//k$ queueing model across different arrival rates.

From the data presented in Table 6.7, it is evident that the control model significantly reduces the mean sojourn time compared to the theoretical uncontrol model, as represented by the $M/G/1/k$ queueing model. Specifically:

- At an arrival rate of $200pcu/h$, the control model achieves an 18% efficiency improvement, reducing the mean sojourn time from 25.64 seconds to 20.97 seconds.
- At an arrival rate of $400pcu/h$, the efficiency improvement increases to78%, with the mean sojourn time dropping from 95.18 seconds to 20.91 seconds.
- At an arrival rate of $600pcu/h$, the improvement further rises to 89%, with the sojourn time decreasing from 206.92 seconds to 22.08 seconds.
- At the highest arrival rate of $800pcu/h$, the control model achieves a 90% efficiency improvement, reducing the mean sojourn time from 213.00 seconds to 22.15 seconds.

These results demonstrate the robustness and effectiveness of the control model in significantly enhancing the roundabout's efficiency, particularly under high traffic volumes.

6.4. Pressure Test

As introduced in Chap.3, to complete answering **Research Question 2**, we will conduct a pressure test in this section. Specifically, we will compare the probability that the control zone is full under controlled and uncontrolled scenarios at an extreme arrival rate of $1200pcu/h$. To achieve this, we

assume that the roundabout, with one of its legs, forms an $M/G/1$ Queueing Model. In this model, vehicles arrive according to a Poisson Process, the service time is generally distributed, there is one server in the system (modeled as the first vehicle attempting to enter the roundabout), and the capacity of the queueing system is infinite. One can also imagine a traffic coordinator standing at the entrance of the roundabout, making decisions on whether to allow the first vehicle to enter based on the current traffic conditions.

The organization of this section is presented in Fig.6.18. At an extreme arrival rate of $1200pcu/h$, to determine the probability that the control zone is full under an uncontrolled scenario, we will first derive the PGF (Probability Generating Function) of the number of vehicles in the system, which will be used to calculate the desired probability. Next, we will estimate the probability that the control zone is full under a controlled scenario based on the control model simulation. Finally, we will compare these two probabilities.

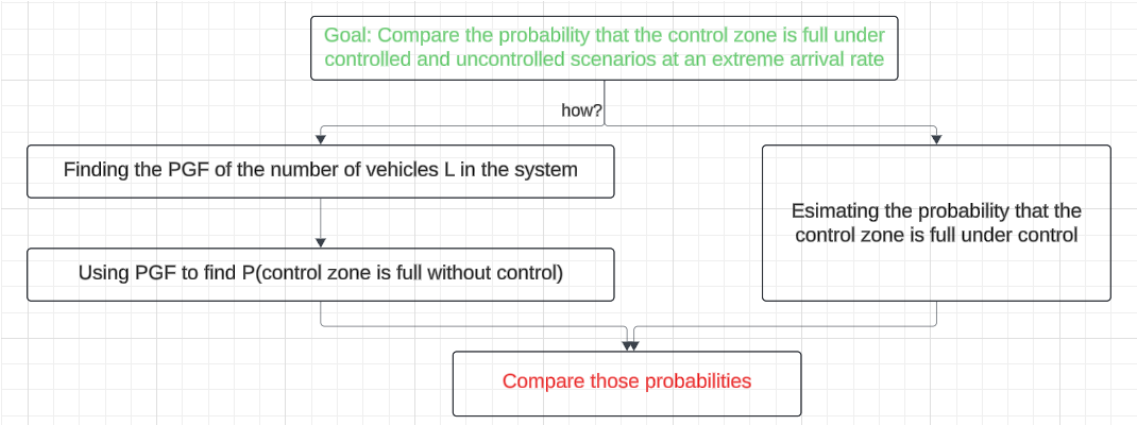

Figure 6.18: Organization of Sec.6.4

PGF of the Number of Vehicles in $M/G/1$ Queueing System

Define the following:

- $L :=$ the number of customers in the system.
- $L_k^d :=$ the number of customers in the system after the $k-$th departure.
- $A_k :=$ the number of arrivals during the service time B_k.
- $p_n := \mathbb{P}(L = n)$, representing the probability of having n customers in the system.
- $a_n := \mathbb{P}(L^a = n)$, representing the probability of having n customers upon arrival.
- $d_n := \mathbb{P}(L^d = n)$, representing the probability of having n customers upon departure.

Then, the relationship between L_{k+1}^d, L_k^d, and A_{k+1} is:

$$L_{k+1}^d = \begin{cases} L_k^d + A_{k+1} - 1 & \text{if } L_k^d > 0, \\ 0 + 1 - 1 + A_{k+1} = A_{k+1} & \text{if } L_k^d = 0. \end{cases} \tag{6.3}$$

Clearly, $\{L_k^d\}_{k=0}^{\infty}$ forms an embedded Discrete Time Markov Chain, with transition probability and transition matrix being:

$$p_{i,j} = \mathbb{P}(L_{k+1}^d = j \mid L_d^k = i), \tag{6.4}$$

$$P = \begin{pmatrix} \alpha_0 & \alpha_1 & \alpha_2 & \alpha_3 & \cdots \\ \alpha_0 & \alpha_1 & \alpha_2 & \alpha_3 & \cdots \\ 0 & \alpha_0 & \alpha_1 & \alpha_2 & \cdots \\ 0 & 0 & \alpha_0 & \alpha_1 & \cdots \\ \vdots & \vdots & \vdots & \vdots & \ddots \end{pmatrix}, \tag{6.5}$$

where

$$\begin{aligned}\alpha_n :&= \mathbb{P}(\text{there are } n \text{ arrivals during a service time } B)\\ &= \int_0^\infty \frac{e^{-\lambda t}(\lambda t)^n}{n!} dF_B(t).\end{aligned} \tag{6.6}$$

The derivations of Eqs.(6.3), (6.5), and (6.6) can be seen in Sec.4.2.3.

The the probability generating function of the random variable L^d_{K+1} can be expressed by:

$$\begin{aligned}P_{L^d_{k+1}}(z) &= \sum_{i=0}^{\infty} \mathbb{E}\Big(z^{L^d_{k+1}} \mid L^d_k = i\Big)\mathbb{P}(L^d_k = i)\\ &= \mathbb{E}\Big(z^{A_{k+1}}\Big)\mathbb{P}(L^d_k = 0) + \sum_{i=1}^{\infty} \mathbb{E}\Big(z^{i-1+A_{k+1}}\Big)\mathbb{P}(L^d_k = i)\\ &= P_{A_{k+1}}(z)\mathbb{P}(L^d_k = 0) + \sum_{i=1}^{\infty} \mathbb{E}\Big(z^{i-1+A_{k+1}}\Big)\mathbb{P}(L^d_k = i).\end{aligned} \tag{6.7}$$

It should be noted that

$$A_{k+1} \overset{d}{=} A_k \overset{d}{=} A, \tag{6.8}$$

where $\overset{d}{=}$ represents 'has the same distribution as'. The first equality in Eq.(6.8) is very obvious. The second equality follows from the PASTA property which states: *For queueing systems with Poisson arrivals, so for $M/\cdot/\cdot$ systems, the very special property holds that arriving customers find on average the same situation in the queueing system as an outside observer looking at the system at an arbitrary point in time* [33].

Let λ be the arrival rate. Since the number of customers up crossing equals the number of customers downcrossing, the rate of $L(t)$ from n to $n+1$ equals the rate of $L(t)$ from $n+1$ to n. Therefore

$$\lambda a_n = \lambda d_n. \tag{6.9}$$

Thus $a_n = d_n$. By PASTA property, $a_n = p_n$, so

$$d_n = p_n. \tag{6.10}$$

Hence we conclude

$$L^d_{k+1} \overset{d}{=} L^d_k \overset{d}{=} L. \tag{6.11}$$

Using Eqs.(6.8) and (6.11), Eq.(6.7) changes to

$$P_L(z) = \mathbb{P}(L = 0)P_A(z) + \sum_{i=1}^{\infty} z^{i-1} P_A(z)\mathbb{P}(L = i). \tag{6.12}$$

Multiplying by z on both sides, one can get

$$\begin{aligned}zP_L(z) &= p_0 P_A(z)z + \sum_{i=1}^{\infty} z^i \mathbb{P}(L = i)P_A(z)\\ &= p_0 P_A(z)z + P_A(z)\Big(P_L(z) - p_0 z^0\Big)\\ &= p_0 P_A(z)z + P_L(z)P_A(z) - p_0 P_A(z).\end{aligned} \tag{6.13}$$

Let ρ be the utilisation of the system, by definition, $\rho = \lambda\mathbb{E}(B) = 1 - p_0$, thus by Eq.(6.13), the PGF of L can be expressed by

$$P_L(z) = \frac{(1-\rho)(1-z)P_A(z)}{P_A(z) - z}. \tag{6.14}$$

Using Eq.(6.6) and the Tower property, the PGF of A can be calculated as:

$$\begin{aligned} P_A(z) &= \mathbb{E}\Big(\mathbb{E}(z^A \mid B)\Big) \\ &= \sum_{n=0}^{\infty} \int_0^{\infty} \frac{(\lambda t)^n}{n!} e^{-\lambda t} f_B(t) dt z^n \\ &= \int_0^{\infty} \sum_{n=0}^{\infty} \frac{(\lambda t z)^n}{n!} e^{-\lambda t} f_B(t) dt \\ &= \int_0^{\infty} e^{-(\lambda - \lambda z)t} f_B(t) dt \\ &= \mathbb{E}\Big(e^{-(\lambda-\lambda z)B}\Big) \\ &= \tilde{B}(\lambda - \lambda z), \end{aligned} \tag{6.15}$$

where $\tilde{B}(\cdot)$ represents the Laplace-Stietjes transform (LST). Substituting Eq.(6.15) into Eq.(6.14), one can express the PGF of L in terms of the LST of B:

$$P_L(z) = \frac{(1-\rho)(1-z)\tilde{B}(\lambda - \lambda z)}{\tilde{B}(\lambda - \lambda z) - z}. \tag{6.16}$$

Probability that the Control Zone is Full under an Uncontrolled Situation

In a single-lane roundabout without traffic control (human-driven), we model it as an $M/G/1$ queuing system. Vehicles arrive at the roundabout according to a Poisson Process, while the distribution of service times is generally distributed. There is one server in the system, represented by an imaginary traffic coordinator stationed at the entry line of the roundabout, who allows the first vehicle on the leg to either enter the roundabout or wait based on traffic conditions. The system has infinite capacity, meaning there is no limit to the number of vehicles that can queue on the leg.

The service time is defined as the duration the first vehicle waits to enter the roundabout. This time is measured from the Vissim simulation as follows:

- Let t_h and t_t be the times when a vehicle's head and tail cross the entry line, respectively.
- The maximum speed at which vehicles can travel inside the roundabout is denoted as v_r.
- The service time is then estimated by $t = t_t - t_h - \frac{L}{v_r}$, where VL is the length of the vehicle.

Since the service time of the current vehicle depends only on the conditions inside the roundabout, rather than on the service time of the previous vehicle, the service time data B_i can be assumed to be approximately i.i.d.

Since $\mathbb{E}(B_i) < \infty$, $\forall i \in \{1, 2, ..., n\}$ from the data, by the Strong Law Of Large Numbers,

$$\begin{aligned} &\frac{(1-\rho)(1-z)\frac{1}{n}\sum_{i=1}^{n} e^{(\lambda z - \lambda)B_i}}{\frac{1}{n}\sum_{i=1}^{n} e^{(\lambda z - \lambda)B_i} - z} \xrightarrow{a.s.} \frac{(1-\rho)(1-z)\mathbb{E}\Big(e^{(\lambda z-\lambda)B}\Big)}{\mathbb{E}\Big(e^{(\lambda z-\lambda)B}\Big) - z} \\ &= \frac{(1-\rho)(1-z)\tilde{B}(\lambda - \lambda z)}{\tilde{B}(\lambda - \lambda z) - z} = P_L(z). \end{aligned} \tag{6.17}$$

If the control zone has a leg distance x_0 of $100m$, the length of vehicle $VL = 4.76m$, and the safety distance between consecutive vehicles $d_{\text{safe}} = 2m$, then the capacity of each leg within the control zone C_l is 17. Under an uncontrolled situation, the probability that the control zone is full is:

$$\begin{aligned} &\mathbb{P}_{uc}(\text{control zone is full}) = \mathbb{P}(L \geq C_l) = 1 - \sum_{i=0}^{16} \mathbb{P}(L = i) \\ &= 1 - P_L(0) - \sum_{i=1}^{16} \frac{1}{i!} \frac{d^{(i)}}{dz^i} P_L(z)\Big|_{z=0}, \end{aligned} \tag{6.18}$$

where the last equality uses the property of PGF. As derived in Eq.(6.17), one can use the data to approximate the PGF of L empirically. Thus

$$\mathbb{P}_{uc}(\text{control zone is full}) \approx 1 - P_L(0) - \sum_{i=1}^{16} \frac{1}{i!} \frac{d^{(i)}}{dz^i} \frac{(1-\rho)(1-z)\frac{1}{n}\sum_{j=1}^{n} e^{(\lambda z-\lambda)B_j}}{\frac{1}{n}\sum_{j=1}^{n} e^{(\lambda z-\lambda)B_j} - z}\bigg|_{z=0}. \tag{6.19}$$

Filling in estimated service time data, we get:

$$\mathbb{P}_{uc}(\text{control zone is full}) \approx 0.45. \tag{6.20}$$

It should be noted that this blocking probability is an estimated value since the service time data is estimated from the Vissim simulation.

Probability that the Control Zone is Full under the Controlled Situation

In the First Phase Optimization simulation, the number of vehicles within the control zone on each leg is recorded every 0.1 seconds. Under controlled conditions, the probability that the control zone is full on each leg is estimated by the fraction of time during which the number of vehicles in each leg exceeds C_l in the simulation. More specifically,

$$\mathbb{P}_c^j(\text{control zone is full}) \approx \frac{\text{time during which there are more than 17 vehicles on leg } j}{\text{total simulation runtime}}, \tag{6.21}$$

where j represents the index of the leg. In the simulation, the number of vehicles on each leg does not change until a new vehicle enters the control zone or a vehicle already inside the control zone merges into the roundabout. Therefore, during the interval between consecutive vehicle entries into the control zone on the same leg, the number of vehicles on that leg will not increase.

Since presenting all data at 0.1-second intervals is not feasible within this thesis, we provide piecewise examples in Tab.6.8 for the number of vehicles inside the control zone at some moments when the maximal number of vehicles within the control zone on each leg is attained under the extreme arrival rate of $1200pcu/h$. These numbers can be regarded as the global maxima between each two consecutive times when new vehicles enter the control zone. From the table, we can conclude that at the extreme

Simulation Time (s)	#vehicles in leg 1	#vehicles in leg 2	#vehicles in leg 3	#vehicles in leg 4
2851.2	6	2	2	2
3095.3	2	8	2	2
3516.5	1	1	10	10
3520.2	2	3	10	10

Table 6.8: Under an arrival rate of $1200pcu/h$, the number of vehicles on each leg at the time when the maximal number of vehicles in the control zone on each leg is attained during a simulation time of $3600s$.

arrival rate of $1200pcu/h$, $\mathbb{P}_c^j(\text{control zone is full}) = 0 \ \forall j = 1,2,3,4$, thus we can conclude that the probability that the control zone is full under the controlled scenario $\mathbb{P}_c(\text{control zone is full}) = 0$ for the extreme arrival rate.

6.4.1. Comparison

If the distance from the boundary of the control zone to the entry line of the roundabout is $x_0 = 100m$, and all vehicles have the same length $VL = 4.76m$, with a safety distance of $d_{\text{safe}} = 2m$, then under an extreme arrival rate of $1200pcu/h$, the probability that the control zone is full under human-driven conditions is 0.45. This means, from a long-run perspective, there is a 0.45 probability that a new vehicle, upon arrival, will find the control zone full and will not be able to enter. In other words, 45% of the vehicles will be unable to enter the control zone.

However, under the controlled scenario, the probability that the control zone is full is estimated to be 0, indicating that, from a long-run perspective, no vehicles will be blocked. In other words, the control

model never fails, as the mathematical optimization always provides feasible solutions. Thus, the control model can effectively manage the traffic.

Therefore, our control model for connected and automated vehicles (CAVs) can significantly reduce the probability of congestion, even under the extreme arrival rate of $1200 pcu/h$.

7

Discussions

7.1. Achievements

This research achieved notable advancements in optimizing the performance of single-lane roundabouts through a microscopic control of CAVs. The findings demonstrated significant improvements in roundabout efficiency, system reliability, and scalability. These achievements contribute to addressing critical challenges in modern traffic management. Key results include:

Effectiveness of the Microscopic Control Model

The microscopic control model formulated in Sec.4.1 significantly reduces the average sojourn time compared to human-driven scenarios, highlighting its effectiveness in enhancing single-lane roundabout efficiency. Empirical results reveal reductions of 26%, 80%, 91%, and 90% across various arrival rates (200, 400, 600, and $800pcu/h$ on each leg). These findings closely align with theoretical predictions of reductions of 18%, 78%, 89%, and 90% under the same conditions. This agreement between empirical and theoretical results underscores the robustness and reliability of the proposed model. These improvements in sojourn time not only mitigate traffic congestion but also establish the model as a scalable and effective solution for real-world applications.

Furthermore, while maximizing the efficiency of the single-lane roundabout, the proposed microscopic control model also ensures driving comfort by providing precise trajectories for individual vehicles. Tabs.7.1, 7.2, 7.3, and 7.4 illustrate examples of how each vehicle within the control zone is guided to follow a specific trajectory. Recall that S_i^j represents the sojourn time for vehicle i from leg j, defined as the time required for the vehicle to travel from entering the control zone to merging into the roundabout, and v_r denotes the speed of vehicles circulating within the single-lane roundabout. These tables can be interpreted as follows: when vehicle i from leg j enters the control zone at time $t_{i,0}$ with an initial speed $v_{i,0}$, it is controlled using acceleration $a_{i,1}$ to travel from $t_{i,0}$ to $t_{i,1}$. At this point, it reaches its cruising speed $v_{i,*}$ and continues traveling from $t_{i,1}$ to $t_{i,2}$. Subsequently, the vehicle is commanded to accelerate at $a_{i,2}$ from $t_{i,2}$ to $t_{i,0} + S_i^j$, at which it attains the speed v_r required to merge into the roundabout (see Fig.4.5).

It should be noted that if $t_{i,1} = t_{i,2}$, the cruising segment depicted in Fig.4.5 does not exist. In such cases, vehicle i from leg j uses acceleration $a_{i,1}$ to travel from $t_{i,0}$ to $t_{i,1}$ (or $t_{i,2}$) and then uses acceleration $a_{i,2}$ to travel from $t_{i,2}$ (or $t_{i,1}$) to $t_{i,0} + S_i^j$. Examples of this scenario include vehicle 256 from leg 2 and vehicle 253 from leg 4 in Tab.7.3, as well as vehicle 316 from leg 2 and vehicle 339 from leg 3 in Tab.7.4.

Integration of Queueing Theory

The research developed an $M/G/1/k$ queueing model to analyze and compare traffic efficiency under controlled and uncontrolled scenarios. For a single-lane roundabout with finite leg capacity (i.e., the maximum number of vehicles that can travel on each leg is limited), the $M/G/1/k$ model provided a critical theoretical baseline. This was achieved by incorporating headway time distributions and service

i	j	$v_{i,0}\ (m/s)$	$t_{i,0}\ (s)$	$a_{i,1}\ (m/s^2)$	$t_{i,1}\ (s)$	$v_{i,*}\ (m/s)$	$t_{i,2}\ (s)$	$a_{i,2}\ (m/s^2)$	$t_{i,0}+S_i^j\ (s)$
33	1	11.4	846.1	-2.15	849.7	3.74	863.10	1.50	867.1
36	2	12.0	864.5	-2.24	850.2	3.69	864.4	1.52	867.5
43	3	13.7	862.2	-2.63	866.0	3.47	880.0	1.60	883.1
45	4	12.1	866.7	-2.26	870.4	3.68	884.7	1.52	887.7

Table 7.1: Examples of the trajectories of controlled vehicles under an arrival rate of $200pcu/h$.

i	j	$v_{i,0}\ (m/s)$	$t_{i,0}\ (s)$	$a_{i,1}\ (m/s^2)$	$t_{i,1}\ (s)$	$v_{i,*}\ (m/s)$	$t_{i,2}\ (s)$	$a_{i,2}\ (m/s^2)$	$t_{i,0}+S_i^j\ (s)$
61	1	11.6	755.7	-2.27	759.8	2.27	765.6	0.55	776.5
67	2	11.8	761.11	-1.73	766.8	1.88	772.0	0.64	782.0
90	3	11.8	769.8	-1.73	775.6	1.88	780.7	0.64	790.6
73	4	12.5	786.6	-2.35	790.4	3.66	804.4	1.54	807.5

Table 7.2: Examples of the trajectories of controlled vehicles under an arrival rate of $400pcu/h$.

time variability to calculate the expected sojourn times. Using the queueing model developed in Sec.4.2 and the estimated distribution for the circulating headway derived in Sec.5.2, we conclude that for arrival rates of 200, 400, 600, and $800pcu/h$ on each leg of the single-lane roundabout with a leg capacity of 17, the expected sojourn times are 25.64, 95.18, 206.92, and 213 seconds, respectively. These values closely align with those under human-driven conditions (simulated by Vissim), which are 28.23, 106.94, 232.49, and 231.52 seconds for the corresponding arrival rates, with a maximum deviation of 11%.

The model was also adapted to the $M/G/1$ queueing system for stress testing under an extreme arrival rate (e.g., $1200pcu/h$ per leg). The results demonstrated the robustness of the control model, maintaining a zero probability of control zone saturation. This indicates that the control model proposed in Sec.4.1 still provides a feasible solution at such a high arrival rate. In contrast, under human-driven conditions, the probability of new vehicles failing to enter the control zone reached as high as 45%. This is calculated by analyzing the $M/G/1$ queueing model and using the estimated service time data from Vissim simulation. These findings confirm the scalability and reliability of the proposed control model in high-demand traffic environments.

Proposed Models are Validated

For the proposed control model and $M/G/1/k$ queueing model, the following aspects are of interest for validation:

(i) Is the control model proposed in Sec.4.1 stable and reliable?

(ii) Are the trajectories of controlled vehicles reasonable? In other words, under the controlled situation, can we ensure that vehicles do not collide with each other from entering the control zone to merging into the roundabout?

(iii) Is the expected sojourn time calculated by the $M/G/1/k$ queueing model reliable?

Validation for (i) is conducted through a stress test at an extreme arrival rate of $1200pcu/h$. Results show that even under this high-demand traffic intensity, the optimization still produces feasible solutions (see Tab.6.8), demonstrating the stability and reliability of the control model.

Validation for (ii) is inherently ensured by the control model itself, as Eq.(4.27) in the Second Phase Optimization serves as a constraint to prevent collisions on all legs of the single-lane roundabout. Therefore, if the optimization model produces a feasible solution, it guarantees that vehicles will not collide from entering the control zone to merging into the roundabout. Additionally, trajectory plots (distance-time plots) provide supplementary evidence. If there are no overlapping lines in the trajectory plot, it indicates no collisions. Since plotting all vehicles' trajectories in a single plot may not be visually clear, we randomly select 10 consecutive vehicles on a random leg to plot their trajectories for various arrival rates as representative examples. Details can be found in Appendix B.

Validation for (iii) involves comparing the expected sojourn time calculated using the $M/G/1/k$ queueing model with the average sojourn time simulated by Vissim across different arrival rates. Although the

i	j	$v_{i,0}\ (m/s)$	$t_{i,0}\ (s)$	$a_{i,1}\ (m/s^2)$	$t_{i,1}\ (s)$	$v_{i,*}\ (m/s)$	$t_{i,2}\ (s)$	$a_{i,2}\ (m/s^2)$	$t_{i,0}+S_i^j\ (s)$
288	1	10.7	2356.0	-1.95	2359.6	3.76	2374.4	1.48	2377.5
256	2	1.4	2370.5	0.25	2391.9	6.87	2391.9	0.98	2393.4
275	3	7.4	2333.8	-1.15	2336.7	4.06	2352.4	1.35	2355.6
253	4	1.8	2358.3	0.22	2379.4	6.47	2379.4	1.10	2381.1

Table 7.3: Examples of the trajectories of controlled vehicles under an arrival rate of $600pcu/h$.

i	j	$v_{i,0}\ (m/s)$	$t_{i,0}\ (s)$	$a_{i,1}\ (m/s^2)$	$t_{i,1}\ (s)$	$v_{i,*}\ (m/s)$	$t_{i,2}\ (s)$	$a_{i,2}\ (m/s^2)$	$t_{i,0}+S_i^j\ (s)$
335	1	4.9	2752.7	-0.40	2754.5	4.17	2771.6	1.28	2774.9
316	2	1.5	2850.0	0.25	2871.3	6.77	2871.3	1.01	2872.9
339	3	1.7	3008.5	0.23	3029.7	6.57	3029.7	1.07	3031.4
372	4	4.7	3384.4	-0.32	3386.0	4.18	3403.4	1.27	3407.9

Table 7.4: Examples of the trajectories of controlled vehicles under an arrival rate of $800pcu/h$.

results show a maximum deviation of 11%, a reasonable explanation for this discrepancy is provided (see the text around Eq.(6.1)). Thus, we conclude that the proposed $M/G/1/k$ queueing model for calculating the expected sojourn time is reliable.

These validations reinforce the accuracy and applicability of the proposed models, ensuring their relevance for real-world implementations.

Other Contributions

An in-depth analysis of headway time distributions has been carried out, leveraging statistical models like shifted exponential, lognormal, M3, and shifted-Erlang distributions. This analysis enriches the understanding of headway time distribution under different arrival rates. Besides, our research advances smart traffic management by proposing an innovative framework for integrating CAVs into existing infrastructure. The developed models and methodologies can serve as a foundation for future studies and the implementation of autonomous traffic systems.

7.2. Limitations

While this study achieved significant advancements in optimizing the efficiency of single-lane roundabouts with all vehicles being CAVs, several limitations should be acknowledged:

Algorithm Efficiency

One of the major limitations of the proposed control model is its computational efficiency. Although, compared to Danesh's work[9], we reformulated the programming method from global optimization to local optimization (see Sec.2.4 and Appendix A), the Second Phase Optimization, which minimizes acceleration fluctuations to enhance driving comfort, remains computationally intensive. For example, simulating an arrival rate of $200pcu/h$ on each leg over a 3600-second period on a supercomputer (e.g., Delft Blue) requires at least 8 hours of processing time. This level of computational demand indicates that the control model is impractical for real-time applications in real-world traffic systems. Further efforts are required to optimize the algorithm's efficiency to ensure its feasibility in operational environments.

Reliance on Simulated Data

The research heavily relies on data generated by VISSIM simulations to evaluate the performance of the proposed models. For example, we did comparison of the sojourn time between the control model and the Vissim simulation, we derived the moments of service time based on the headway time generated by Vissim, and we calculate the blocking probability that the control zone is full under an uncontrolled scenario using the service time data estimated from Vissim simulation. Although VISSIM is a widely recognized and validated tool, simulation-based results may not fully capture the complexities of real-world traffic dynamics. Factors such as driver behavior, environmental variability, and unexpected disruptions in real-world scenarios are not accounted for, potentially limiting the generalizability of the

findings.

Simplified Traffic Assumptions

The $M/G/1/k$ queueing model and microscopic control model operate under several simplified assumptions, such as Poisson Process arrival, uniform vehicle size, constant safety distance, idealized control zones, the same arrival rates on each leg, and no path guidance. These assumptions, while necessary for analytical tractability, may not fully reflect the diversity of traffic conditions in real-world applications, particularly in heterogeneous traffic environments.

The Used Maximal Acceleration and Minimal Acceleration Might be Uncomfortable

In the literature study, different researchers have proposed their own comfort thresholds for maximal acceleration a_{max} and minimal acceleration a_{min}. A summary of their findings, as discussed in Sec.2.2, is presented in Tab.7.5. To implement the Python code for our control model, we adopt the values of $a_{\text{max}} = -a_{\text{min}} = 3.6m/s^2$. This is because, when using Vissim to simulate the human-driven condition, the default values for these two parameters are $3.6m/s^2$ and $-3.6m/s^2$, respectively. To ensure that our control model is comparable to the uncontrolled scenario (human-driven condition simulated by Vissim), we use these default values provided by the Vissim software.

However, if some vehicles are controlled to use a_{max} or a_{min} in their trajectories, it may cause discomfort for the driver. Additionally, it should be noted that reducing the absolute values of a_{max} and a_{min} could lead to an increase in sojourn time. Intuitively, given the arrival speed of a vehicle i to the control zone $v_{i,0}$ and the speed of merging into the roundabout v_r, for a fixed distance x_0, a higher absolute value of acceleration results in shorter travel times. Thus, a trade-off exists between the driving comfort and the roundabout's efficiency.

a_{max} (m/s^2)	a_{min} (m/s^2)	Reference
1.02	Not Mentioned	[25]
$0.9 \sim 1.47$	Not Mentioned	[3]
Not Mentioned	-2	[24]

Table 7.5: Comfort thresholds for a_{max} and a_{min} from different references.

Lack of Experimental Validation

Although theoretical and simulation-based results are promising, the proposed models have not yet been validated through field experiments or pilot implementations. Without such real-world validation, the practical applicability and robustness of the models under varying traffic conditions remain uncertain.

Limited Scope of Application

This study focuses exclusively on single-lane roundabouts with 100% CAV penetration. In mixed traffic conditions, where human-driven vehicles coexist with CAVs, the performance of the proposed models may differ significantly. Moreover, the findings may not directly extend to other traffic scenarios, such as multi-lane roundabouts, turbo-roundabout, intersections, or urban street networks.

Assumption of Perfect Communication

The microscopic control model assumes flawless communication and cooperation among CAVs, facilitated by a central control system. In reality, communication delays, system failures, or security vulnerabilities could affect the model's effectiveness and reliability.

Sensitivity Analysis to High Traffic Volumes and Local Failures

While the pressure tests demonstrate the robustness of the control model at high arrival rates, further analysis is required to explore its performance under extreme congestion (arrival rate more than $1200pcu/h$) or network-wide traffic disruptions. The potential cascading effects of localized failures on the broader traffic system remain unexamined.

7.3. Future Research Direction

This study has laid a solid foundation for understanding the optimization of single-lane roundabouts with CAVs. However, further research is essential to address unresolved challenges and explore new opportunities. Key future research directions include:

Building a Bridge between Mathematics and Civil Engineering

In our control model, the parameter values t_C (critical gap) and t_F (follow-on time) are adopted from Fortuijn and Salomons' thesis[15]. Therefore, it is of interest to compare our results with their findings. Their research indicates that the capacity of a single-lane roundabout (i.e., the number of vehicles a single-lane roundabout can handle per unit time until one of its legs becomes saturated) is roughly doubled for AVG through headway time optimization.

In contrast, our study focuses on minimizing the sojourn time (i.e., improving efficiency), achieving reduction levels of 18%, 78%, 89%, and 90% for arrival rates of 200, 400, 600, and $800 pcu/h$, respectively, compared to human-driven conditions (simulated by Vissim). It is important to note that the capacity of a single-lane roundabout and its efficiency, as defined by sojourn time, are two distinct measures for evaluating roundabout performance. This difference makes a direct comparison between our results and those of Fortuijn and Salomons infeasible.

Thus, establishing a connection between mathematics and civil engineering is of great interest. Future work is recommended as follows:

- Deriving a formula that establishes a relationship between the sojourn time and the capacity of the roundabout.
- Plotting the probability that our control model fails to provide feasible solutions across different arrival rates, followed by deriving a regression line for these points and identifying the 90% quantile.
- Exploring additional metrics to evaluate the interplay between capacity and efficiency under varying traffic conditions.

Validation Through Real-World Experiments

While this research relies on theoretical models and simulations, real-world experiments are necessary to validate the proposed methods. Pilot studies involving single-lane roundabouts with varying levels of CAV penetration could provide valuable insights into the practical challenges and effectiveness of the models in real traffic scenarios.

Complicated Traffic Conditions

Future work should investigate the performance of the microscopic control model and the $M/G/1/k$ queueing framework under complex traffic conditions, where human-driven vehicles coexist with CAVs and the arrival rates at different legs are uneven. This includes exploring the impact of varying CAVs penetration rates and differing arrival rates at each leg on system efficiency, as well as identifying strategies to ensure the seamless integration of autonomous and conventional vehicles.

Application to Multi-Lane Roundabouts

Expanding the scope of the study to multi-lane roundabouts would enable a broader understanding of CAV-based traffic optimization. Multi-lane roundabouts introduce additional complexities such as lane-changing behavior and higher traffic volumes, which require advanced models and control strategies.

Robustness to Communication Failures

The current models assume perfect communication among CAVs and the central control system. Future research should address the robustness of the control strategies in the presence of communication delays, failures, or cybersecurity threats. This could involve developing decentralized or hybrid control methods to enhance system resilience.

Integration with Broader Traffic Systems

To fully realize the potential of CAVs, future studies should explore their integration into larger traffic networks, such as urban intersections and highways. Investigating how CAV-controlled roundabouts interact with surrounding traffic systems and developing multi-node optimization frameworks could significantly enhance traffic efficiency on a city-wide scale.

Improving Algorithm Efficiency

Future research should focus on enhancing the computational efficiency of the control model to facilitate real-time applications. Potential strategies include developing more efficient optimization algorithms, leveraging parallel computing, and utilizing high-performance hardware such as GPUs or TPUs. Additionally, employing machine learning techniques to approximate optimization results could significantly reduce computational overhead while maintaining acceptable accuracy. These improvements would make the model more suitable for deployment in practical traffic systems.

Addressing Extreme Traffic Scenarios

Future research could also explore the performance of the control model under extreme conditions, such as traffic surges or network-wide disruptions. Investigating adaptive mechanisms to manage sudden changes in traffic flow could enhance the robustness and scalability of the proposed solutions. Additionally, studying the boundary value of the arrival rate at which the control model fails to produce a feasible solution would provide valuable insights. This boundary can be considered the limiting arrival rate of the model, offering a critical metric for evaluating its operational capacity.

.

References

[1] Hirotugu Akaike. “A new look at the statistical model identification”. In: *IEEE transactions on automatic control* 19.6 (1974), pp. 716–723.

[2] Austroads. *Guide to Traffic Engineering Practice: Bicycles*. Austroads, 1993.

[3] Il Bae, Jaeyoung Moon, and Jeongseok Seo. “Toward a comfortable driving experience for a self-driving shuttle bus”. In: *Electronics (Switzerland)* 8 (9 2019). comfortable acceleration. ISSN: 20799292. DOI: 10.3390/electronics8090943.

[4] ASM Bakibillah, Md Abdus Samad Kamal, CP Tan, et al. “The optimal coordination of connected and automated vehicles at roundabouts”. In: *2019 58th annual conference of the society of instrument and control engineers of Japan (SICE)*. IEEE. 2019, pp. 1392–1397.

[5] J Ben-Edigbe, R Rahman, and N Mashros. “Research Article Headway Distributions Based on Empirical Erlang and Pearson Type III Time Methods Compared”. In: *Res. J. Appl. Sci. Eng. Technol* 7 (2014), pp. 4410–4414.

[6] Transportation Research Board. *Highway Capacity Manual*. Washington, D.C.: National Research Council, 2000.

[7] KL Chung. *JL Doob, Stochastic processes*. 1954.

[8] Alan Cobham. “Priority assignment in waiting line problems”. In: *Journal of the Operations Research Society of America* 2.1 (1954), pp. 70–76.

[9] Ali Danesh et al. “Optimal roundabout control under fully connected and automated vehicle environment”. In: *IET Intelligent Transport Systems* 15.11 (2021), pp. 1440–1453.

[10] Robert Frank Dawson and LA Chimini. *The Hyperlang probability distribution: A generalized traffic headway model*. University of Connecticut, School of Engineering, Civil Engineering Department, 1967.

[11] Yiheng Feng, Chunhui Yu, and Henry X Liu. “Spatiotemporal intersection control in a connected and automated vehicle environment”. In: *Transportation Research Part C: Emerging Technologies* 89 (2018), pp. 364–383.

[12] Aimee Flannery et al. “Estimating Delay at Roundabouts”. In: *Institute of Transportation Engineers* (703 2000). Estimating delay using queueing models.

[13] Aimee Flannery et al. “Queuing delay models for single-lane roundabouts”. In: *Civil Engineering and Environmental Science* 22 (3 2005). mean and variance of waiting time in single-roundabout. ISSN: 10286608. DOI: 10.1080/10286600500279949.

[14] Lambertus G.H. Fortuijn. “Turbo roundabouts: Estimation of capacity”. In: *Transportation Research Record* (2130 2009). capacity model for turbo-roundabout, gap acceptance and conflicting stream. ISSN: 03611981. DOI: 10.3141/2130-11.

[15] LGH Bertus Fortuijn and A Maria Salomons. “Capacity Increase through connectivity for the i-Roundabout and i-Turbo roundabout”. In: *2020 Forum on Integrated and Sustainable Transportation Systems (FISTS)*. IEEE. 2020, pp. 83–88.

[16] Xiaozheng He, Henry X Liu, and Xiaobo Liu. “Optimal vehicle speed trajectory on a signalized arterial with consideration of queue”. In: *Transportation Research Part C: Emerging Technologies* 61 (2015), pp. 106–120.

[17] Bryan Higgs, Montasir Abbas, and Alejandra Medina. “Analysis of the Wiedemann car following model over different speeds using naturalistic data”. In: *Procedia of RSS Conference*. 2011, pp. 1–22.

[18] Martijn A.M. De Leeuw, Hein Botma, and Piet H.L. Bovy. “Capacity of single-lane roundabouts with slow traffic”. In: *Transportation Research Record* (1678 1999). gap acceptance theory. ISSN: 03611981. DOI: 10.3141/1678-08.

[19] Li Li and Xiqun Michael Chen. “Vehicle headway modeling and its inferences in macroscopic/microscopic traffic flow theory: A survey”. In: *Transportation Research Part C: Emerging Technologies* 76 (2017), pp. 170–188.

[20] R Tapio Luttinen et al. *Statistical analysis of vehicle time headways*. Helsinki University of Technology, 1996.

[21] R. Tapio Luttinen. “Properties of Cowan’s M3 Headway Distribution”. In: *Transportation Research Record* 1678 (1999), pp. 189–196.

[22] Sindhura Mandava, Kanok Boriboonsomsin, and Matthew Barth. “Arterial velocity planning based on traffic signal information under light traffic conditions”. In: *2009 12th International IEEE Conference on Intelligent Transportation Systems*. IEEE. 2009, pp. 1–6.

[23] Marilo Martin-Gasulla and Lily Elefteriadou. “Traffic management with autonomous and connected vehicles at single-lane roundabouts”. In: *Transportation research part C: emerging technologies* 125 (2021), p. 102964.

[24] Seungwuk Moon and Kyongsu Yi. “Human driving data-based design of a vehicle adaptive cruise control algorithm”. In: *Vehicle System Dynamics* 46 (8 2008). comfortable deceleration, max acceleration, deceleration. ISSN: 00423114. DOI: 10.1080/00423110701576130.

[25] Arup K. Nandi, Debasri Chakraborty, and Warren Vaz. “Design of a comfortable optimal driving strategy for electric vehicles using multi-objective optimization”. In: *Journal of Power Sources* 283 (2015). comfortable acceleration. ISSN: 03787753. DOI: 10.1016/j.jpowsour.2015.02.109.

[26] Engineering National Academies of Sciences, Medicine, et al. *Highway capacity manual 7th edition: A guide for multimodal mobility analysis*. 1930.

[27] Johan Janson Olstam and Andreas Tapani. *Comparison of Car-following models*. Vol. 960. Swedish National Road and Transport Research Institute Linköping, Sweden, 2004.

[28] R. J. Salter. *Road Traffic Analysis and Design*. Translated by Zhang Zuozhou et al. Beijing: China Architecture & Building Press, 1982.

[29] Gideon Schwarz. “Estimating the dimension of a model”. In: *The annals of statistics* (1978), pp. 461–464.

[30] J MacGregor Smith. “Optimal design and performance modelling of M/G/1/K queueing systems”. In: *Mathematical and computer modelling* 39.9-10 (2004), pp. 1049–1081.

[31] R. J. Troutbeck. “AVERAGE DELAY AT AN UNSIGNALIZED INTERSECTION WITH TWO MAJOR STREAMS EACH HAVING A DICHOTOMIZED HEADWAY DISTRIBUTION.” In: *Transportation Science* 20 (4 1986). ISSN: 00411655. DOI: 10.1287/trsc.20.4.272.

[32] RJ Troutbeck. *Evaluating the Performance of a Roundabout*. SR No. 45. 1989.

[33] Ronald W Wolff. “Poisson arrivals see time averages”. In: *Operations research* 30.2 (1982), pp. 223–231.

[34] Jin Xu et al. “An experimental study on lateral acceleration of cars in different environments in Sichuan, Southwest China”. In: *Discrete Dynamics in nature and Society* 2015 (2015).

[35] Shengchao Yin et al. “Headway distribution modeling with regard to traffic status”. In: *2009 IEEE intelligent vehicles symposium*. IEEE. 2009, pp. 1057–1062.

[36] Chunhui Yu et al. “Integrated optimization of traffic signals and vehicle trajectories at isolated urban intersections”. In: *Transportation Research Part B: Methodological* 112 (2018). boundary of arrival time. ISSN: 01912615. DOI: 10.1016/j.trb.2018.04.007.

[37] Chang Yulin, Wang Wei, et al. “Research and Application of Headway Time Distribution Models for Two-Lane Highways”. In: *Journal of Southeast University* 29.6 (1999).

[38] Nidzamuddin Md Yusof et al. “The exploration of autonomous vehicle driving styles: Preferred longitudinal, lateral, and vertical accelerations”. In: comfortable lateral acceleration. 2016. DOI: 10.1145/3003715.3005455.

[39] Guohui Zhang et al. “Examining headway distribution models with urban freeway loop event data”. In: *Transportation Research Record* 1999.1 (2007), pp. 141–149.

A

Codes for Microscopic Control Model

The codes are divided into three parts: **Executer**, **First Phase Optimization**, and **Second Phase Optimization**. The mathematical formulations for the First Phase Optimization and the Second Phase Optimization, as described in Sec. 4.1.3 and Sec. 4.1.4, are encapsulated into two Python objects, namely `First_Phase_Optimization` and `Second_Phase_Optimization`. The attributes of these objects are accessed and utilized in the Python script `Executer`.

Executer

```
import os
import First_Phase_Optimization as ot
import Second_Phase_Optimization as st
import pandas as pd

class Vehicle:
    def __init__(self, id, approach, destination, position, speed, arrivaltime, start_time,
        arrived):
        self.id = id
        self.approach = approach
        self.destination = destination
        self.position = position
        self.speed = speed
        self.arrivaltime = arrivaltime
        self.start_time = start_time
        self.arrived = False

        # add attributes to for the second stage
        self.a1 = None
        self.a2 = None
        self.t1 = None
        self.t2 = None
        self.v_star = None
        self.x_t0_t1 = 0

        self.x_t1_t2 = 100
        self.current_speed = speed
        self.isoptimized = False

    def __repr__(self):
        return f"Vehicle(ID={self.id}, Approach={self.approach}, Dest={self.destination}, Pos
            ={self.position}, Speed={self.speed}, ArrTime={self.arrivaltime}, StartTime={self
            .start_time }Arrived= {self.arrived})"
# Road destinations mapping
road_destinations = {
    1: ['b', 'c', 'd'],
    2: ['a', 'c', 'd'],
    3: ['a', 'b', 'd'],
    4: ['a', 'b', 'c']
}
```

```
# read csv
df = pd.read_csv('1200roaddata.csv')
df['arrived'] = False


# create vehicle object
vehicles = [Vehicle(**row) for index, row in df.iterrows()]

# Categorize vehicles by approach or destination
active_vehicles = {road: [] for road in road_destinations}
for vehicle in vehicles:
    active_vehicles[vehicle.approach].append(vehicle)

# Print the categorized vehicles
for approach in active_vehicles:
    print(f"Approach {approach}:")
    for vehicle in active_vehicles[approach]:
        print(vehicle)


# Initialize global variables
v_max = 50/3.6
amax = 3.6
dec_max = 3.6
x_cd = 100 #control distance
vr = 30/3.07
x_dest = 100

# Initialize optimizers
optimizer = ot.TrafficOptimizer(v_max, amax, dec_max, x_cd, vr)
second_stage_optimizer = st.SecondStageOptimization(optimizer.T, v_max, amax, dec_max, vr,
    x_cd)

# # Initialize dictionaries to track positions and speeds
# vehicle_positions = {(vehicle.approach, vehicle.id): [] for vehicle in vehicles}

def compare_dicts(dict1, dict2):
    """
    Compare two dictionaries to determine if they are equal.
    This function handles nested dictionaries as well.

    Args:
    dict1 (dict): The first dictionary to compare.
    dict2 (dict): The second dictionary to compare.

    Returns:
    bool: True if both dictionaries are equal, False otherwise.
    """
    if dict1 is dict2:
        # Check if both references point to the same object
        return True
    if not isinstance(dict1, dict) or not isinstance(dict2, dict):
        # Ensure both are dicts, otherwise, they're not equal
        return False
    if len(dict1) != len(dict2):
        # Different number of keys means they are not equal
        return False
    for key, val1 in dict1.items():
        if key not in dict2:
            # Key is not present in both dicts
            return False
        val2 = dict2[key]
        if isinstance(val1, dict) and isinstance(val2, dict):
            # If the value is a dict, perform a recursive call
            if not compare_dicts(val1, val2):
                return False
        elif val1 != val2:
            # Check value equality
            return False
    return True
def update_vehicle_arrivals(current_vehicles, current_time):
```

```
    for road, vehicles in current_vehicles.items():
        for vehicle in vehicles:
            if vehicle.arrivaltime >= current_time:
                vehicle.arrived = True  # set the situation that vehicle has arrived

def clear_first():
    to_be_first_optimize = {road: [] for road in road_destinations}



to_be_first_optimize_privious_t = {road: [] for road in road_destinations}
current_vehicles_t = {road: [] for road in road_destinations}
# Simulation loop
t = 1

while t <= 3600:
    #       update the information of vehicle at current time
    for road in road_destinations:
        #           only include the vehicle that are already in the control zone
        current_vehicles_t[road] = [vehicle for vehicle in active_vehicles[road] if vehicle.
            start_time <= t]

    # for road in road_destinations:
    # Check each road and each vehicle on that road
    to_be_first_optimize = {road: [] for road in road_destinations}
    for road, vehicle_list in current_vehicles_t.items():
        for vehicle in vehicle_list:
            if vehicle.start_time <= t and vehicle.arrived == False:
                to_be_first_optimize[road].append(vehicle)
            else:
                pass

    # print(f"current t is: {t}")
    # print(f"Current vehicles: {to_be_first_optimize.items()}")
    # print(f"priviou vehicles:{to_be_first_optimize_privious_t.items()}")
    # print(compare_dicts(to_be_first_optimize,to_be_first_optimize_privious_t))



    if(compare_dicts(to_be_first_optimize, to_be_first_optimize_privious_t) == True):
        print(f"At time {t},skipped &&&&&&&&&&&&&&&&&&&&&&&&&&&&&&&&&&&&")

    # optimizer.optimize(to_be_first_optimize, t)
    # optimizer.print_optimization_results(to_be_first_optimize)
    # to_be_first_optimize_privious_t = to_be_first_optimize
    # print(f"current t is {t}")

    if (compare_dicts(to_be_first_optimize, to_be_first_optimize_privious_t) == False):
        optimizer.optimize(to_be_first_optimize, t)
        optimizer.print_optimization_results(to_be_first_optimize)
        to_be_first_optimize_privious_t = to_be_first_optimize
        print(f"current t is {t}")

        data = []

        vehicle_count1 = len(to_be_first_optimize[1])
        vehicle_count2 = len(to_be_first_optimize[2])
        vehicle_count3 = len(to_be_first_optimize[3])
        vehicle_count4 = len(to_be_first_optimize[4])
        data.append({
            'current_t': t,
            'v_count_r1': vehicle_count1,
            'v_count_r2': vehicle_count2,
            'v_count_r3': vehicle_count3,
            'v_count_r4': vehicle_count4,
        })
        df = pd.DataFrame(data)
        df.to_csv('current_count.csv', mode='a', header=not os.path.exists('current_count.csv
            '),
                  index=False)
    #     update_vehicle_arrivals(current_vehicles_t, t)
```

```
177
178         to_be_second_optimized = {}
179         for road, vehicles in to_be_first_optimize.items():
180             not_optimized_vehicles = [vehicle for vehicle in vehicles if not vehicle.
                isoptimized]
181             if not_optimized_vehicles:
182                 to_be_second_optimized[road] = not_optimized_vehicles
183                 print("$$$$$$$$$$$$$$$$$$$$$$$$$$$$$")
184                 print(f"Current state of to_be_second_optimized: {to_be_second_optimized}")
185
186
187         second_stage_optimizer.optimize(to_be_second_optimized)
188         second_stage_optimizer.print_optimization_results(to_be_second_optimized)
189
190     # update_vehicle_arrivals(to_be_first_optimize,t)
191     # clear_first()
192
193     for road, vehicles in to_be_first_optimize.items():
194         for vehicle in vehicles:
195             if not vehicle.isoptimized:
196                 vehicle.isoptimized = True
197             else:
198                 pass
199
200     for road, vehicles in current_vehicles_t.items():
201         for vehicle in vehicles:
202             if not vehicle.arrivaltime > t:
203                 vehicle.arrived = True
204             else:
205                 pass
206
207     t += 0.1
```

First Phase Optimization

```
1     from gurobipy import Model, GRB
2 import math
3 import pandas as pd
4 import os
5
6 class TrafficOptimizer:
7     def __init__(self, v_max, amax, dec_max, x_cd, vr):
8         self.v_max = v_max
9         self.amax = amax
10        self.dec_max = dec_max
11        self.x_cd = x_cd
12        self.vr = vr
13        self.model = None
14        self.T = {}
15
16    def optimize(self, active_vehicles, t):
17        self._initialize_model()
18        self._define_decision_variables(active_vehicles)
19        self._add_constraints(active_vehicles)
20        self._set_objective()
21        self.model.optimize()
22        self._update_vehicle_arrival_times(active_vehicles)
23
24    def _initialize_model(self):
25        self.model = Model('TrafficOptimization')
26        self.T.clear()
27
28    def _define_decision_variables(self, active_vehicles):
29        for road, vehicles in active_vehicles.items():
30            for i, vehicle in enumerate(vehicles):
31                self.T[(i, road)] = self.model.addVar(vtype=GRB.CONTINUOUS, name=f"T_{i}_{
                    road}")
32        self.model.update()
33
34    def _add_constraints(self, active_vehicles):
```

```
35
36          for road, vehicles in active_vehicles.items():
37              for i, vehicle in enumerate(vehicles):
38                  T_var = self.T[(i, road)]
39                  # calculating T_min and T_max
40                  if (self.v_max ** 2 - vehicle.speed ** 2) / (2 * self.amax) + (self.v_max **
                        2 - self.vr ** 2) / (
41                          2 * self.dec_max) > self.x_cd:
42                      v_1i = math.sqrt((
43                                                2 * self.amax * self.dec_max * self.x_cd +
                                                      self.dec_max * vehicle.speed ** 2 + self
                                                      .amax * self.vr ** 2) / (
44                                                self.amax + self.dec_max))
45                      T_min = (v_1i - vehicle.speed) / self.amax + (v_1i - self.vr) / self.
                            dec_max
46                      if self.x_cd > self.vr ** 2 / (2 * self.amax) and vehicle.speed < math.
                            sqrt(
47                              2 * self.x_cd * self.dec_max - (self.vr ** 2 * self.dec_max /
                                    self.amax)):
48                          T_max = GRB.INFINITY
49                      else:
50                          T_max = (vehicle.speed - v_1i) / self.dec_max + (self.vr - v_1i) /
                                self.amax
51                  else:
52                      delta_t1 = (self.v_max - vehicle.speed) / self.amax
53                      delta_t2 = (self.x_cd - (self.v_max ** 2 - vehicle.speed ** 2) / (2 *
                            self.amax) - (
54                              self.v_max ** 2 - self.vr ** 2) / (2 * self.dec_max)) / self.
                                v_max
55                      delta_t3 = (self.v_max - self.vr) / self.dec_max
56                      T_min = delta_t1 + delta_t2 + delta_t3
57                      T_max = GRB.INFINITY  # infinity
58
59                  # add constraints
60                  self.model.addConstr(T_var >= T_min, f"T_min_{road}_{i}")
61                  self.model.addConstr(T_var <= T_max, f"T_max_{road}_{i}")
62          tf = 1.12  #
63          for road, vehicles in active_vehicles.items():
64              for i in range(len(vehicles) - 1):
65                  T_i_j = self.T[(i, road)]
66                  T_i1_j = self.T[(i + 1, road)]
67                  car = vehicles[i]
68                  car_next = vehicles[i + 1]
69
70                  # arrival time difference constraint
71                  self.model.addConstr(T_i_j + car.start_time + tf <= T_i1_j + car_next.
                        start_time,
72                                       f"departure_interval_{road}_{i}")
73
74          omega = {}
75          # define omega
76          for road, vehicles in active_vehicles.items():
77              for i, vehicle_i in enumerate(vehicles):
78                  for road_prime, vehicles_prime in active_vehicles.items():
79                      if road_prime == (road + 2) % 4 or road_prime == (road + 3) % 4:
80                          for i_prime, vehicle_i_prime in enumerate(vehicles_prime):
81                              omega[(i, road, i_prime, road_prime)] = self.model.addVar(vtype=
                                    GRB.BINARY,
82                                    name=f"omega_{i}_{road}_{i_prime}_{road_prime}")
83          self.model.update()  # update
84
85          # constraint
86          for (i, road, i_prime, road_prime), omega_var in omega.items():
87              x = 100 if road_prime == (road + 2) % 4 else 50
88              self.model.addGenConstrIndicator(omega_var, True,
89                                               self.T[(i, road)] + x / self.vr <= self.T[(
                                                     i_prime, road_prime)],
90                               name=f"omega_true_{i}_{road}_{i_prime}_{road_prime}")
91
92          # constraint on conflict point
93          t_C = 2.24  # critical time
```

```
        M = 1000  # sufficient large number
        for (i, road, i_prime, road_prime), omega_var in omega.items():
            self.model.addConstr(self.T[(i, road)] + t_C <= self.T[(i_prime, road_prime)] + M * (1 - omega_var),
                                 name=f"conflict_{i}_{road}_{i_prime}_{road_prime}")




    def _set_objective(self):
        self.model.setObjective(sum(self.T.values()), GRB.MINIMIZE)

    def _update_vehicle_arrival_times(self, active_vehicles):
        if self.model.status == GRB.OPTIMAL:
            for road, vehicles in active_vehicles.items():
                for i, vehicle in enumerate(vehicles):
                    vehicle.arrivaltime = self.T[(i, road)].X + vehicle.start_time

    def _calculate_T_min_max(self, vehicle):
        T_min = vehicle.position / max(vehicle.speed, 1)
        T_max = GRB.INFINITY
        return T_min, T_max

    def print_optimization_results(self, active_vehicles):
        if self.model.status == GRB.OPTIMAL:
            print("Optimization results:")
            data = []
            for road, vehicles in active_vehicles.items():
                for i, vehicle in enumerate(vehicles):
                    T_var = self.T[(i, road)]  # decision variable
                    vehicle.arrival_time = T_var.X  # optimal arrival time
                    data.append({
                        'Vehicle_ID': vehicle.id,
                        'Approach': road,
                        'Target_Exit': vehicle.destination,
                        'Tij': vehicle.arrival_time,
                        'starttime': vehicle.start_time,
                        'arrivaltime': vehicle.arrivaltime
                    })
            #         print(
            #             f"Vehicle {vehicle.id} at approach {road} has target exit {vehicle.destination} and optimized arrival time: {vehicle.arrival_time}")
            # # Create a DataFrame
            df = pd.DataFrame(data)
            df_cleaned = df.drop_duplicates()


            # print(df_cleaned)

            # Append DataFrame to a CSV file
            df_cleaned.to_csv('optimization_results.csv', mode='a', header=not os.path.exists('optimization_results.csv'),
                              index=False)
        else:
            print("No optimal solution found.")
```

Second Phase Optimization

```
 import os

from gurobipy import Model, GRB
import gurobipy as gp
import math
import pandas as pd
class SecondStageOptimization:
    def __init__(self , T, v_max, amax, dec_max, vr, x_cd):
        self.T = T
        self.v_max = v_max
        self.amax = amax
        self.dec_max = dec_max
```

```
        self.vr = vr
        self.x_cd = x_cd
        self.model = Model("SecondStageOptimization")

    def _define_variables(self,active_vehicles):
        for road, vehicles in active_vehicles.items():
            for i, vehicle in enumerate(vehicles):
                # define decision variables
                vehicle.a1 = self.model.addVar(name=f"a1_{vehicle.id}_{road}", lb=-self.
                    dec_max, ub=self.amax)
                vehicle.a2 = self.model.addVar(name=f"a2_{vehicle.id}_{road}", lb=-self.
                    dec_max, ub=self.amax)
                vehicle.t1 = self.model.addVar(name=f"t1_{vehicle.id}_{road}", lb=0)
                vehicle.t2 = self.model.addVar(name=f"t2_{vehicle.id}_{road}", lb=0)
                vehicle.v_star = self.model.addVar(name=f"v_star_{vehicle.id}_{road}", lb=0,
                    ub=self.v_max)

        self.model.update()

    def _add_constraints(self,active_vehicles):
        for road, vehicles in active_vehicles.items():
            for vehicle in vehicles:
                # speed constaint
                self.model.addConstr(vehicle.v_star == vehicle.current_speed + vehicle.a1 * (
                    vehicle.t1 - vehicle.start_time),
                                     name=f"v_star_{vehicle.id}_{road}")
                self.model.addConstr(vehicle.v_star + vehicle.a2 * (vehicle.arrivaltime -
                    vehicle.t2) == self.vr,
                                     name=f"v_end_{vehicle.id}_{road}")

                # time constraint on t1 t2
                self.model.addConstr(vehicle.t1 >= vehicle.start_time, name=f"t1_start_{
                    vehicle.id}_{road}")
                self.model.addConstr(vehicle.t1 <= vehicle.t2, name=f"t1_t2_{vehicle.id}_{
                    road}")
                self.model.addConstr(vehicle.t2 <= vehicle.arrivaltime, name=f"t2_Ti_j_{
                    vehicle.id}_{road}")

                # a1 a2 constraint
                self.model.addConstr(vehicle.a1 >= -self.dec_max, name=f"a1_min_{vehicle.id}_
                    {road}")
                self.model.addConstr(vehicle.a1 <= self.amax, name=f"a1_max_{vehicle.id}_{
                    road}")
                self.model.addConstr(vehicle.a2 >= -self.dec_max, name=f"a2_min_{vehicle.id}_
                    {road}")
                self.model.addConstr(vehicle.a2 <= self.amax, name=f"a2_max_{vehicle.id}_{
                    road}")

                #Gurobi constraint(for square)
                car_t_diff_sqr = self.model.addVar(name=f"car_t_diff_sqr_{vehicle.id}_{road}"
                    )
                car_ij_t2_sqr = self.model.addVar(name=f"car_ij_t2_sqr_{vehicle.id}_{road}")

                # components of distance constraint
                aa1 = vehicle.current_speed * (vehicle.t1 - vehicle.start_time)
                aa2 = 0.5 * vehicle.a1 * car_t_diff_sqr
                aa3 = vehicle.v_star * (vehicle.t2 - vehicle.t1)
                aa4 = vehicle.v_star * (vehicle.arrivaltime - vehicle.t2)
                aa5 = 0.5 * vehicle.a2 * car_ij_t2_sqr
                aa6 = aa1 + aa2 + aa3 + aa4 + aa5

                # Gurobi language for square
                self.model.addConstr(
                    car_t_diff_sqr == (vehicle.t1 - vehicle.start_time) * (vehicle.t1 -
                        vehicle.start_time),
                    name=f"car_t_diff_sqr_constr_{vehicle.id}_{road}")
                self.model.addConstr(car_ij_t2_sqr == (vehicle.arrivaltime - vehicle.t2) * (
                    vehicle.arrivaltime - vehicle.t2),
                                     name=f"car_ij_t2_sqr_constr_{vehicle.id}_{road}")

                # distance constraint
```

```
                self.model.addConstr(aa6 == 100, name=f"dynamic_constraint_{vehicle.id}_{road}")



                #Collision Avoidance Constraint
                for i in range(len(vehicles) - 1):

                    current_vehicle = vehicles[i]
                    next_vehicle = vehicles[i + 1]
                    current_v_position = current_vehicle.position
                    next_v_position = next_vehicle.position

                    if current_v_position >= current_vehicle.x_t0_t1:
                        current_v_next_t_position = current_vehicle.position - current_vehicle.current_speed*0.5 - 0.5 * current_vehicle.a1*(0.5**2)


                    elif current_vehicle.x_t0_t1 >= current_v_position > current_vehicle.x_t1_t2:

                        current_v_next_t_position = current_vehicle.position - current_vehicle.v_star
                    else:


                        current_v_next_t_position = current_vehicle.position - current_vehicle.current_speed*0.5 - 0.5 * current_vehicle.a2*(0.5**2)

                    if next_v_position >= next_vehicle.x_t0_t1:
                        next_v_next_t_position = next_vehicle.position - next_vehicle.current_speed*0.5 - 0.5 * next_vehicle.a1*(0.5**2)

                    elif next_vehicle.x_t0_t1 >= next_v_position > next_vehicle.x_t1_t2:
                        next_v_next_t_position = next_vehicle.position - next_vehicle.v_star

                    else:
                        next_v_next_t_position = next_vehicle.position - next_vehicle.current_speed*0.5 - 0.5 * next_vehicle.a2*(0.5**2)

                    self.model.addConstr(next_v_next_t_position - current_v_next_t_position >= 2)


        self.model.update()

    def _set_objective(self,active_vehicles):
        # Initialization
        objective = 0


        for road, vehicles in active_vehicles.items():
            for vehicle in vehicles:

                objective += vehicle.a1 * vehicle.a1 + vehicle.a2 * vehicle.a2


                objective += (vehicle.v_star - self.vr) * (vehicle.v_star - self.vr)


        self.model.setObjective(objective, GRB.MINIMIZE)

    def _update_vehicle_parameters(self,active_vehicles):
        if self.model.status == GRB.OPTIMAL:
            print("Optimization results:")
            for road, vehicles in active_vehicles.items():
                for vehicle in vehicles:
                    # update decision variable
```

```
                    vehicle.a1 = vehicle.a1.X
                    vehicle.a2 = vehicle.a2.X
                    vehicle.t1 = vehicle.t1.X
                    vehicle.t2 = vehicle.t2.X
                    vehicle.v_star = vehicle.v_star.X

                    # print
                    print(f"Vehicle ID: {vehicle.id}, Approach: {road}")
                    print(f"  a1: {vehicle.a1}, a2: {vehicle.a2}")
                    print(f"  t1: {vehicle.t1}, t2: {vehicle.t2}")
                    print(f"  v_star: {vehicle.v_star}\n , arrivaltime:{vehicle.arrivaltime}"
                        )
        else:
            print("Optimization was not successful. Parameters are not updated.")

    def print_optimization_results(self,active_vehicles):
        print("Second Stage Optimization results:")
        data = []
        for road, vehicles in active_vehicles.items():
            for vehicle in vehicles:
                data.append(
                    {'Vehicle_ID': vehicle.id,
                    'Approach': road,
                    'Target_Exit': vehicle.destination,
                    'Tij': vehicle.arrival_time,
                    'starttime': vehicle.start_time,
                    'arrivaltime': vehicle.arrivaltime,
                    'v_0': vehicle.speed,
                     'a1':vehicle.a1,
                     'a2':vehicle.a2,
                     't1':vehicle.t1,
                     't2':vehicle.t2,
                     'v_star':vehicle.v_star
                     }
                )
        df = pd.DataFrame(data)
        df_cleaned = df.drop_duplicates()
        print(df_cleaned)
# Append DataFrame to a CSV file
        df_cleaned.to_csv('optimization_results_second_stage.csv', mode='a', header=not os.
            path.exists('optimization_results_second_stage.csv'),
                                index=False)
```

B

Examples of Trajectories of Controlled Vehicles

The constraint (4.27) in the Second Phase Optimization guarantees that vehicles on the same leg will not collide with each other. Consequently, as long as the optimization model yields feasible solutions, collisions between vehicles are inherently avoided. Since plotting the trajectories of all vehicles in the control model is not visually practical, we provide examples by randomly selecting 10 consecutive vehicles from a randomly chosen leg. These examples serve as supporting evidence to demonstrate the effectiveness and reliability of our optimization model.

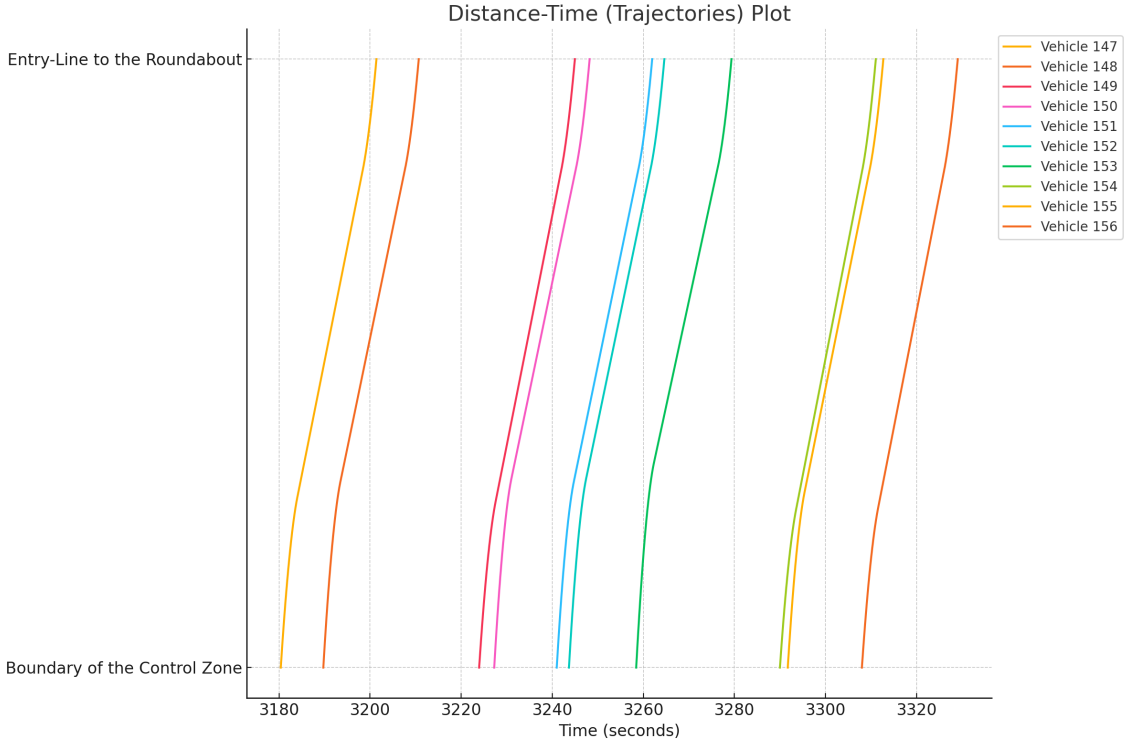

Figure B.1: Examples of controlled vehicles' trajectories on leg 1 at an arrival rate of $200pcu/h$.

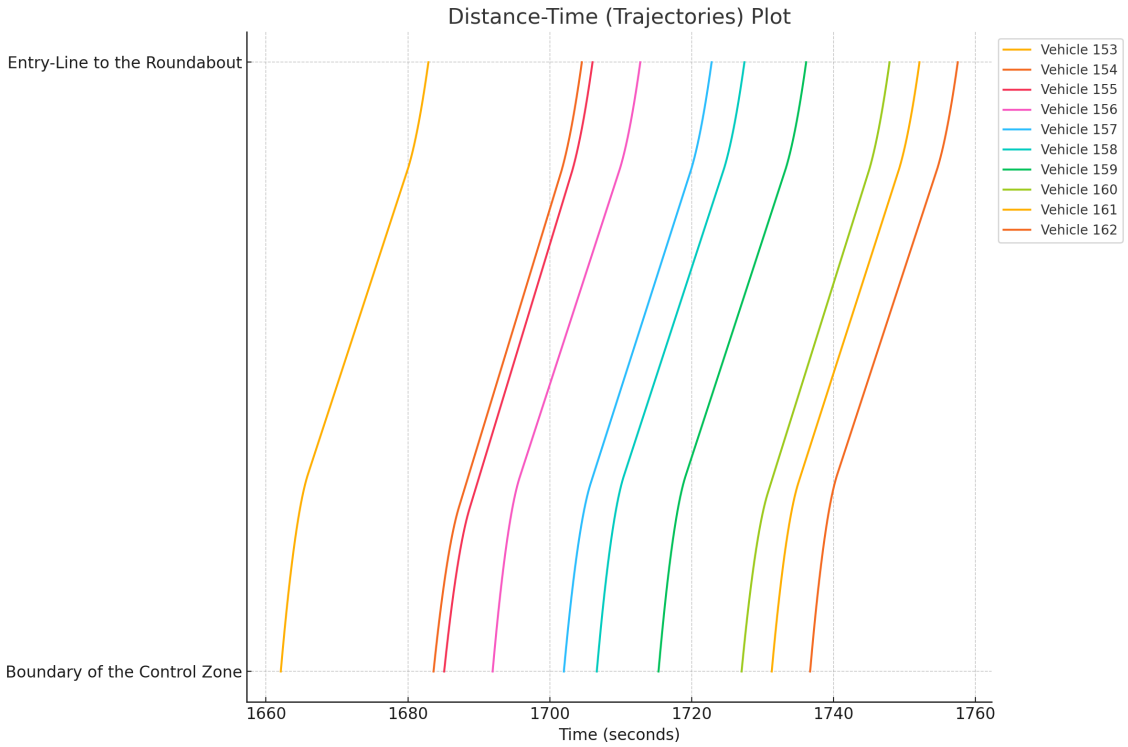

Figure B.2: Examples of controlled vehicles' trajectories on leg 2 at an arrival rate of $400pcu/h$.

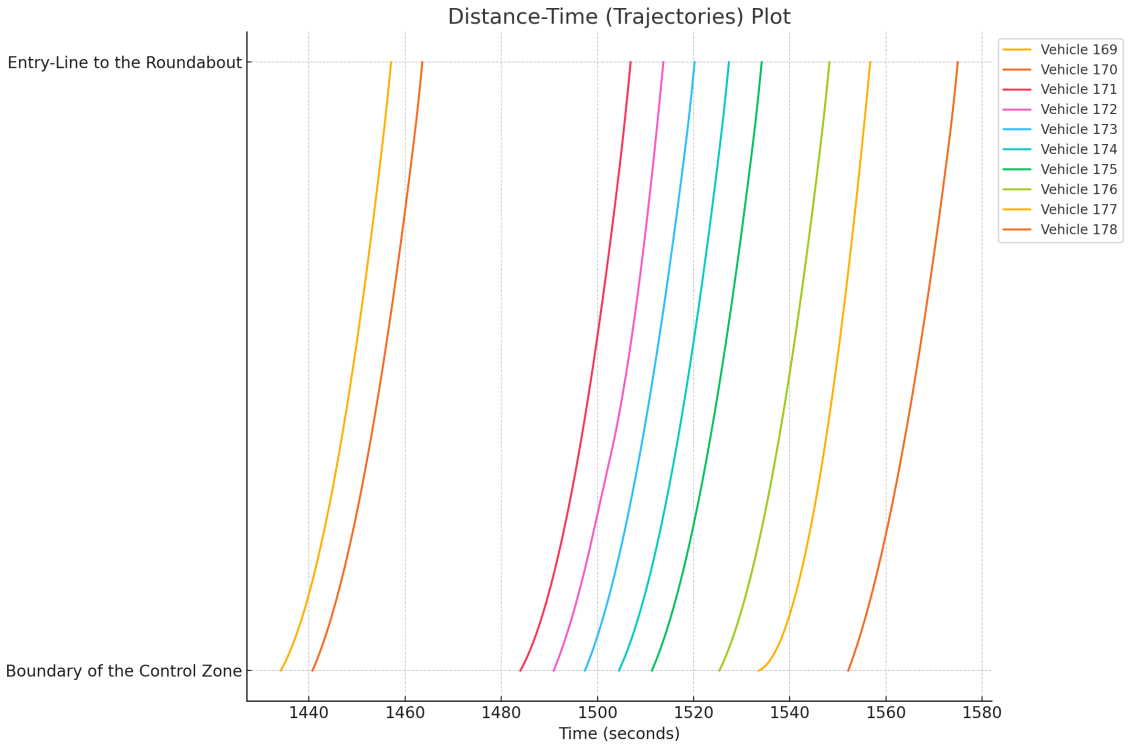

Figure B.3: Examples of controlled vehicles' trajectories on leg 3 at an arrival rate of $600pcu/h$.

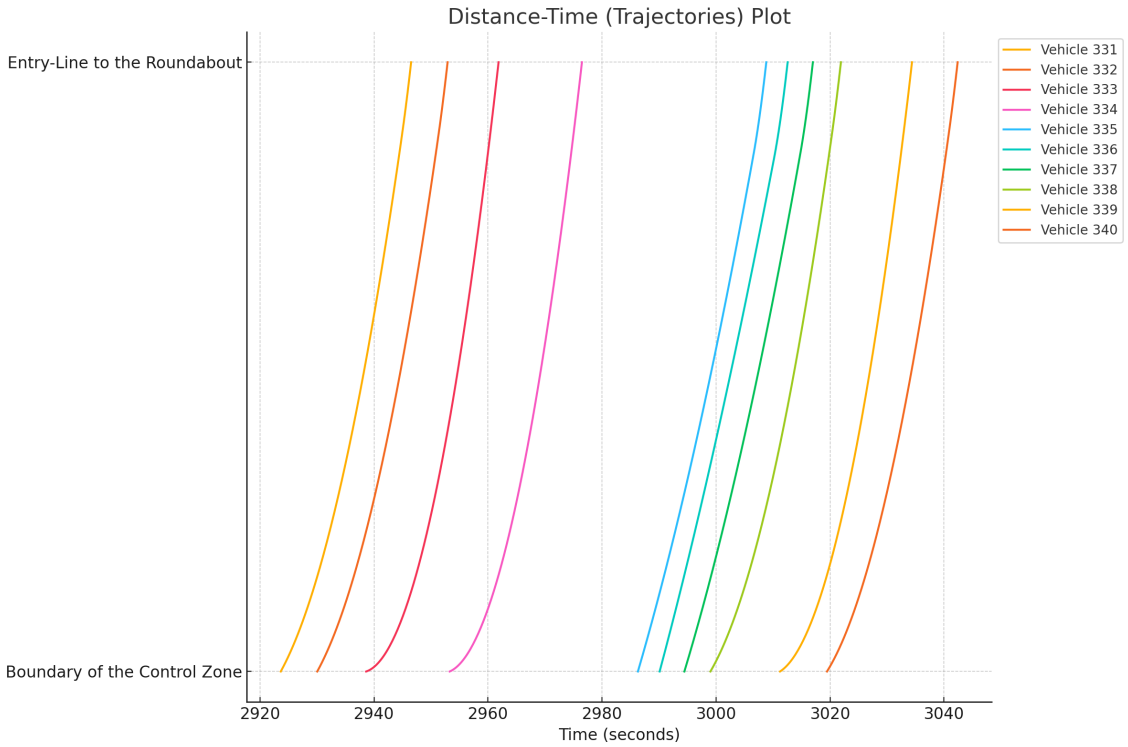

Figure B.4: Examples of controlled vehicles' trajectories on leg 4 at an arrival rate of $800pcu/h$.